Application of Bayesian Inference Techniques for Calibrating Eutrophication Models

by

Weitao Zhang

A thesis submitted in conformity with the requirements

for the degree of Master of Science

Graduate Department of Geography

University of Toronto

Application of Bayesian Inference Techniques for Calibrating Eutrophication Models

by Weitao Zhang (2008)
for the degree of Master of Science,
Graduate Department of Geography, University of Toronto

Abstract

This research aims to integrate mathematical water quality models with Bayesian inference techniques for obtaining effective model calibration and rigorous assessment of the uncertainty underlying model predictions. The first part of my work combines a Bayesian calibration framework with a complex biogeochemical model to reproduce oligo-, meso- and eutrophic lake conditions. The model accurately describes the observed patterns and also provides realistic estimates of predictive uncertainty for water quality variables. The Bayesian estimations are also used for appraising the exceedance frequency and confidence of compliance of different water quality criteria. The second part introduces a Bayesian hierarchical framework (BHF) for calibrating eutrophication models at multiple systems (or sites of the same system). The models calibrated under the BHF provided accurate system representations for all the scenarios examined. The BHF allows overcoming problems of insufficient local data by "borrowing strength" from well-studied sites. Both frameworks can facilitate environmental management decisions.

Acknowledgments

Foremost, I would like to express my deepest gratitude to my advisor, Prof. George Arhonditsis, for his encouragement, patience, support, and constant invaluable advice. I have been amazingly fortunate to have him as an advisor, who has the rich knowledge and perspicacious intuition on ecological modeling problems. I enjoyed my research experience so much during last two years.

I would also like to give a special thanks to my committee, Prof. Myrna Simpson and Prof. Miriam Diamond, for volunteering their time and providing me their feedback through this process.

At the same time, I wish to thank all the members of the Ecological Modeling Lab for their help. We also spent great times together just for random talks that usually had nothing to do with modeling.

Finally, I would like to give thanks to my parents for all their love and support throughout my life. I also would like to dedicate this to my wife, Jing Wu, for all her support while I pursued my educational goals and for enduring all the evenings and weekends that I was busy with school. I am finally done!

This work was supported by Ontario Graduate Scholarship (OGS) and funding from the Department of Geography, University of Toronto.

Table of Contents

List of Tables

List of Figures

List of Appendices

Glossary of Terms

Bayes' Theorem: is a theorem of probability theory originally stated by the Reverend Thomas Bayes. The theorem relates the conditional and marginal probability distributions of random variables, and tells how to update or revise beliefs in the light of new evidence from the study system.

Bayesian Inference: is a statistical approach in which all forms of uncertainty are expressed in terms of probability, and concerns with the consequences of modifying our previous beliefs as a result of receiving new data. In the inference process, Bayes' Theorem is applied to obtain a posterior probability for a specific hypothesis, which considers both the prior probability and the observations from the study system.

Convergence: is the point in which MCMC sampling techniques eventually reach a stationary distribution. From this point on, the MCMC scheme moves around this distribution.

Credible Interval: is a posterior probability interval of a parameter or a model output. Credible intervals are the Bayesian counterparts of the confidence intervals used in frequentist statistics.

Likelihood Function: is a conditional function [$p(y|\theta)$] considered as a function of its second argument (θ, model parameters) with its first argument (y, the data) held fixed. The likelihood function indicates how likely a particular population (model parameter set) can produce an observed sample.

Model Calibration: Calibration is the procedure by which the modeler attempts to find the best fit between computed and observed data by adjusting model parameters.

Markov chain Monte Carlo (MCMC) methods: are a class of algorithms for sampling from probability distributions based on the construction of a Markov chain that has the desired distribution as its stationary distribution. This procedure is used to generate a

sequence of samples from a probability distribution that is difficult to be directly sampled.

Metropolis-Hastings Algorithm: is a rejection sampling algorithm, which generates a random walk using a proposal density and contains a method for rejecting proposed steps. It is one algorithm of Markov chain Monte Carlo methods.

NPZD model: model consists of four state variables: nutrient (N) (phosphate, PO_4^{3-}), phytoplankton (*P*), zooplankton (*Z*), and detritus (*D*)

Over relaxation: At each MCMC iteration, a number of candidate samples are generated and one that is negatively correlated with the current value is selected. The time per iteration will be increased, but the within-chain correlations should be reduced and hence less iteration may be necessary.

Posterior Distribution: is the conditional probability of a random event or an uncertain proposition, and it is assigned when the relevant evidence from the study system is taken into account.

Prior Distribution: is a marginal probability and interpreted as a description of what is known about a variable in the absence of evidence from the study system.

Runge-Kutta Method: is a family of implicit and explicit iterative methods for the numerical approximation of solutions of ordinary differential equations.

Sensitivity Analysis: is the process by which the modeler attempts to evaluate the model sensitivity to the parameters selected, the forcing functions, or the state-variable submodels.

Chapter 1: Introduction

The importance of investigating the effects of uncertainty on mathematical model predictions has been extensively highlighted in the modelling literature. Nonetheless, in a recent meta-analysis, Arhonditsis and Brett (2004) showed that the large majority of the aquatic biogeochemical models published over the last decade did not properly assess prediction error and reliability of the critical planning information generated by the models. Thorough quantification of model sensitivity to parameters, forcing functions and state variable submodels, was only reported in 27.5% of the studies, while 45.1% of the published models did not report any results of uncertainty/sensitivity analysis. The question of model credibility is important because models are used to identify polluters, to direct the use of research dollars, and to determine management strategies that have considerable social and economic implications. Erroneous model outputs and failure to account for uncertainty could produce misleading results and misallocation of limited resources during the costly implementation of alternative environmental management schemes. For better model-based decision making, the uncertainty in model projections must be reduced, or at least explicitly acknowledged, and reported in a straightforward way that can be easily used by policy planners and decision makers.

Another problematic aspect of the current modelling practice is that the usual calibration methods do not address the well-known equifinality (poor model identifiability), where several distinct choices of model inputs lead to the same model outputs (many sets of parameters fit the data about equally well). A main reason for the equifinality problem is that the ecological processes/causal mechanisms used for

understanding how the system works internally is of substantially higher order than what can be externally observed. However, having a model that realistically reflects the natural system dynamics is particularly important when the model is intended for making predictions in the extrapolation domain, i.e., predict future conditions significantly different from those used to calibrate the mode. For example, when a water quality model does not operate with realistic relative/absolute magnitudes of biological rates and transport processes, even if the fit between model outputs and observations is satisfactory ("good results for the wrong reasons"), its credibility to provide predictions about how the system will respond under different external nutrient loading conditions is very limited. In this case, the application of mathematical models for extrapolative tasks is "an exercise in prophecy" rather than scientific action based on robust prognostic tools. Another problem that modellers do not always acknowledge is that the conventional model calibration, may provide the best fit of model input parameters to the dataset available at the moment, but it is specific to the given dataset at hand. As new data become available, the model should be recalibrated and in the common calibration practice there is no way of considering previous results. In this sense, we do not update previous knowledge about model input parameters, but rather we make the models dataset-specific.

The first part of this dissertation (Chapter 2) aims to attain effective model calibration and rigorous uncertainty assessment by integrating complex mathematical modeling with Bayesian analysis. We used a complex aquatic biogeochemical model that simulates multiple elemental cycles (org. C, N, P, Si, O), multiple functional phytoplankton (diatoms, green algae and cyanobacteria) and zooplankton (copepods and cladocerans) groups. The Bayesian calibration framework is illustrated using three

synthetic datasets that represent oligo-, meso- and eutrophic lake conditions. Scientific knowledge, expert judgment, and observational data were used to formulate prior probability distributions and characterize the uncertainty pertaining to a subset of the model parameters, i.e., a vector comprising the 35 most influential parameters based on an earlier sensitivity analysis of the model. The study also underscores the lack of perfect simulators of natural system dynamics using a statistical formulation that explicitly accounts for the discrepancy between mathematical models and environmental systems. The analysis also aimed to illustrate how the Bayesian parameter estimation can be used for assessing the exceedance frequency and confidence of compliance of different water quality criteria. The proposed methodological framework can be very useful in the policy-making process and can facilitate environmental management decisions in the Laurentian Great Lakes region.

The second part of this dissertation (Chapter 3) presents a Bayesian hierarchical formulation for simultaneously calibrating aquatic biogeochemical models at multiple systems (or sites of the same system) with differences in their trophic conditions, prior precisions of model parameters, available information, measurement error or inter-annual variability. Model practitioners increasingly place emphasis on rigorous quantitative error analysis in aquatic biogeochemical models and the existing initiatives range from the development of alternative metrics for goodness of fit, to data assimilation into operational models, to parameter estimation techniques. However, the treatment of error in many of these efforts is arguably selective and/or ad hoc. A Bayesian hierarchical framework enables the development of robust probabilistic analysis of error and uncertainty in model predictions by explicitly accommodating measurement error, parameter uncertainty, and model structure imperfection. Our statistical formulation also

explicitly considers the uncertainty in model inputs (model parameters, initial conditions), the analytical/sampling error associated with the field data, and the discrepancy between model structure and the natural system dynamics (e.g., missing key ecological processes, erroneous formulations, misspecified forcing functions). The Bayesian hierarchical approach allows overcoming problems of insufficient local data by "borrowing strength" from well-studied sites and this feature will be highly relevant to conservation practices of regions with a high number of freshwater resources for which complete data could never be practically collected.

Chapter 2: Predicting the Frequency of Water Quality Standard Violations Using Bayesian Calibration of Eutrophication Models [1]

2.1 Introduction

In his 2006 review paper, D.W. Schindler highlighted the cultural eutrophication as one of the preeminent threats to the integrity of freshwater ecosystems worldwide. He also emphatically argued that our current understanding and management of eutrophication has evolved from simple control of point and non-point nutrient sources to the explicit recognition that it often stems from the cumulative effects of the human activities on climate, global element cycles, land use, and fisheries. Therefore, alleviating eutrophication problems often involves complex policy decisions aiming to protect the functional properties of the freshwater ecosystem community as well as to restore many of the features of the surrounding watershed. In the Great Lakes region, the growing appreciation of the complexity pertaining to eutrophication control and the need for addressing the combined effects of a suite of tightly intertwined stressors has sparked considerable confusion and disagreements (Hartig *et al.* 1998, Bowerman *et al.* 1999). Much of this controversy has arisen as to whether the Great Lakes Water Quality Agreement is a thrust for improving water quality or for maintaining ecosystem integrity, and the proposed transition from the Water Quality/Fisheries Exploitation paradigms into the Ecosystem Management paradigm has been repeatedly debated in the literature (Bowerman *et al*. 1999, Minns and Kelso 2000). The defenders of the traditional

[1] In press: *J. Great Lakes Res.* 2008

paradigms have argued that the shift of focus from water quality to ecosystem management has also been accompanied by a shift from the traditional identification of simple cause–effect relationships to a multi-causal way of thinking to accommodate the complexity of ecosystems. In this context, the crux of the problem is that the ecological complexity along with the underlying uncertainty can be a major impediment for deriving the straightforward scientific answers required from the regulatory agencies to implement the provisions of the Great Lakes Water Quality Agreement (Bowerman *et al.* 1999, Krantzberg 2004).

Aside from the environmental thinking, the emergence of the ecosystem approach has also pervaded the contemporary mathematical modeling practice, increasing the demand for more complex ecosystem models. Earlier eutrophication modeling studies in the Great Lakes provided long-term forecasts and insightful retrospective analysis using as foundation the interplay among nutrient loading, hydrodynamics, phytoplankton response, and sediment oxygen demand (Bierman and Dolan 1986, Lam *et al.* 1987a, DiToro *et al.* 1987). Yet, the current challenges make compelling the development of more realistic platforms (i) to elucidate causal mechanisms, complex interrelationships, direct and indirect ecological paths of the Great Lakes basin ecosystem; (ii) to examine the interactions among the various stressors (e.g., climate change, urbanization/land-use changes, alternative management practices, invasion of exotic species); and (iii) to assess their potential consequences on the lake ecosystem functioning (e.g., food web dynamics, benthic-pelagic coupling, fish communities) (Mills *et al.* 2003, Leon *et al.* 2005). In this regard, a characteristic example is the integrated eutrophication-zebra mussel bioenergetic model developed for identifying the factors that promote the re-occurrence of *Microcystis* blooms in the Saginaw Bay, Lake Huron (Bierman *et al.* 2005). It was

shown that the zebra mussels through selective cyanobacteria rejection, increased sediment-water phosphorus fluxes can cause structural shifts in the phytoplankton community, and the impact of these perturbations varies depending on the magnitude of the zebra mussel densities and their distribution among different age groups. The Bierman *et al.* (2005) study is an example of how the increase of the articulation level of our mathematical models allows performing experiments that are technologically or economically unattainable by other means, thereby gaining insights into the direct and synergistic effects induced from the multitude of stressors on the various lake ecosystem components.

While the development of more holistic modeling constructs is certainly the way forward, the question arising is: do we have the knowledge to parameterize or even to mathematically depict the new biotic relationships and their interactions with the abiotic environment? More importantly, how reliable are the long-term projections generated from the current generation of mathematical models? Our experience is that the performance of existing mechanistic biogeochemical models declines as we move from physical-chemical to biological components of aquatic ecosystems (Arhonditsis and Brett 2004). Because of the still poorly understood ecology, we do not have robust parameterizations to support predictions in a wide range of spatiotemporal domains (Anderson 2005). Despite the repeated efforts to explicitly treat multiple biogeochemical cycles, to increase the functional diversity of biotic communities, and to refine the mathematical description of the higher trophic levels, modelers still haven't gone beyond the phase of identifying the unforeseeable ramifications and the challenges that we need to confront so as to strengthen model foundation (Anderson 2006). Furthermore, the additional model complexity will increase the disparity between what ideally we want to

learn (internal description of the system and model endpoints) and what can realistically be observed, thereby reducing our ability to properly constrain the model parameters from observations (Denman 2003). The poor model identifiability undermines the predictive power of our models and their ability to support environmental management decisions (Arhonditsis *et al.* 2006). Thus, the most prudent strategy is to incorporate complexity gradually and this process should be accompanied by critical evaluation of the model outputs; the latter concern highlights the central role of uncertainty analysis.

Uncertainty analysis of mathematical models has received considerable attention in aquatic ecosystem research, and there have been several attempts to rigorously address issues pertaining to model structure and input error (Beck 1987, Reichert and Omlin 1997, Stow *et al.* 2007). In this direction, Arhonditsis *et al.* (2007) recently introduced a Bayesian calibration scheme using intermediate complexity mathematical models (4-8 state variables) and statistical formulations that explicitly accommodate measurement error, parameter uncertainty, and model structure imperfection. The Bayesian calibration methodology offers several technical advances, such as alleviation of the identification problem, sequential updating of the models, realistic uncertainty estimates of ecological predictions, and ability to obtain weighted averages of the forecasts from different models, that can be particularly useful for environmental management (Arhonditsis *et al.* 2007, 2008a, b). Nonetheless, the capacity of this approach to be coupled with complex mathematical models has not been demonstrated yet and recent studies have cautioned that this modeling framework will possibly require substantial modifications to accommodate highly multivariate outputs (Arhonditsis *et al.* 2008b).

In this paper, our main objective is to integrate the Bayesian calibration framework with a complex aquatic biogeochemical model that simulates multiple

elemental cycles (org. C, N, P, Si, O), multiple functional phytoplankton (diatoms, green algae and cyanobacteria) and zooplankton (copepods and cladocerans) groups. Because the model structure and complexity is suitable for addressing a variety of eutrophication-related problems (chlorophyll *a*, water transparency, cyanobacteria dominance, hypoxia), our presentation is highly relevant to the Great Lakes modeling practice. This illustration is based on three synthetic datasets representing oligo-, meso- and eutrophic lake conditions. Our analysis also shows how the Bayesian parameter estimation can be used for assessing the exceedance frequency and confidence of compliance of different water quality criteria. We conclude by pinpointing some of the anticipated benefits from the proposed approach, such as the assessment of uncertainty in model predictions and expression of model outputs as probability distributions, the optimization of the sampling design of monitoring programs, and the alignment with the policy practice of adaptive management, which can be particularly useful for stakeholders and policy makers when making decisions for sustainable environmental management in the Laurentian Great Lakes region.

2.2 Methods

2.2.1 Model Description

Model spatial structure and forcing functions: The spatial structure of the model is simpler than the two-compartment vertical system of the original model application in Lake Washington (Arhonditsis and Brett 2005a, b). We considered a single compartment model representing the lake epilimnion, whereas the hypolimnion was treated as boundary conditions to emulate mass exchanges across the thermocline. The external

forcing encompasses river inflows, precipitation, evaporation, solar radiation, water temperature, and nutrient loading. The reference conditions for our analysis correspond to the average epilimnetic temperature, solar radiation, vertical diffusive mixing, hydraulic and nutrient loading in Lake Washington (Arhonditsis and Brett 2005b, Brett *et al*. 2005). The hydraulic renewal rate in our hypothetical system is 0.384 $year^{-1}$. The fluvial and aerial total nitrogen inputs are 1114×10^3 kg $year^{-1}$, and the exogenous total phosphorus loading contributes approximately 74.9×10^3 kg $year^{-1}$. The exogenous total organic carbon supplies in the system are 6685×10^3 kg $year^{-1}$. In our analysis, the average input nutrient concentrations for the oligo-, meso-, and eutrophic environments correspond to 50 (2.9 mg TOC/L, 484 μg TN/L and 32.5 μg TP/L), 100 (5.8 mg TOC/L, 967 μg TN/L and 65 μg TP/L), and 200% (11.6 mg TOC/L, 1934 μg TN/L and 130 μg TP/L) of the reference conditions, respectively. Based on these nutrient loading scenarios, the model was run using the calibration vector presented in Arhonditsis and Brett (2005a; see their Appendix B for parameter definitions and calibration values). The simulated monthly averages provided the mean values of normal distributions with standard deviations assigned to be 15 % of the monthly values for each state variable; a fraction that comprises both analytical error and inter-annual variability at the deeper (middle) sections of the lake. These distributions were then sampled to generate the oligo-, meso- and eutrophic datasets used for the Bayesian model calibration.

Plankton community structure: The ecological submodel consists of 24 state variables and simulates five elemental cycles (organic C, N, P, Si, O) as well as three phytoplankton (diatoms, green algae and cyanobacteria) and two zooplankton (copepods and cladocerans) groups (Arhonditsis and Brett 2005a, b). The three phytoplankton functional groups differ with regards to their strategies for resource competition

(nitrogen, phosphorus, light, temperature) and metabolic rates as well as their morphological features (settling velocity, shading effects) (Fig. 2.1a). Phytoplankton growth temperature dependence has an optimum level and is modeled by a function similar to a Gaussian probability curve (Cerco and Cole, 1994). Phosphorus and nitrogen dynamics within the phytoplankton cells account for luxury uptake, and phytoplankton uptake rates depend on both intracellular and extracellular nutrient concentrations (Schladow and Hamilton 1997, Arhonditsis *et al*. 2002). We used Steele's equation to describe the relationship between photosynthesis and light intensity along with Beer's law to scale photosynthetically active radiation to depth (Jassby and Platt 1976). Diatoms are modeled as r-selected organisms with high maximum growth rates and higher metabolic losses, strong phosphorus and weak nitrogen competitors, lower tolerance to low light availability, low temperature optima, silica requirements, and high sinking velocities. By contrast, cyanobacteria are modeled as K-strategists with low maximum growth and metabolic rates, weak P and strong N competitors, higher tolerance to low light availability, low settling velocities, and high temperature optima. The parameterization of the third functional group (labelled as "Green Algae") aimed to provide an intermediate competitor and more realistically depict the continuum between diatom- and cyanobacteria-dominated phytoplankton communities.

The two zooplankton functional groups (cladocerans and copepods) differ with regards to their grazing rates, food preferences, selectivity strategies, elemental somatic ratios, vulnerability to predators, and temperature requirements (Arhonditsis and Brett 2005a, b). Cladocerans are modeled as filter-feeders with an equal preference among the four food-types (diatoms, green algae, cyanobacteria, detritus), high maximum grazing rates and metabolic losses, lower half saturation for growth efficiency, high temperature

optima and high sensitivity to low temperatures, low nitrogen and high phosphorus content. In contrast, copepods are characterized by lower maximum grazing and metabolic rates, capability of selecting on the basis of food quality, higher feeding rates at low food abundance, slightly higher nitrogen and much lower phosphorus content, lower temperature optima with a wider temperature tolerance. Fish predation on cladocerans is modeled by a sigmoid function, while a hyperbolic form is adopted for copepods (Edwards and Yool 2000). Both forms exhibit a plateau at high zooplankton concentrations representing satiation of the fish predation, e.g., the fish can only process a certain number of food items per unit time or there is a maximum limit on predator density caused by direct interference among the predators themselves. The S-shaped curve, however, is more appropriate for reproducing the tight connection between planktivorous fish and large *Daphnia* adults at higher zooplankton densities, due to fish specialisation (learning ability of fish to capture large animals) or lack of escape behaviour of the prey (Lampert and Sommer 1997).

Carbon cycle: The inorganic carbon required for algal photosynthesis is assumed to be in excess and thus is not explicitly modeled. Dissolved organic carbon (DOC) and particulate organic carbon (POC) are the two carbon state variables considered by the model (Fig. 2.1b). Phytoplankton basal metabolism, zooplankton basal metabolism and egestion of excess carbon during zooplankton feeding release particulate and dissolved organic carbon in the water column. A fraction of the particulate organic carbon undergoes first-order dissolution to dissolved organic carbon, while another fraction settles to the sediment. Particulate organic carbon is grazed by zooplankton (detrivory), dissolved organic carbon is lost through a first-order denitrification and respiration during heterotrophic activity.

Nitrogen cycle: There are four nitrogen forms considered by the model: nitrate (NO_3^-), ammonium (NH_4^+), dissolved organic nitrogen (DON), particulate organic nitrogen (PON) (Fig. 2.1c). Both ammonium and nitrate are utilized by phytoplankton during growth and Wroblewski's model (1977) was used to describe ammonium inhibition of nitrate uptake. Phytoplankton basal metabolism, zooplankton basal metabolism and egestion of excess nitrogen during zooplankton feeding release ammonium and organic nitrogen in the water column. A fraction of the particulate organic nitrogen hydrolyzes to dissolved organic nitrogen. Dissolved organic nitrogen is mineralized to ammonium. In an oxygenated water column, ammonium is oxidized to nitrate through nitrification and its kinetics are modeled as a function of available ammonium, dissolved oxygen, temperature and light (Cerco and Cole 1994, Tian *et al*. 2001). During anoxic conditions, nitrate is lost as nitrogen gas through denitrification.

Phosphorus cycle: Three phosphorus state variables were considered in the model: phosphate (PO_4^{3-}), dissolved organic phosphorus (DOP), and particulate organic phosphorus (POP) (Fig. 2.1d). Phytoplankton uptakes phosphate and redistributes the three forms of phosphorus through basal metabolism. Zooplankton basal metabolism and egestion of excess phosphorus during feeding release phosphate and dissolved/particulate organic phosphorus. Particulate organic phosphorus can be hydrolyzed to dissolved organic phosphorus, and another fraction settles to the sediment. Dissolved organic phosphorus is mineralized to phosphate through a first-order reaction.

2.2.2 Bayesian Framework

i) *Statistical formulation:* Our presentation examines a statistical formulation founded on the assumption that the eutrophication model is an imperfect simulator of the

environmental system and the model discrepancy is invariant with the input conditions, i.e., the difference between model and lake dynamics was assumed to be constant over the annual cycle for each state variable. This formulation aims to combine field observations with simulation model outputs to update the uncertainty of model parameters, and then use the calibrated model to give predictions (along with uncertainty bounds) of the natural system dynamics. An observation i for the state variable j, y_{ij}, can be described as:

$$y_{ij} = \underbrace{f(\theta, x_i, y_0) + \delta_j}_{g(\theta, x_i, y_0, \delta_j) \sim N(f(\theta, x_i, y_0), \sigma_j^2)} + \varepsilon_{ij}, \quad i = 1, 2, 3, \ldots\ldots n \text{ and } j = 1, \ldots, m \qquad \textbf{(2-1)}$$

where $f(\theta, x_i, y_0)$ denotes the eutrophication model, x_i is a vector of time dependent control variables (e.g., boundary conditions, forcing functions) describing the environmental conditions, the vector θ is a time independent set of the calibration model parameters, y_0 corresponds to the vector of the concentrations of the twenty four state-variables at the initial time point t_0 (initial conditions), the stochastic term δ_j accounts for the discrepancy between the model and the natural system, ε_{ij} denotes the observation (measurement) error that is usually assumed to be independent and identically distributed following a Gaussian distribution, and $g(\theta, x_i, y_0, \delta_j)$ represents a normally distributed variable with first and second order moments based on the model predictions and the time independent model structural error σ_j^2. In this study, as a result of the scheme followed to generate the three datasets, we assumed a multiplicative measurement error with standard deviations proportional (15%) to the average monthly values for each state variable (Van Oijen *et al*. 2005). With this assumption, the likelihood function (see Glossary of Terms) will be:

$$p\left(y\middle|f(\theta,x,y_0)\right)=\prod_{j=1}^{m}(2\pi)^{-n/2}\left|\Sigma_{Totj}\right|^{-1/2}\exp\left[-\frac{1}{2}\left[y_j-f_j(\theta,x,y_0)\right]^T\Sigma_{Totj}^{-1}\left[y_j-f_j(\theta,x,y_0)\right]\right] \quad \textbf{(2-2)}$$

$$\Sigma_{Totj}=\Sigma_{\delta j}+\Sigma_{\varepsilon j} \quad \textbf{(2-3)}$$

where m and n correspond to the number of state variables (m = 24) and the number of observations in time used to calibrate the model (n = 12 average monthly values), respectively; $y_j = [y_{1j},...,y_{nj}]^T$ and $f_j(\theta, x, y_0) = [f_{1j}(\theta, x_1, y_0),..., f_{nj}(\theta, x_n, y_0)]^T$ correspond to the vectors of the field observations and model predictions for the state variable j; $\Sigma_{\delta j} = I_n \cdot \sigma_j^2$ corresponds to the stochastic term of the model; and $\Sigma_{\varepsilon j} = I_n \cdot (0.15)^2 \cdot y_j^T \cdot y_j$. In the context of the Bayesian statistical inference, the posterior density of the parameters θ and the initial conditions of the twenty four state variables y_0 given the observed data y is defined as:

$$p\left(\theta,y_0,\sigma^2\middle|y\right)=\frac{p\left(y\middle|f(\theta,x,y_0,\sigma^2)\right)p(\theta)p(y_0)p(\sigma^2)}{\iiint p\left(y\middle|f(\theta,x,y_0,\sigma^2)\right)p(\theta)p(y_0)p(\sigma^2)d\theta dy_0 d\sigma^2}\propto p\left(y\middle|f(\theta,x,y_0,\sigma^2)\right)p(\theta)p(y_0)p(\sigma^2) \quad \textbf{(2-4)}$$

$p(\theta)$ is the prior density of the model parameters θ and $p(y_0)$ is the prior density of the initial conditions of the twenty four state variables y_0. In a similar way to the measurement errors, the characterization of the prior density $p(y_0)$ was based on the assumption of a Gaussian distribution with a mean value derived from the January monthly averages during the study period and standard deviation that was 15% of the mean value for each state variable j; the prior densities $p(\sigma_j^2)$ were based on the conjugate inverse-gamma distribution (Gelman *et al*. 1995). Thus, the resulting posterior distribution for θ, y_0, and σ^2 is:

$$p\left(\theta, y_0, \sigma^2 \middle| y\right) \propto \prod_{j=1}^{m} (2\pi)^{-n/2} \left|\Sigma_{Totj}\right|^{-1/2} \exp\left[-\frac{1}{2}\left[y_j - f_j(\theta, x, y_0)\right]^T \Sigma_{Totj}^{-1}\left[y_j - f_j(\theta, x, y_0)\right]\right]$$

$$\times (2\pi)^{-l/2} \left|\Sigma_\theta\right|^{-1/2} \prod_{k=1}^{l} \frac{1}{\theta_k} \exp\left[-\frac{1}{2}\left[\log\theta - \theta_0\right]^T \Sigma_\theta^{-1}\left[\log\theta - \theta_0\right]\right]$$

$$\times (2\pi)^{-m/2} \left|\Sigma_{y0}\right|^{-1/2} \exp\left[-\frac{1}{2}\left[y_0 - y_{0m}\right]^T \Sigma_{y0}^{-1}\left[y_0 - y_{0m}\right]\right]$$

$$\times \prod_{j=1}^{m} \frac{\beta_j^{\alpha j}}{\Gamma(\alpha_j)} \sigma_j^{-2(\alpha_j+1)} \exp(-\frac{\beta_j}{\sigma_j^2}) \qquad \textbf{(2-5)}$$

where l is the number of the model parameters θ used for the model calibration ($l = 35$); θ_0 indicates the vector of the mean values of θ in logarithmic scale; $\Sigma_\theta = I_l \cdot \sigma_\theta^T \cdot \sigma_\theta$ and $\sigma_\theta = [\sigma_{\theta 1}, \ldots, \sigma_{\theta l}]^T$ corresponds to the vector of the shape parameters of the l lognormal distributions (standard deviation of *log* θ); the vector $y_{0m} = [y_{1,1}, \ldots, y_{1,24}]^T$ corresponds to the January values of the twenty four state variables; $\Sigma_{y0} = I_m \cdot (0.15)^2 \cdot y_{0m}^T \cdot y_{0m}$; α_j (= 0.01) and β_j (= 0.01) correspond to the shape and scale parameters of the m non-informative inverse-gamma distributions used in this analysis.

ii) *Prior parameter distributions:* The calibration vector consists of the 35 most influential parameters as identified from an earlier sensitivity analysis of the model (Arhonditsis and Brett 2005a). The prior parameter distributions reflect the existing knowledge (field observations, laboratory studies, literature information and expert judgment) on the relative plausibility of their values. For example, based on the previous characterization of the three functional groups, we assigned probability distributions that represent their differences in growth and storage strategies, basal metabolism, nitrogen and phosphorus kinetics, light and temperature requirements, and settling velocity. In this study, we used the following protocol to formulate the parameter distributions: i) we identified the global (not the group-specific) minimum and maximum values for each

parameter from the pertinent literature; ii) we partitioned the original parameter space into three subregions reflecting the functional properties of the phytoplankton groups; and then iii) we assigned lognormal distributions parameterized such that 98% of their values were lying within the identified ranges (Steinberg *et al*. 1997). The group-specific parameter spaces were also based on the calibration vector presented during the model application in Lake Washington (Arhonditsis and Brett 2005a). For example, the identified range for the maximum phytoplankton growth rate was 1.0-2.4 day^{-1}, while the three subspaces were 2.2 ± 0.2 day^{-1} for diatoms (calibration value ± literature range), 1.8 ± 0.2 day^{-1} for greens and 1.3 ± 0.3 day^{-1} for cyanobacteria. We then assigned lognormal distributions formulated such that 98% of their values were lying within the specified ranges, i.e., $growth_{max(diat)} \sim \Lambda(2.19, 1.040)$, $growth_{max(greens)} \sim \Lambda(1.79, 1.049)$, $growth_{max(cyan)} \sim \Lambda(1.26, 1.106)$. The prior distributions of all the parameters of the model calibration vector are presented in Table 2.1.

iii) *Numerical approximations for posterior distributions:* Sequence of realizations from the posterior distribution of the model were obtained using Markov chain Monte Carlo (MCMC) simulations (Gilks *et al*. 1998). We used the general normal-proposal Metropolis algorithm coupled with an ordered over-relaxation to control the serial correlation of the MCMC samples (Neal 1998). In this study, we present results using two parallel chains with starting points: (i) a vector that consists of the mean values of the prior parameter distributions, and (ii) the calibration vector of the application Lake Washington. We used 30,000 iterations and convergence was assessed with the modified Gelman–Rubin convergence statistic (Brooks and Gelman 1998). The accuracy of the posterior estimates was inspected by assuring that the Monte Carlo error (an estimate of the difference between the mean of the sampled values and the true posterior mean; see

Spiegelhalter *et al*. 2003) for all the parameters was less than 5% of the sample standard deviation. Our framework was implemented in the WinBUGS Differential Interface (WBDiff); an interface that allows numerical solution of systems of ordinary differential equations within the WinBUGS software.

2.3 Results

The MCMC sequences of the three applications of the model converged rapidly (≈ 5,000 iterations) and the statistics reported were based on the last 25,000 draws by keeping every 4th iteration (thin = 4). The uncertainty underlying the values of the 35 model parameters after the MCMC sampling is depicted on the respective marginal posterior distributions (Table 2.1 and Fig. 2.2). Generally, the moments of the posterior parameter distributions indicate that the knowledge gained for the 35 parameters after the Bayesian updating of the complex eutrophication model was fairly limited. [It should be noted that for the sake of consistency all the parameter posteriors were presented as lognormal distributions, although in several cases the shape is better approximated by a uniform distribution.] Namely, most of the calibration parameters were characterized by minor or no shifts of their central tendency relative to the prior assigned values, such as the half saturation constants for nitrogen uptake ($KN_{(i);\ i=\ diatoms,\ greens,\ cyanobacteria}$), the half saturation constants for grazing ($KZ_{(j);\ j=\ cladocerans,\ copepods}$), and the half saturation constants for growth efficiency ($ef_{2(j);\ j=\ cladocerans,\ copepods}$). Nonetheless, there were parameters with moderate shifts of their posterior mean values; characteristic examples were the nitrogen mineralization rate ($KN_{refmineral}$) with relative percentage changes of 14, 23, and 11% in the oligo-, meso-, and eutrophic environments, respectively; the light

attenuation coefficient for chlorophyll ($K_{EXTchla}$) with 6, 15, and 14% relative changes in the three nutrient enrichment conditions; settling velocity for diatoms ($V_{settling(diat)}$) with 9, 13, and 7% relative shifts. Furthermore, the vast majority of the posterior standard deviations increased or remained unaltered relative to the prior assigned values, and several parameter posteriors were almost uniformly distributed within the specified ranges prior to the model calibration. Notable exceptions were the dissolution/hydrolysis rates for particulate carbon ($KC_{refdissolution}$), nitrogen ($KN_{refdissolution}$), phosphorus ($KP_{refdissolution}$), and silica ($KSi_{refdissolution}$) with approximately 2-6% relative decrease of the respective standard deviations. The standard deviation of the diatom settling velocity ($V_{settling(diat)}$) was also reduced by 3% in the mesotrophic state.

The comparison between the observed and posterior predictive monthly distributions for the three trophic states indicates that the eutrophication model combined with the Bayesian calibration scheme provides an accurate representation of the system dynamics. In the oligotrophic environment, the observed monthly values were included within the 95% credible intervals of the model predictions throughout the simulation period, while the median values of model predictions closely matched the observed patterns (Fig. 2.3). In a similar manner, all the observed values of the dataset representing the mesotrophic conditions were included within the 95% credible intervals, although the median model predictions slightly underestimated the spring biomass peaks of three phytoplankton groups (Fig. 2.4). In the eutrophic scenario, the model closely reproduced the summer prey-predator oscillations between cladocerans and the three phytoplankton groups and also accurately simulated the nutrient dynamics, i.e., total nitrogen, nitrate, ammonium, total phosphorus, and phosphate (Fig. 2.5). However, the central tendency and uncertainty bounds of the copepod biomass predictive distribution failed to capture

the late-spring peak, while the upper (97.5%) and lower (2.5%) uncertainty boundaries showed convexo-convex shape during the same period.

The model performance for each trophic state was evaluated by three measures of fit: root mean squared error (RMSE), relative error (RE) and average error (AE) (Table 2.2). These comparisons aimed to assess the goodness-of-fit between the medians of the predictive distributions and the observed values. The application of the model to the oligotrophic environment was characterized by the lowest RE values (1.19-10.6%), while the mesotrophic and eutrophic scenarios resulted in moderate (3.37-13.6%), and relatively larger RE values (6.03-21.2%), respectively. We also highlight the fairly high RE values for cyanobacteria and copepod biomass in the eutrophic environment, whereas total nitrogen and dissolved oxygen had consistently low REs in the three nutrient loading scenarios. The average error is a measure of aggregate model bias, though values near zero can be misleading because negative and positive discrepancies can cancel each other. In most cases, we found that the medians of the state variable predictive distributions underestimated the observed levels, whereas dissolved oxygen was overestimated with an AE value of 0.482, 0.356, and 0.628 mg L^{-1} in the oligo-, meso-, and eutrophic environment, respectively. The root mean square error is another measure of the model prediction accuracy that overcomes the shortcoming of the average error by considering the magnitude rather than the direction of each difference. The RMSE for the copepod biomass increased across the trophic gradient examined from 5.19 μg C L^{-1} in the oligotrophic to 13.2 and 48.3 μg C L^{-1} in the meso- and eutrophic datasets, respectively. We also note the approximately 0.5 μg chla L^{-1} mean discrepancy between the predictive medians and the observed cyanobacteria biomass values.

The seasonally invariant error terms (σ_j) delineate a constant zone around the model predictions for the 24 state variables that accounts for the discrepancy between the model simulation and the natural system dynamics (Table 2.3). The majority of the discrepancy terms increased as we move from the oligotrophic to the eutrophic state, providing evidence that these terms play an important role in accommodating the increased intra-annual variability of the meso- and eutrophic datasets. On the other hand, the error terms associated with the phytoplankton intracellular nutrient storage (e.g., $\sigma_{N, P(i);\ i=\ diatoms,\ greens,\ cyanobacteria}$, and $\sigma_{Si(diatoms)}$) were characterized by similar mean and standard deviation values across the trophic gradient examined. Finally, high coefficients of variation (standard deviation/mean) were found for the dissolved oxygen, dissolved organic carbon, and dissolved silica error terms.

Exceedance frequency and confidence of compliance with water quality standards: The MCMC posterior samples were also used to examine the exceedance frequency and confidence of compliance with different water quality standards under the three nutrient loading scenarios. For illustration purposes, we selected three water quality variables of management interest, i.e., chlorophyll *a* concentration, total phosphorus, and percentage cyanobacteria contribution to the total phytoplankton biomass, and then specified their threshold values (numerical criteria) at 5 μg Chl *a* L^{-1}, 25 μg TP L^{-1}, and 30%, respectively. For each iteration, we calculated the monthly predicted values and the corresponding probabilities of exceeding the three water quality criteria. The latter probabilities were calculated as follows:

$$p = P(c > c' \mid \theta, x, y_0) = 1 - F\left(\frac{c' - g(\theta, x, y_0, \delta)}{\sigma_\varepsilon}\right) \qquad \textbf{(2-6)}$$

where p is the probability of the response variable exceeding a numerical criterion c', given values of θ, x, and y_0, σ_ε is the measurement error/within-month variability, and $F(\cdot)$ is the value of the cumulative standard normal distribution. The monthly predicted values along with the calculated exceedance frequencies were then averaged over the summer stratified period (June-September). The distribution of these statistics across the posterior space (12,500 MCMC samples) can be used to assess the expected exceedance frequency and the confidence of compliance with the three water quality standards, while accounting for the uncertainty that stems from the model parameter uncertainty. It should be noted that the exceedance frequency is not necessarily normally distributed, especially since this value is calculated as the average over the stratified period (Borsuk *et al.* 2002).

In our example, no violations of the 5 μg Chl *a* L^{-1} numerical criterion are predicted in the oligo- and mesotrophic scenarios (Fig. 2.6). On the other hand, the chlorophyll *a* standard is likely to be violated in the eutrophic environment, and the corresponding expected exceedance (the mean of the distributions in Fig. 2.7) and confidence of compliance (the proportion of the exceedance frequency distribution that lies below the EPA's 10% guideline; CC) were approximately 30 and 3.5%, respectively. This probabilistic assessment of the water quality conditions should make model results more useful to decision makers and stakeholders, because the deterministic statements are avoided and the optimal management schemes (e.g., reduction of nutrient loading) are determined by explicitly acknowledging an inevitable risk of non-attainment. Similar insights can be gained by the other two water quality criteria (total phosphorus and cyanobacteria percentage). In the eutrophic conditions, the exceedance frequency distribution of the 25 μg TP L^{-1} criterion was lying within the 30-100% range, and therefore it is nearly impossible to comply with the 10% EPA guideline. The latter

conclusion can also be drawn with regards to the 30% cyanobacteria biomass criterion, although in this case a fairly low confidence of compliance also characterizes the mesotrophic state. Analogous statements can be made with other model endpoints of management interest, such as the spatiotemporal dissolved oxygen levels in systems experiencing problems of prolonged hypoxia (e.g., Lake Erie).

2.4 Discussion

The water quality management usually relies on mathematical models with strong mechanistic basis, as this improves the confidence in predictions made for a variety of conditions. From an operational standpoint, the interpretation of model results should explicitly consider two sources of model error, i.e., the observed variability that is not explained by the model and the uncertainty arising from the model parameters and/or the misspecification of the model structure (Arhonditsis *et al*. 2007, Stow *et al*. 2007). In this study, we illustrated a methodological framework that can accommodate rigorous and complete error analysis, thereby allowing for the direct assessment of the frequency of water quality standard violations along with the determination of an appropriate margin of safety (Borsuk *et al*. 2002). The latter term refers to the *probability distribution of the predicted exceedance probabilities* and represents the degree of confidence that the true value of the violation frequency is below a specified value (Wild *et al*. 1996, McBride and Ellis 2001). The presentation of the model outputs as probabilistic assessment of water quality conveys significantly more information than the point predictions and is conceptually similar to the percentile-based standards proposed by the EPA-guidelines (Office of Water 1997). In this regard, our analysis also builds upon the

recommendations of an earlier modeling work by Lam *et al.* (1987b), which advocated the use of probability indicators in water quality assessment in the Great Lakes area, recognizing the importance of the variability pertaining to nutrient loading and weather conditions. This type of probabilistic information is certainly more appealing to decision makers and stakeholders, as it acknowledges the knowledge gaps, the inherent uncertainty, and the interannual variability typically characterizing freshwater ecosystems (Ludwig 1996). The latter feature is particularly important in the most degraded and highly variable nearshore zones or enclosed bays/harbours in the Great Lakes. These areas are transitional zones in that they receive highly polluted inland waters from watersheds with significant agricultural, urban and/or industrial activities while mixing with offshore waters having different biological and chemical characteristics. Generally, we believe that the Bayesian calibration presented herein can be particularly useful in the context of the Great Lakes modeling, although our analysis highlighted several technical features that need to be acknowledged so as to put this framework into perspective.

As demonstrated in several recent studies (Arhonditsis *et al*. 2007, 2008a, b), the inclusion of the monthly invariant stochastic terms that account for model structure imperfection resulted in a close reproduction of the epilimnetic patterns. Even though the median model predictions tend to slightly underestimate the spring plankton bloom, all the observed monthly values of the datasets representing the three trophic states were included within the 95% credible intervals. It is important to note, however, that the updating of the model mainly changed the discrepancy error terms instead of the model input parameters; namely, the terms that reflect the model inadequacy and not the mathematical model itself were used to accommodate the temporal variability across the trophic gradient examined. The latter result does not fully satisfy the basic premise of our

framework to attain realistic forecasts while gaining insight into the ecological structure (e.g., cause-effect relationships, feedback loops) underlying system dynamics. Similar results were also reported in an earlier exercise of sequential model updating (Arhonditsis *et al*. 2008a), but here the increased complexity of the model has further reduced the updating of the posterior parameter distributions. A more parsimonious statistical configuration of the model will assume a "perfect" model structure, i.e., the difference between model and lake dynamics is only caused by the observation/measurement error (Higdon *et al*. 2004, Arhonditsis *et al*. 2007). Applications of this statistical formulation resulted in narrow-shaped posterior parameter distributions but also in substantial misrepresentation of the calibration dataset (Arhonditsis *et al*. 2008a, b). Both features were attributed to the overconditioning of the parameter estimates because the lack of potential for model error tends to overestimate the information content of the observations (Beven 2006). These contradictory results highlight the pivotal role of the assumptions pertaining to model error structure and invite further examination of statistical formulations that objectively weigh the relative importance of the discrepancy terms vis-à-vis the model parameters on the calibration results. For example, future research should evaluate formulations that explicitly consider the dependence patterns of the error terms in time/space along with the covariance between measurement error and model structural error (Beven 2006, Arhonditsis *et al*. 2008b).

The determination of the model structure (and associated parameter values) that realistically represents the natural system dynamics is the basic foundation for developing robust prognostic tools (Reichert and Omlin, 1997). However, most of the calibration schemes in the modeling literature have not adequately addressed the problem of uncertainty, and sometimes generate more questions than answers. Model calibration is

mainly presented as an inverse solution exercise (i.e., the data for the model endpoints are used to learn something about the parameters) or as an exercise for delineating uncertainty zones around the mean predictions (Beven 1993, Beven 2001). In ecological modeling, the model parameters correspond to ecological processes for which we usually have substantial amount of information on the relative plausibility of their values (e.g., Jorgensen *et al*. 1991). Thus, it is a significant omission to ignore this knowledge and solely let the data to offer insights into the parameter marginal distributions. In this study, prior information of the magnitudes of ecological processes (based on field observations from the lake, laboratory studies, literature information, and expert judgment) was used to formulate probability distributions that reflect the relative likelihood of different values of the respective model parameters. Earlier studies have indicated that the inclusion of these informative distributions into the "prior-likelihood-posterior" update cycles of intermediate complexity models favours solutions that more realistically depict the internal structure of the system and avoid getting "good results for the wrong reasons"; the latter finding has been reported even when the mathematical models were coupled with statistical formulations that explicitly consider discrepancy error terms (Arhonditsis *et al*. 2007, 2008a, b). In this analysis, however, the relatively uninformative patterns of the posterior parameter space suggest that the efficiency of this scheme can be compromised with complex model structures ($\geq$ 15-20 state variables). Interestingly, our analysis showed a relatively higher change (central tendency shifts and standard deviation reductions) of the posterior moments of some parameters associated with the nutrient recycling in the system, i.e., dissolution and mineralization rates. Despite the aforementioned role of the model structure error terms and the high dimensional input space (35 model parameters) of the complex simulation model examined, some of the parameters representing feedback loops of the system played a somewhat more active

role during the Bayesian updating process. Finally, the high coefficients of variation for the DO, DOC, and DSi error terms are indicative of the relatively low intra-annual variability characterizing these state variables (Arhonditsis *et al*. 2008a).

Aside from the probabilistic assessment of the water quality conditions, another benefit of the Bayesian parameter estimation is the alignment with the policy practice of adaptive management, i.e., an iterative implementation strategy that is recommended to address the often-substantial uncertainty associated with water quality model forecasts, and to avoid the implementation of inefficient and flawed management plans (Walters 1986). Adaptive implementation or "learning while doing" supports initial model forecasts of management schemes with post-implementation monitoring, i.e., the initial model forecast serves as the Bayesian prior, the post-implementation monitoring data serve as the sample information (the likelihood), and the resulting posterior probability (the integration of monitoring and modeling) provides the basis for revised management actions (Qian and Reckhow 2007). The probabilistic predictions for water quality variables of management interest (e.g., chlorophyll *a*, dissolved oxygen) can also be used to optimize water quality monitoring programs (Van Oijen *et al*. 2005). For example in Fig. 2.8, the sections of the system where water quality conditions are more uncertain ("flat" distributions; C and D in the first map) should be more intensively monitored. These model predictions form the Bayesian prior which then is integrated (updated) with additional monitoring data to provide the posterior distribution. Based on the patterns of the posterior predictive distributions (where the predictive distribution for one site indicates a "high" probability of non-attaining water quality goals or, alternatively, an "unacceptably high" variance), we can determine again the optimal sampling design for water quality monitoring and assess the value of information (value of additional

monitoring; *"Where should additional water quality data collection efforts be focused?"*). The Bayesian inference and decision theory can also provide a coherent framework for decision making in problems of natural resources management (Dorazio and Johnson 2003). Management objectives can be evaluated by integrating the probability of use attainment for a given water quality goal with utility functions that reflect different socioeconomic costs and benefits. The water quality goals (resulting from specific management schemes) associated with the highest expected utility might then be chosen (Dorazio and Johnson 2003).

2.5 Conclusions

We illustrated a novel methodological framework that effectively addresses several aspects of model uncertainty (model structure, model parameters, initial conditions, and forcing functions) and explicitly examines how they can undermine the credibility of model predictions. We also demonstrated how the Bayesian parameter estimation can be used for assessing the exceedance frequency and confidence of compliance of different water quality criteria. The present analysis also highlighted the difficulty in unequivocally dissaggregating the role of the uncertainty in model inputs and the error associated with the model structure (parameters versus model imperfection error terms); especially when using complex statistical formulations and models with multivariate outputs. Generally, our study provides overwhelming evidence that the coupling of the Bayesian calibration framework with complex overparameterized simulation models can negate the premise of attaining realistic forecasts while gaining mechanistic insights into the ecosystem dynamics. Thus, the use of complex models is

advised only if existing prior information from the system can reasonably constrain the input parameter space, thereby ensuring model fit that is not founded on uninformative and/or fundamentally flawed ecological structures (e.g., unrealistic magnitudes of the various ecological processes). In cases where prior knowledge does not exist, it is advised to start with intermediate complexity models (4-10 state variables) and then gradually increase the complexity as more information becomes available (Arhonditsis *et al.* 2008b).

The latter assertions do not imply that this framework cannot accommodate the enormous complexity characterizing environmental systems, but rather are an indication that the rigid structure of complex mathematical models can be replaced by more flexible modeling tools (e.g., Bayesian networks) with the ability to integrate quantitative descriptions of ecological processes at multiple scales and in a variety of forms (intermediate complexity mathematical models, empirical equations, expert judgments), depending on available information (Borsuk *et al*. 2004). Regarding the spatial model resolution, our presentation was based on a single-compartment model for the sake of simplicity, but it should be acknowledged that the Bayesian framework can be easily employed with the segmentations of existing Great Lakes models, i.e., 5-10 completely-mixed boxes (Lam *et al.* 1987a; DiToro *et al.* 1987; Bierman *et al.* 2005). It is expected though that the use of finer grid resolutions will significantly increase the computation demands along with the simulation time required. To overcome this impediment, on-going research should focus on the use of more flexible schemes, such as nested grid configurations that can reduce the computational time compared to the standard approach (one fixed grid size) and better capture the interplay between pollutant mixing/dispersion and food web dynamics in the nearshore areas, while the offshore water dynamics can be

sufficiently reproduced with coarser spatio-temporal resolution. The patterns of the posterior uncertainty can then be used to further optimize the spatial model segmentation (e.g., splitting-up segments with flat posteriors or lumping segments with similar, narrow-shaped predictions) and avoid overly cumbersome modeling constructs that profoundly violate the parsimony principle.

Bearing in mind the pending reevaluation of the Great Lakes Water Quality Agreement, the Great Lakes community -as it did in the 1970s- has the opportunity to set the standard for the innovative use of mathematical models in support of decision-making. Despite the unresolved technical issues, we believe that the benefits from the Bayesian calibration scheme proposed, such as the assessment of uncertainty in model predictions and expression of model outputs as probability distributions, the alignment with the policy practice of adaptive management, and the optimization of the sampling design of monitoring programs can be particularly useful for stakeholders and policy makers when making decisions for sustainable environmental management in the Laurentian Great Lakes region.

Tables

Table 2.1 Prior and posterior parameter distributions in three trophic states: Λ– lognormal distribution, $\theta \sim \Lambda(\mu^*, \sigma^*)$ is a mathematical expression meaning that θ is lognormally distributed, μ^* and σ^* correspond to the median and multiplicative standard deviation.

Parameters	*Prior*	*Oligotrophic*	*Mesotrophic*	*Eutrophic*
$bm_{ref(clad)}$	Λ(0.0495, 1.161)	Λ(0.0491, 1.236)	Λ(0.0490, 1.239)	Λ(0.0491, 1.241)
$bm_{ref(cop)}$	Λ(0.0442, 1.181)	Λ(0.0441, 1.271)	Λ(0.0438, 1.271)	Λ(0.0444, 1.265)
$bm_{ref(cyan)}$	Λ(0.0775, 1.116)	Λ(0.0774, 1.168)	Λ(0.0789, 1.163)	Λ(0.0808, 1.162)
$bm_{ref(diat)}$	Λ(0.0980, 1.091)	Λ(0.0978, 1.144)	Λ(0.0951, 1.125)	Λ(0.0946, 1.120)
$bm_{ref(green)}$	Λ(0.0775, 1.116)	Λ(0.0760, 1.170)	Λ(0.0753, 1.164)	Λ(0.0753, 1.163)
$ef_{2(clad)}$	Λ(18.3, 1.123)	Λ(18.3, 1.183)	Λ(18.3, 1.181)	Λ(18.1, 1.183)
$ef_{2(cop)}$	Λ(19.4, 1.116)	Λ(19.3, 1.174)	Λ(19.3, 1.172)	Λ(19.4, 1.166)
$growth_{max(cyan)}$	Λ(1.26, 1.106)	Λ(1.29, 1.155)	Λ(1.28, 1.158)	Λ(1.22, 1.145)
$growth_{max(diat)}$	Λ(2.19, 1.040)	Λ(2.23, 1.050)	Λ(2.24, 1.049)	Λ(2.22, 1.055)
$growth_{max(greens)}$	Λ(1.79, 1.049)	Λ(1.80, 1.070)	Λ(1.80, 1.073)	Λ(1.81, 1.070)
$grazing_{max(clad)}$	Λ(0.837, 1.080)	Λ(0.837, 1.118)	Λ(0.839, 1.115)	Λ(0.844, 1.121)
$grazing_{max(cop)}$	Λ(0.490, 1.091)	Λ(0.489, 1.134)	Λ(0.477, 1.125)	Λ(0.490, 1.139)
$KC_{refdisslution}$	Λ(0.00200, 2.691)	Λ(0.00194, 2.573)	Λ(0.00198, 2.588)	Λ(0.00206, 2.643)
$K_{eddyref}$	Λ(0.0316, 1.218)	Λ(0.0351, 1.277)	Λ(0.0325, 1.340)	Λ(0.0322, 1.277)
$K_{EXTback}$	Λ(0.265, 1.084)	Λ(0.256, 1.106)	Λ(0.244, 1.075)	Λ(0.252, 1.097)
$K_{EXTchla}$	Λ(0.0200, 1.347)	Λ(0.0187, 1.489)	Λ(0.0169, 1.424)	Λ(0.0173, 1.452)
$KN_{(cyan)}$	Λ(22.9, 1.200)	Λ(22.8, 1.308)	Λ(22.9, 1.298)	Λ(23.0, 1.306)
$KN_{(diat)}$	Λ(64.2, 1.069)	Λ(64.1, 1.101)	Λ(64.1, 1.101)	Λ(64.2, 1.101)
$KN_{(greens)}$	Λ(43.9, 1.102)	Λ(43.9, 1.151)	Λ(43.9, 1.150)	Λ(43.7, 1.149)
$KN_{refdisslution}$	Λ(0.00200, 2.691)	Λ(0.00201, 2.663)	Λ(0.00199, 2.613)	Λ(0.00195, 2.594)
$KN_{refmineral}$	Λ(0.00775, 1.503)	Λ(0.00884, 1.622)	Λ(0.00594, 1.559)	Λ(0.00691, 1.716)
$KP_{(cyan)}$	Λ(19.4, 1.116)	Λ(19.2, 1.174)	Λ(19.7, 1.168)	Λ(19.5, 1.174)
$KP_{(diat)}$	Λ(5.66, 1.161)	Λ(5.28, 1.216)	Λ(5.36, 1.226)	Λ(5.46, 1.235)
$KP_{(greens)}$	Λ(10.6, 1.128)	Λ(10.4, 1.187)	Λ(10.3, 1.187)	Λ(10.4, 1.188)
$KP_{refdisslution}$	Λ(0.00200, 2.691)	Λ(0.00202, 2.604)	Λ(0.00198, 2.603)	Λ(0.00202, 2.668)
$KP_{refmineral}$	Λ(0.0245, 1.470)	Λ(0.0220, 1.644)	Λ(0.0235, 1.691)	Λ(0.0235, 1.716)
$KSi_{(diat)}$	Λ(40.0, 1.347)	Λ(39.7, 1.542)	Λ(39.8, 1.536)	Λ(39.8, 1.527)
$KSi_{refdisslution}$	Λ(0.00200, 2.691)	Λ(0.00198, 2.631)	Λ(0.00197, 2.613)	Λ(0.00194, 2.533)
$KZ_{(clad)}$	Λ(114, 1.058)	Λ(114, 1.087)	Λ(114, 1.087)	Λ(113, 1.085)
$KZ_{(cop)}$	Λ(93.8, 1.071)	Λ(93.6, 1.104)	Λ(94.5, 1.104)	Λ(93.3, 1.100)
$pred_1$	Λ(0.141, 1.161)	Λ(0.139, 1.238)	Λ(0.138, 1.233)	Λ(0.136, 1.224)
$pred_2$	Λ(34.6, 1.266)	Λ(36.1, 1.400)	Λ(35.5, 1.412)	Λ(39.4, 1.330)
$V_{settling(cyan)}$	Λ(0.0224, 1.413)	Λ(0.0205, 1.590)	Λ(0.0224, 1.605)	Λ(0.0232, 1.610)
$V_{settling(diat)}$	Λ(0.316, 1.106)	Λ(0.289, 1.112)	Λ(0.275, 1.072)	Λ(0.293, 1.118)
$V_{settling(greens)}$	Λ(0.245, 1.091)	Λ(0.237, 1.128)	Λ(0.231, 1.108)	Λ(0.235, 1.120)

Table 2.2 Goodness-of-fit statistics for the model state variables in three trophic states*.

State Variables	*Oligotrophic*			*Mesotrophic*			*Eutrophic*		
	RMSE	*RE*	*AE*	*RMSE*	*RE*	*AE*	*RMSE*	*RE*	*AE*
Green Algae Biomass (μg Chl a/L)	0.118	7.03%	-0.050	0.223	8.49%	-0.092	0.251	7.63%	-0.117
Diatom Biomass (μg Chl a/L)	0.307	10.4%	-0.139	0.467	13.6%	-0.215	0.275	7.17%	-0.139
Cyanobacteria Biomass (μg Chl a/L)	0.059	8.26%	-0.028	0.235	10.7%	-0.082	0.552	12.8%	-0.188
Copepod Biomass (μg C/L)	5.19	10.6%	-2.00	13.2	12.6%	-4.74	48.3	21.2%	-15.6
Cladoceran Biomass (μg C/L)	3.41	7.04%	-1.62	4.40	5.92%	-2.20	8.42	6.03%	-4.23
Total Silica (mg Si/L)	0.097	7.50%	0.019	0.136	8.25%	-0.0085	0.222	8.61%	-0.0030
Total Nitrogen (μg N/L)	4.06	1.19%	-2.77	14.4	3.37%	-9.48	45.4	7.64%	-12.5
Total Phosphorus (μg P/L)	0.627	4.16%	-0.350	1.17	4.62%	-0.648	4.74	9.81%	-1.16
Dissolved Oxygen (mg DO/L)	0.655	4.92%	0.482	0.629	5.04%	0.356	0.763	6.37%	0.628

* RMSE – Root Mean Square Error

RE – Relative Error

AE – Average Error

Table 2.3 Markov Chain Monte Carlo posterior estimates of the mean values and standard deviations of the model discrepancies in three trophic states.

Discrepancy terms	*Oligotrophic*		*Mesotrophic*		*Eutrophic*	
	Mean	*Std. Dev.*	*Mean*	*Std. Dev.*	*Mean*	*Std. Dev.*
$\sigma_{green\ algae}$	25.8	7.32	33.9	10.3	46.0	14.9
$\sigma_{diatoms}$	38.4	15.8	35.6	21.4	58.4	19.3
$\sigma_{cyanobacteria}$	10.5	2.93	23.3	7.62	39.2	17.6
$\sigma_{N(greens)}$	0.0494	0.0111	0.0496	0.0113	0.0495	0.0114
$\sigma_{P(greens)}$	0.0434	0.0098	0.0435	0.0098	0.0436	0.0098
$\sigma_{N(diatoms)}$	0.0492	0.0113	0.0496	0.0117	0.0493	0.0116
$\sigma_{P(diatoms)}$	0.0436	0.0099	0.0438	0.0102	0.0438	0.0097
$\sigma_{Si(diatoms)}$	0.0618	0.0163	0.0612	0.0159	0.0608	0.0156
$\sigma_{N(cyanobacteria)}$	0.0498	0.0117	0.0497	0.0117	0.0496	0.0116
$\sigma_{P(cyanobacteria)}$	0.0436	0.0099	0.0436	0.0098	0.0438	0.0098
$\sigma_{copepods}$	19.3	5.25	29.7	9.53	33.2	17.0
$\sigma_{cladocerans}$	20.5	5.43	34.8	8.84	73.8	17.9
σ_{NO3}	53.4	15.9	92.7	23.5	157	35.7
σ_{NH4}	1.77	0.784	7.76	2.09	18.6	4.71
σ_{DON}	1.56	1.93	2.32	3.23	3.56	5.24
σ_{PON}	10.8	2.55	16.6	3.89	19.0	4.62
σ_{PO4}	3.00	0.726	5.09	1.25	10.2	2.58
σ_{DOP}	0.608	0.219	1.09	0.401	1.30	0.925
σ_{POP}	0.820	0.192	1.54	0.374	1.90	0.462
σ_{DOC}	10.3	19.0	26.4	44.5	48.2	112
σ_{POC}	54.3	13.1	90.7	20.8	109	25.8
σ_{DSi}	12.3	23.5	18.1	33.0	29.7	54.7
σ_{PSi}	119	30.1	232	56.4	461	116
σ_{DO}	67.0	158	87.4	177	93.8	190

Figures

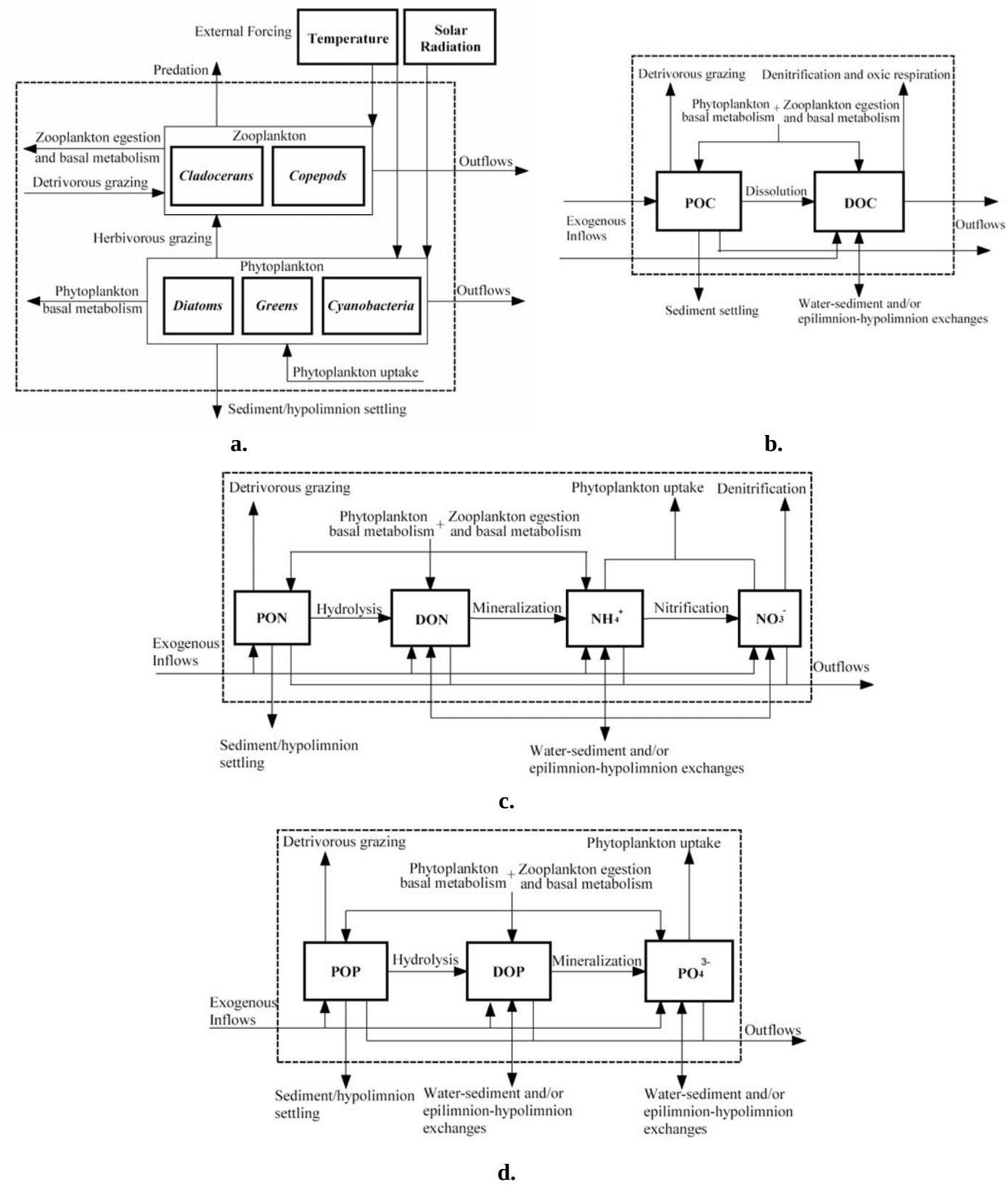

Figure 2.1 The structure of the complex aquatic biogeochemical model. Arrows indicate flows of matter through the system: **a.** plankton submodel; **b.** carbon cycle; **c.** nitrogen cycle; **d.** phosphorus cycle.

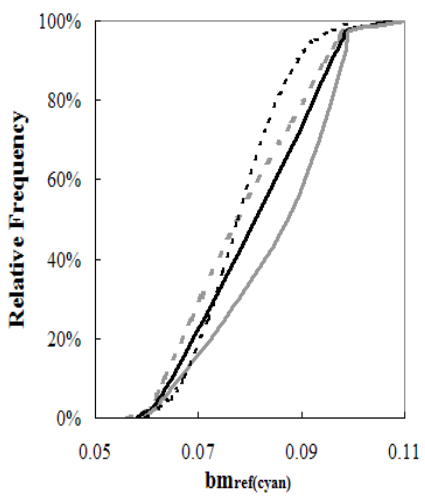
Relative Frequency
100%
80%
60%
40%
20%
0%
0.05
0.07
0.09
0.11
bmref(cyan)

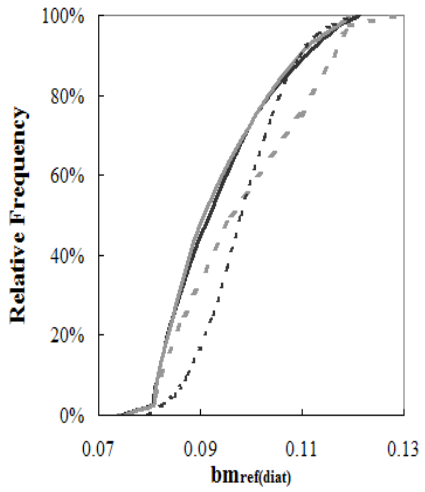
Relative Frequency
100%
80%
60%
40%
20%
0%
0.07
0.09
0.11
0.13
bmref(diat)

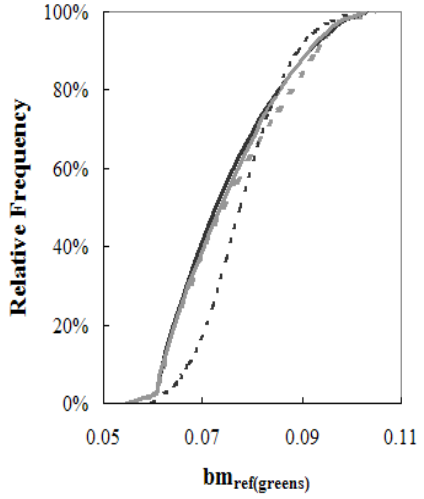
Relative Frequency
100%
80%
60%
40%
20%
0%
0.05
0.07
0.09
0.11
bmref(greens)

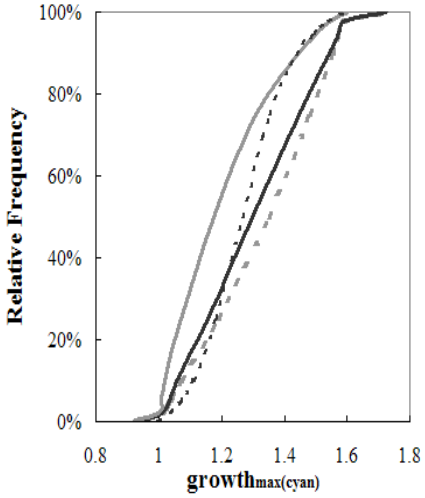
Relative Frequency
100%
80%
60%
40%
20%
0%
0.8
1
1.2
1.4
1.6
1.8
growthmax(cyan)

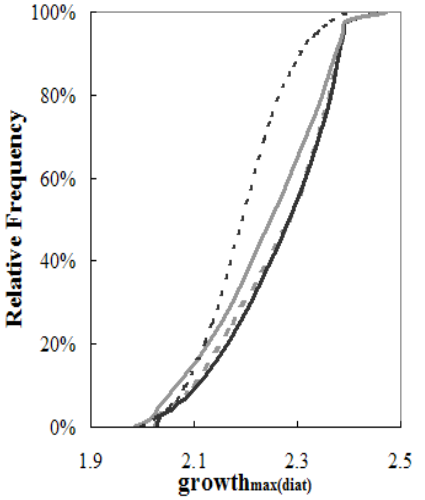
Relative Frequency
100%
80%
60%
40%
20%
0%
1.9
2.1
2.3
2.5
growthmax(diat)

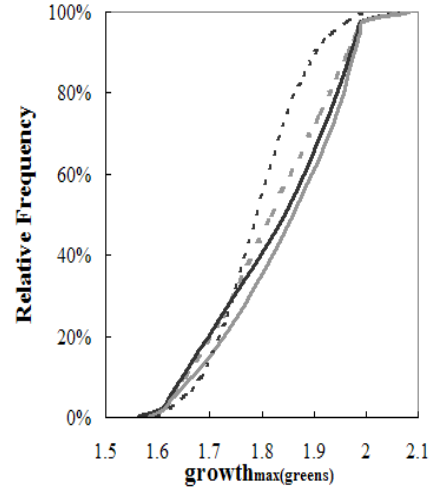
Relative Frequency
100%
80%
60%
40%
20%
0%
1.5
1.6
1.7
1.8
1.9
2
2.1
growthmax(greens)

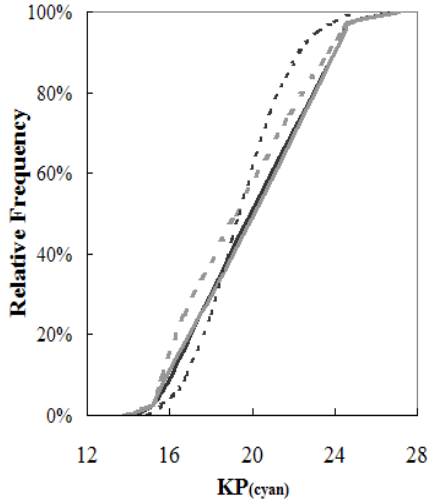
Relative Frequency
100%
80%
60%
40%
20%
0%
12
16
20
24
28
KP(cyan)

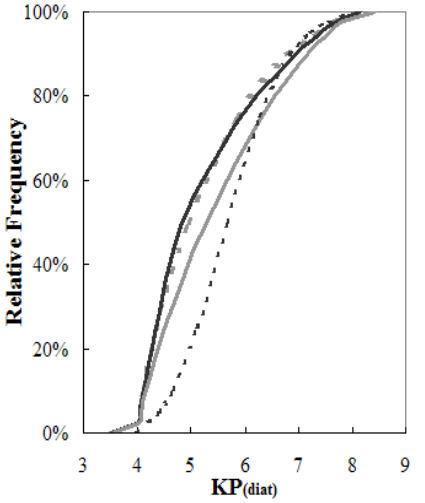
Relative Frequency
100%
80%
60%
40%
20%
0%
3
4
5
6
7
8
9
KP(diat)

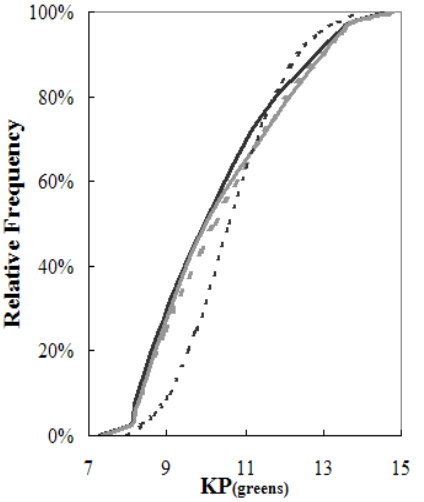
Relative Frequency
100%
80%
60%
40%
20%
0%
7
9
11
13
15
KP(greens)

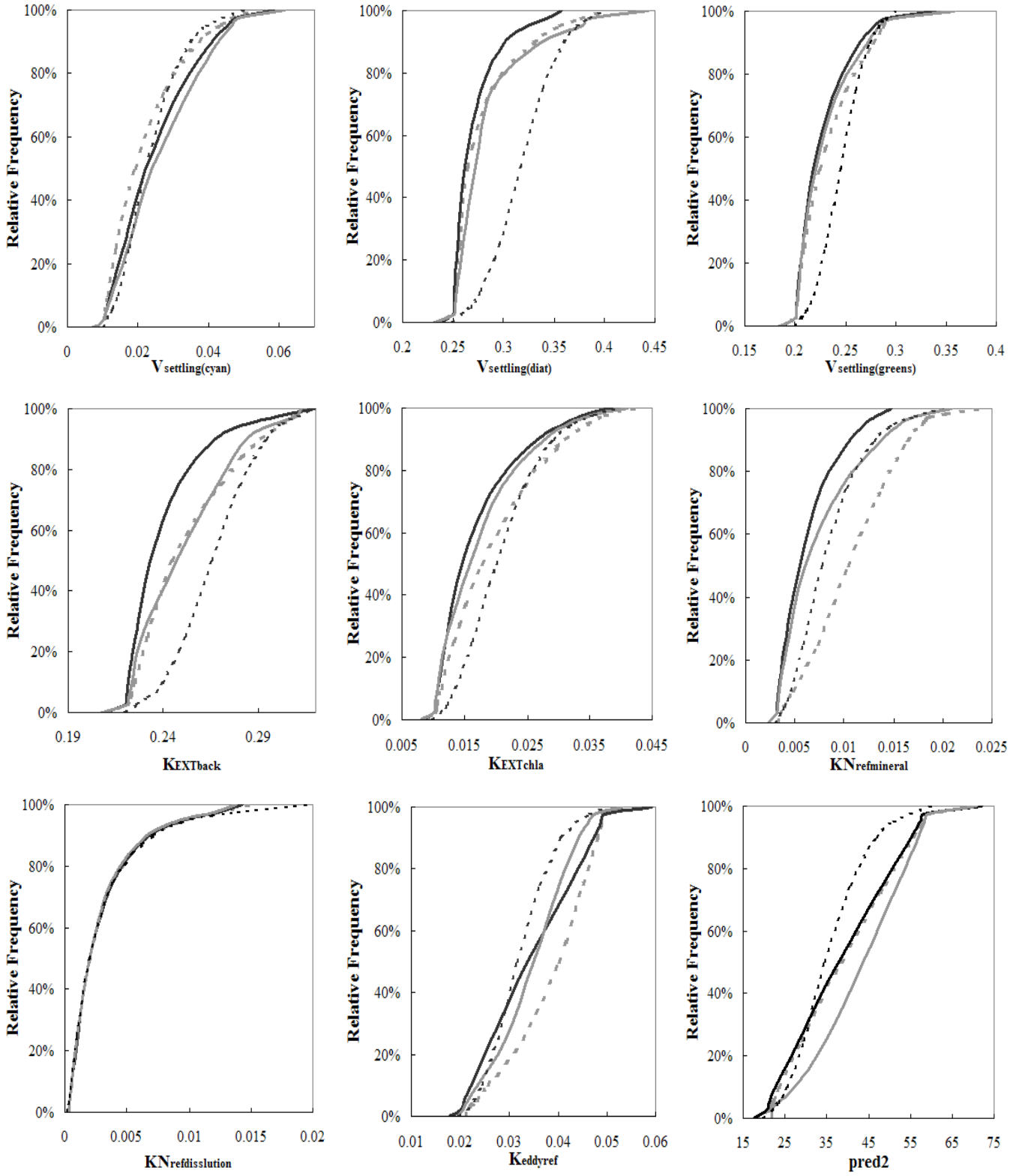

Figure 2.2 Prior (thin black dashed lines) and posterior (eutrophic environment: thick grey lines, mesotrophic environment: thick black lines, and oligotrophic environment: thick grey dashed lines,) cumulative distributions of the aquatic biogeochemical model.

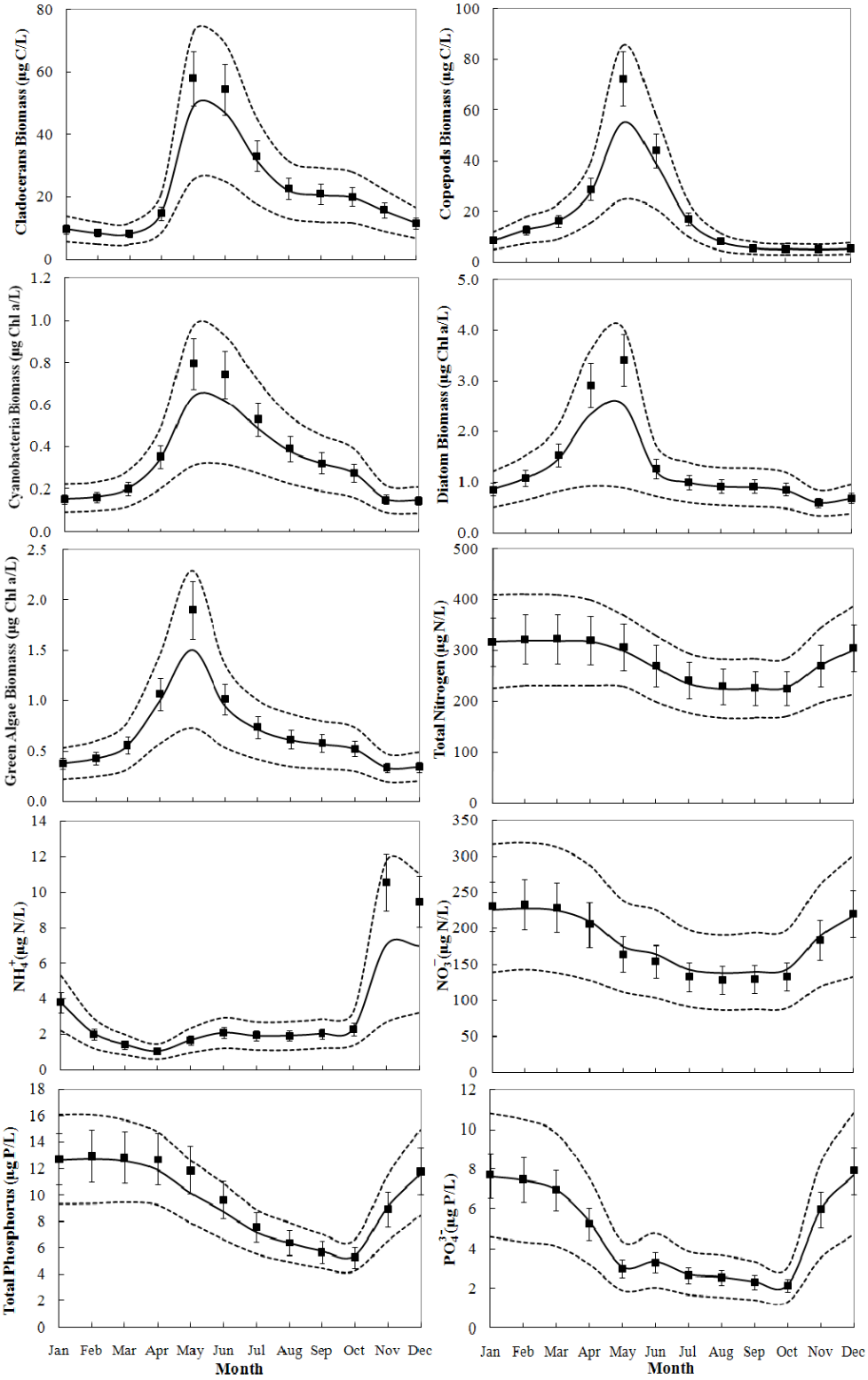

Figure 2.3 Comparison between the observed and posterior predictive monthly distributions for 10 water quality variables based on Markov chain Monte Carlo posterior samples from the model application in the oligotrophic environment. Solid line corresponds to the median value of model prediction and dashed lines correspond to the 2.5 and 97.5% credible intervals. The square dots represent the observed data, while the error bars correspond to the measurement error.

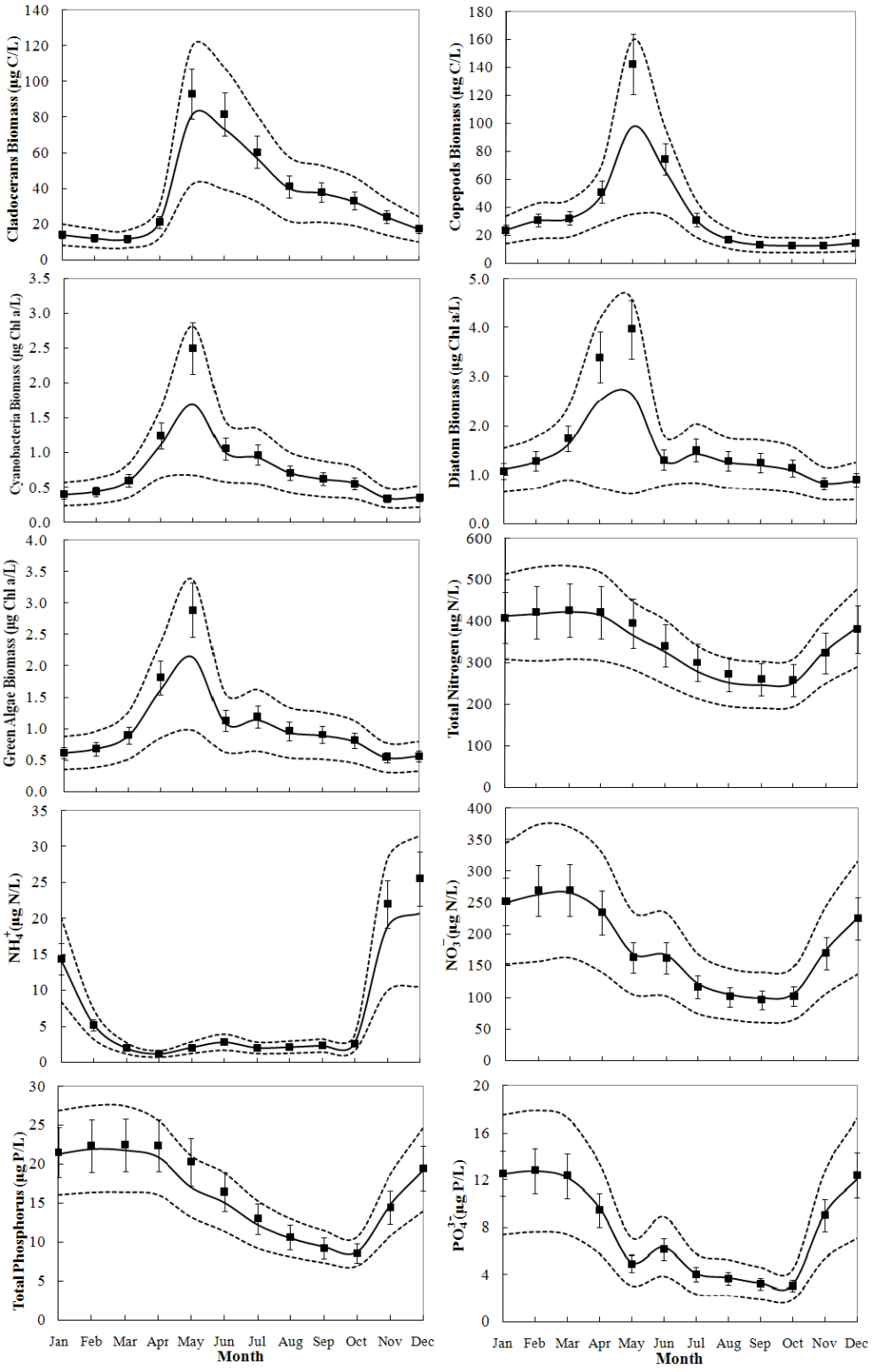

Figure 2.4 Comparison between the observed and posterior predictive monthly distributions for 10 water quality variables based on Markov chain Monte Carlo posterior samples from the model application in the mesotrophic environment. Solid line corresponds to the median value of model prediction and dashed lines correspond to the 2.5 and 97.5% uncertainty bounds. The square dots represent the observed data, while the error bars correspond to the measurement error.

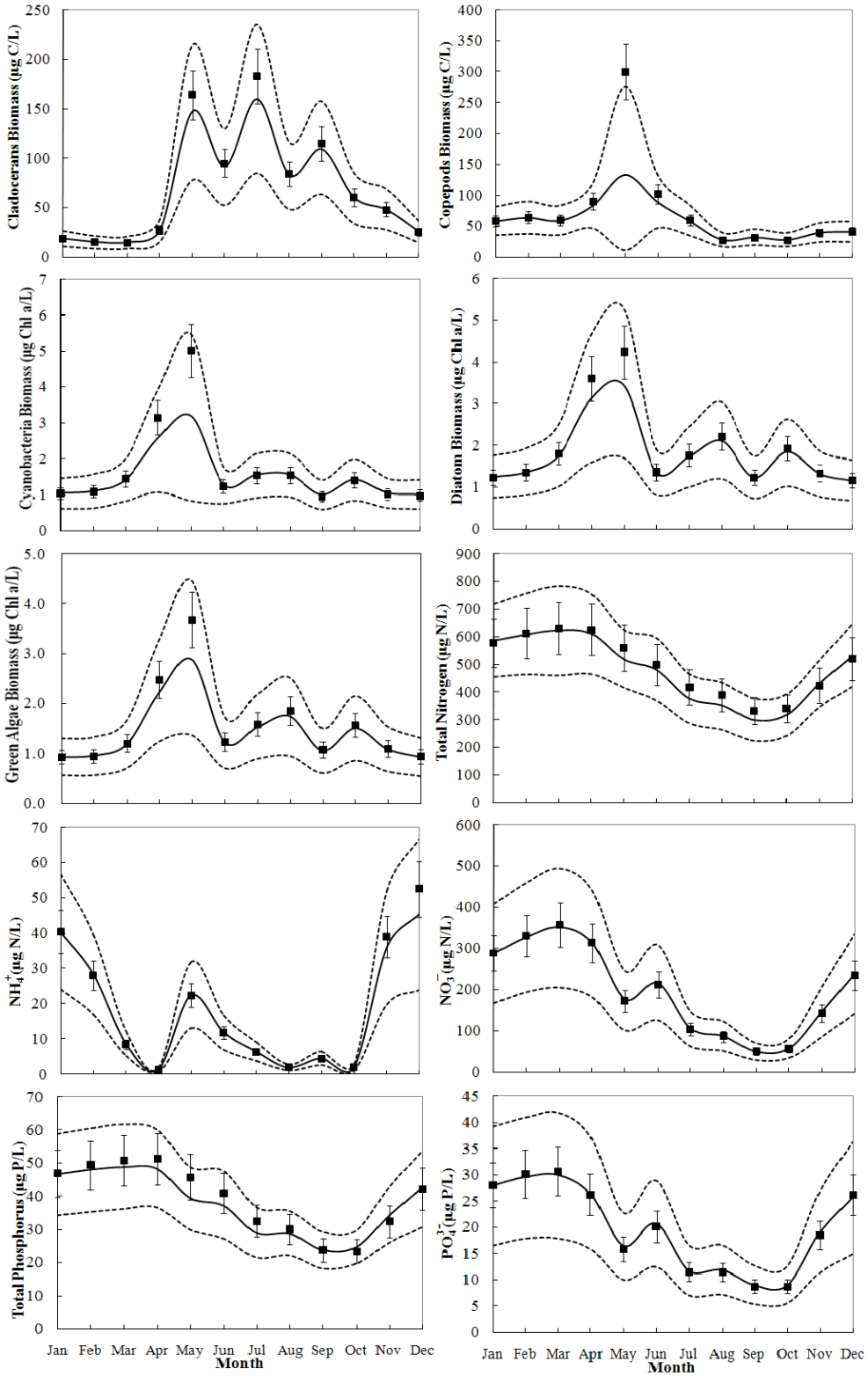

Figure 2.5 Comparison between the observed and posterior predictive monthly distributions for 10 water quality variables based on Markov chain Monte Carlo posterior samples from the model application in the eutrophic environment. Solid line corresponds to the median value of model prediction and dashed lines correspond to the 2.5 and 97.5% uncertainty bounds. The square dots represent the observed data, while the error bars correspond to the measurement errors.

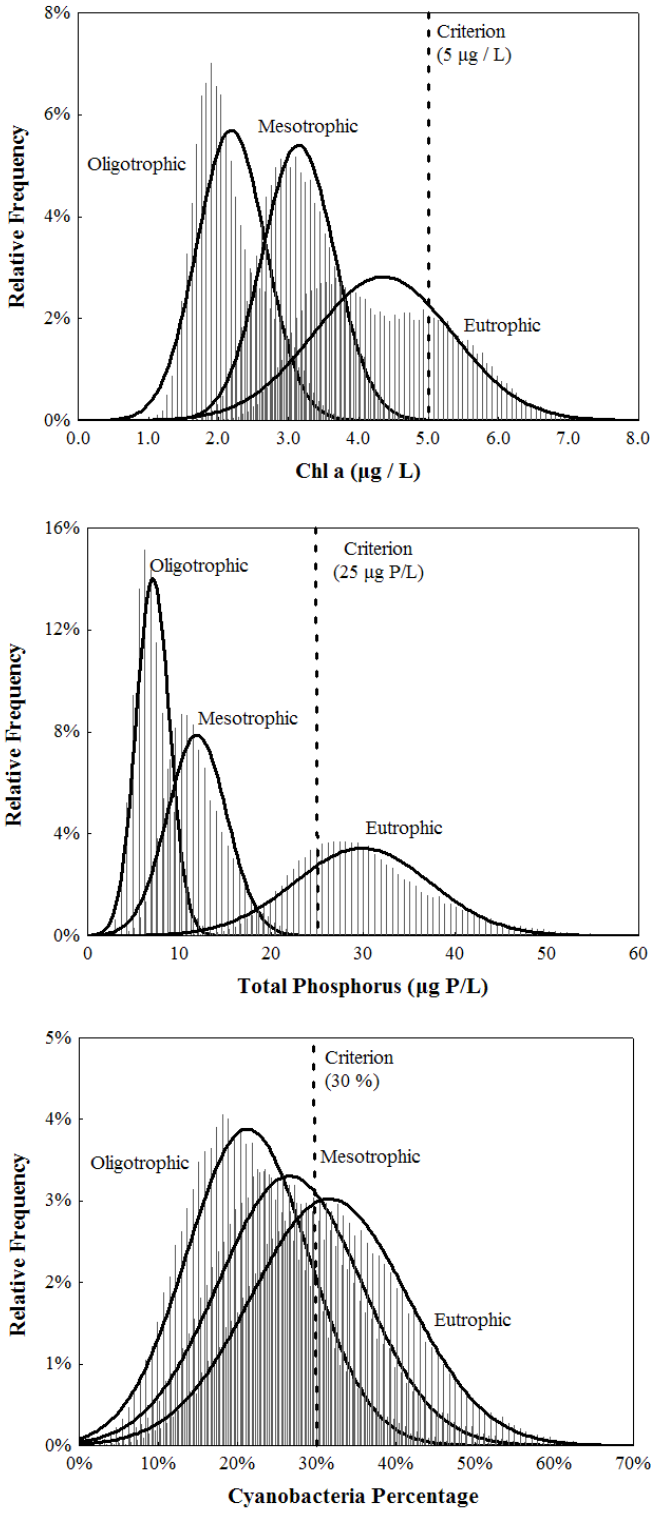

Figure 2.6 Predictive distributions for water quality variables of management interest (chlorophyll a, total phosphorus, and cyanobacteria percentage) during the summer stratified period (June to September). The dashed lines correspond to the numerical criteria used to determine the frequency of violations under different trophic conditions.

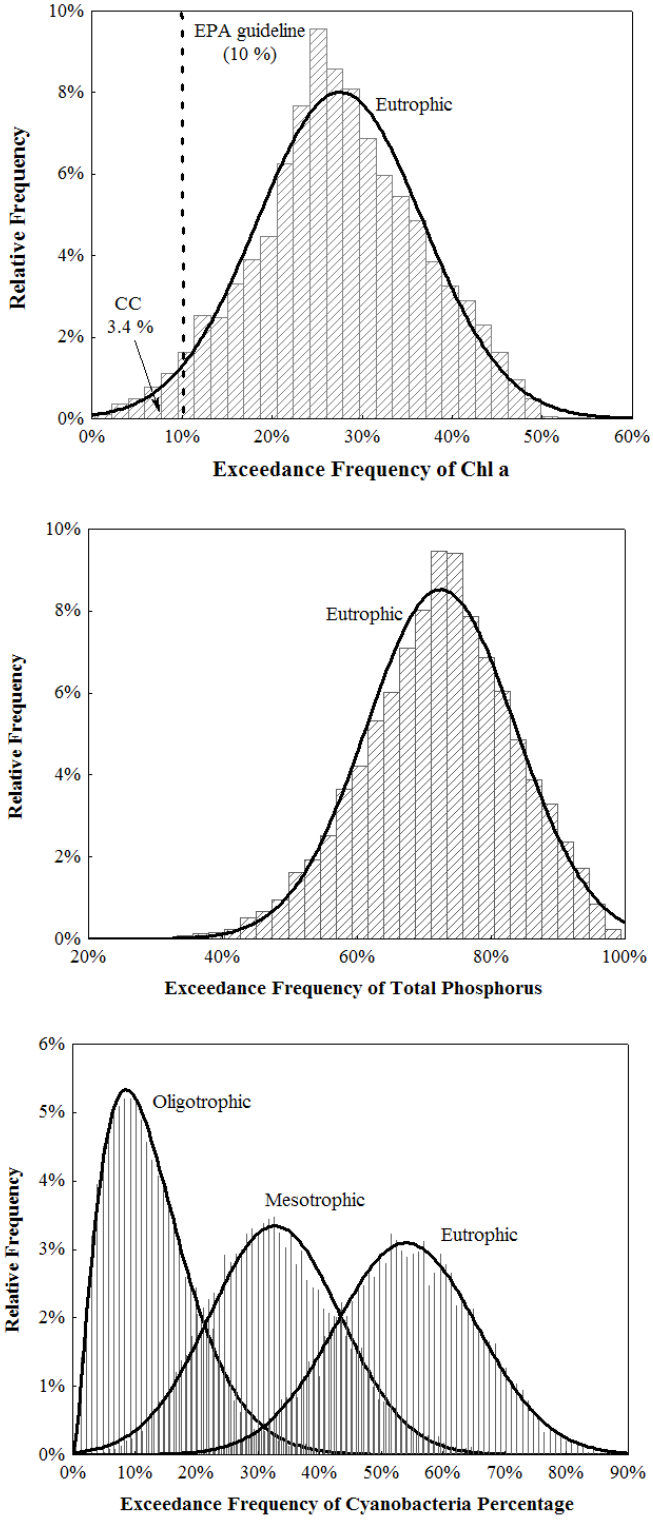

Figure 2.7 The exceedance frequency of the different water quality standards (chlorophyll a: 5 µg/L, total phosphorus: 25 µg/L, and cyanobacteria percentage: 30%) during the summer stratified period (June to September) under the different trophic conditions. In these distributions, the area below the 10% cutoff point is termed the confidence of compliance (CC), and represents the probability that the true exceedance frequency is below the 10% EPA guideline.

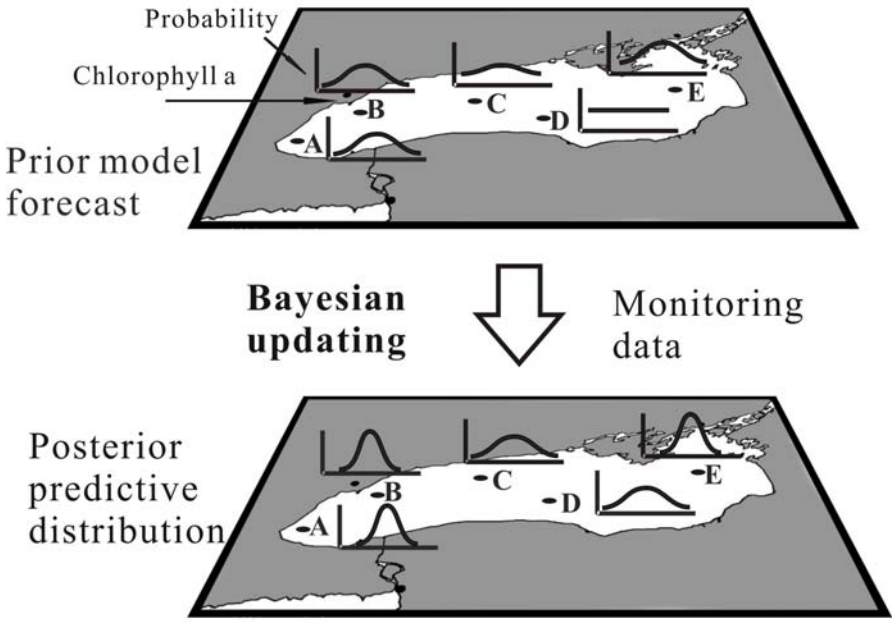

Figure 2.8 Bayesian parameter estimation and optimization of the water quality monitoring using value of information concepts from decision theory.

Chapter 3: A Bayesian Hierarchical Framework for Calibrating Aquatic Biogeochemical Models

3.1 Introduction

Many freshwater ecosystems are currently jeopardized by human intrusion, without proper documentation of their baseline state and how humans have altered their biotic communities and biogeochemical cycles. The invasion of biotic communities by non-native species is perhaps the greatest threat to the integrity of lakes and rivers (Schindler, 2001). Climate-induced chemical and biological responses in lakes are another important issue, and several ecological and biogeochemical studies have shown a coupling among lake temperatures and water chemistry, individual organism physiology, population abundance, and community structure (Schindler, 1997; Straile, 2002; Weyhenmeyer, 2004). Climate forcing can have different effects on various taxonomic groups/trophic levels, and decouple species from favorable food conditions with dire consequences on ecosystem functioning (Thomas et al., 2001, Hampton, 2005). Therefore, the development of holistic understanding of the climate-driven aquatic ecosystem responses requires consideration of the complex interplay between physical, chemical factors and multiple trophic levels at a variety of spatial and temporal scales. Given the increasingly ominous context, the demand for reliable modeling tools that can offer insights into the ecosystem dynamics and effectively support environmental management is more pressing than ever before (Arhonditsis and Brett, 2004, Arhonditsis et al., 2006). However, the general lack of uncertainty estimates for most environmental

models, the arbitrary selection of higher, more costly, and often unattainable threshold values for environmental variables as a hedge against unknown prediction errors, risky model-based management decisions and unanticipated system responses are often experienced in the current management practice.

Uncertainty analysis of mathematical models has been a central topic in aquatic ecosystem research, and there have been several attempts to rigorously assess model error associated with model structure and parameter uncertainty (Omlin and Reichert, 1999; Brun et al., 2001; Reichert et al., 2002; Chen et al., 2007). Model uncertainty analysis essentially aims to make inference about the joint probability distribution of model inputs, reflecting the amount of knowledge available for model parameters, initial conditions, forcing functions, and model structure. In this regard, Bayes' Theorem provides a convenient means to combine existing information (prior) with current observations (likelihood) for projecting future ecosystem response (posterior). Hence, the Bayesian techniques are more informative than the conventional model calibration practices (i.e., mere adjustment of model parameters until the discrepancy between model outputs and observed data is minimized), and can be used to refine our knowledge of model input parameters, and obtain predictions along with uncertainty bounds for output variables (Arhonditsis et al., 2007). Despite the compelling arguments for considering Bayesian inference techniques as an integral part of the model development process, their high computational demands along with the lack of analytical expressions for the posterior distributions was until recently a major impediment for their broader application (Reichert and Omlin, 1997).

Elucidation of the uncertainty patterns in the multidimensional parameter spaces of mathematical models involves two critical steps: i) selection of the likelihood function

to quantify model misfit, and ii) selection of the sampling scheme for generating input vectors which then are evaluated with regards to the model performance. The latter decision addresses the sampling efficiency of the approach, e.g., Random sampling, Latin hypercube, Markov chain Monte Carlo (MCMC). Many Bayesian or non-Bayesian uncertainty analysis applications (e.g., Generalized Likelihood Uncertainty Estimation, Bayesian Monte Carlo) have been combined with sampling algorithms which draw samples uniformly and independently from the prior parameter space. These strategies often result in Monte Carlo samples that misrepresent (or insufficiently cover) regions of high model likelihood; especially, when the joint prior parameter distribution is very wide or the parameters are highly correlated (Qian et al., 2003). To address this problem, several recent studies advocate the use of MCMC sampling schemes that are specifically designed to sample directly from the posterior distribution and to converge to the higher model likelihood regions (Gelman et al., 1995; Arhonditsis et al., 2007; Stow et al., 2007). On the other hand, the selection of the model likelihood function entails conceptual dilemmas involving the selection of generalized (e.g., Root Mean Square Error, Reliability Index, U-uncertainty) or purely probabilistic (e.g., Normal, Lognormal or Poisson error) likelihood functions that can significantly alter the results (Beven, 2001). In typical uncertainty analysis applications, the likelihood function is broadly specified as any measure of goodness of-fit that can be used to compare observed data with model predictions, e.g., sum of squared errors, fuzzy measures or even qualitative measures for model evaluation (Franks et al., 1998; Beven, 2001; Page et al., 2004). However, it has been argued that unless the likelihood function corresponds to a formal probability distribution that directly connects the data with model input parameters and output state variables, the uncertainty analysis results do not have a clear Bayesian interpretation (Engeland and Gottschalk, 2002; Hong et al., 2005).

In the context of water quality modeling, there are several recent studies illustrating how the Bayesian inference techniques combined with MCMC sampling schemes can improve model forecasts and management actions over space and time. For example, Malve et al. (2005) showed how the Bayesian parameter estimation of a dynamic non-linear model can be used for quantifying the winter respiration rates (oxygen depletion per unit area of hypolimnetic surface) in a hyper-eutrophic shallow Finnish lake. A conceptually similar modeling approach was also used to elucidate the confounded bottom-up and top-down effects on the phytoplankton community structure of the shallow, mesotrophic Lake Pyhäjärvi (Malve et al., 2007). Arhonditsis et al. (2007; 2008a) introduced a Bayesian calibration scheme using intermediate complexity mathematical models (4-8 state variables) and statistical formulations that explicitly accommodate measurement error, parameter uncertainty, and model structure imperfection; this framework was then used to quantify the information the data contain about model inputs, to offer insights into the covariance structure among parameter estimates, and to obtain predictions along with credible intervals for model outputs. A follow-up study examined the efficiency of two uncertainty analysis strategies, a typical Generalized Likelihood Uncertainty Estimation (GLUE) approach combined with random sampling scheme vis-á-vis a formal probabilistic model configuration updated with MCMC simulations, to elucidate the propagation of uncertainty in the input spaces of intermediate complexity numerical aquatic biogeochemical models (Arhonditsis et al., 2008b). Finally, a recent study integrated the Bayesian calibration framework with a complex aquatic biogeochemical model simulating multiple elemental cycles and functional plankton groups to illustrate how the Bayesian parameter estimation can be used for assessing the exceedance frequency and confidence of compliance of different water quality criteria (Zhang and Arhonditsis, 2008).

In this paper, we present another prospect of the Bayesian inference techniques by introducing a hierarchical formulation for calibrating aquatic biogeochemical models at multiple sites. This illustration is based on several synthetic datasets representing oligo-, meso- and eutrophic lake conditions. Our objective is to examine if the incorporation of mathematical models into Bayesian hierarchical frameworks can assist the effective modeling of systems with limited information by enabling the transfer of information across systems. With the hierarchical model configuration, we can potentially overcome problems of insufficient local data by "borrowing strength" from well-studied sites on the basis of distributions that connect systems in space. This outcome is highly relevant to conservation practices of regions with a high number of freshwater resources for which complete data could never be practically gathered. Finally, we discuss the prospect of extending this framework to coupled physical-biogeochemical models along with its benefits to environmental management, such as the optimization of the sampling design of monitoring programs and the alignment with the policy practice of adaptive management.

3.2 Methods

Hierarchical Bayes allows decomposing the environmental problems into intuitively manageable levels, thereby offering a conceptually plausible means for addressing the complexity pervading the natural systems (Clark, 2005). As such, the Bayesian hierarchical modeling can be an indispensable methodological framework to disentangle complex ecological patterns, to exploit disparate sources of ecological information, to accommodate tightly intertwined environmental processes operating at

different spatiotemporal scales, and to explicitly consider the variability pertaining to latent variables or other inherently "unmeasurable" quantities (Wikle, 2003a; Clark, 2005). Furthermore, Wikle (2003a) argued that rather than specifying the ecological dynamics as joint multivariate spatiotemporal covariance structures, it would also be statistically easier to factor such joint distributions into a series of conditional models, i.e., dissect the total process into a number of connected subprocesses. The essence of the Bayesian hierarchical thinking is that the environmental complexity can be decomposed into the following series of models coherently linked together via Bayes' rule (Berliner, 1996):

$$\underbrace{[process, parameters \mid data]}_{\text{Posterior Distribution}} \propto \underbrace{[data \mid process, parameters]}_{\text{Data Model}} \times \underbrace{[process \mid parameters]}_{\text{Process Model}} \times \underbrace{[parameters]}_{\text{Parameter Model}} \quad \textbf{(3-1)}$$

where the posterior distribution reflects our beliefs on the levels of the process and parameters after the data updating, which can be thought of as the product of the data model, specifying the dependence of the observed data on the process of interest and parameters, with the process model, describing the process conditional on other parameters, and the parameter model, quantifying the uncertainty in parameter values. Each of these models may then consist of multiple substages to account for the role of an inconceivably complex array of environmental functions that comes into play in real world applications (Wikle, 2003a). In environmental science, the general formula (1) has been used to predict demographic processes and spatiotemporal population spread (Wikle, 2003b; Clark, 2005), to incorporate physically based prior information on simulated geophysical processes (Royle et al., 1999; Wikle et al., 2001), to stochastically

treat boundary conditions in coupled atmospheric-ocean models (Wikle et al., 2003), and more recently to resolve the mechanisms of species coexistence and the biodiversity paradox (Clark et al., 2007).

In the context of aquatic ecosystem management, Borsuk et al. (2001) introduced a Bayesian hierarchical framework to model the relationship between organic matter loading and benthic oxygen demand using data from 34 estuarine and coastal systems. The basic premise of the hierarchical structure was to relax the typical assumption of common parameter values across systems, while overcoming problems of overfitting with models of entirely site-specific parameters. The Borsuk et al. (2001) study showed that the hierarchical model improved the model fit to the observed data and also provided more realistic estimates of the predictive uncertainty. The latter feature has important implications for environmental management and allows establishing water quality criteria that explicitly acknowledge an inevitable risk of non-attainment (Arhonditsis et al., 2007). Likewise, Malve and Qian (2006) developed a Bayesian hierarchical linear model to assess compliance of the chlorophyll *a* concentration standards under different nitrogen and phosphorus loads using data from the national water quality monitoring program of Finnish lakes. The same study also highlighted the ability of hierarchical modeling to transfer information across systems and support predictions in lakes with few observations and limited observational range. Similar findings have also been reported in fisheries ecology underscoring the importance of the methodology to the treatment of aquatic ecological data (Rivot and Prévost, 2002; Wyatt, 2002; Michielsen and McAllister, 2004; Rivot et al., 2008). In this study, we extend the application of Bayesian hierarchical structures with process-based models and our aim is (i) to illustrate how they can assist in sharing information among different systems (or sites), and (ii) to obtain

predictions along with uncertainty bounds that take into account the insufficient amount of information in less studied systems as well as the variability observed across systems.

3.2.1. Bayesian Hierarchical Framework

Our statistical formulation explicitly considers the uncertainty in model inputs (model parameters, initial conditions), the analytical/sampling error associated with the field data, and the discrepancy between model structure and the natural system dynamics (e.g., missing key ecological processes, erroneous formulations, misspecified forcing functions). Earlier applications of this formulation have resulted in an improvement of the model performance, i.e., the median predictions along with the 95% credible intervals delineate zones that accurately describe the observed data (Arhonditsis et al., 2007; 2008a, b). In this study, the Bayesian hierarchical framework builds upon the assumption that the model discrepancy is invariant with the input conditions, and thus the difference between model and system dynamics is constant over the annual cycle for each state variable. The hierarchical structures examined consist of two submodels representing two local aquatic systems (or two sites of the same system) with differences in their trophic conditions, prior precisions of model parameters, available information, measurement error or inter-annual variability (Table 3.1). In particular, the first scenario considers a mesotrophic system combined with an oligotrophic or eutrophic one, aiming to examine the posterior patterns when crossing different trophic states under the hierarchical framework. Two mesotrophic datasets with different inter-annual variability (15 and 30%) were used in scenario *B*, thereby assessing the robustness of the results if, for example, we explicitly consider both dynamic (inshore) and static (offshore) areas of the same system during the model calibration process. The focus of the third scenario was to compare how the two submodels will be calibrated when combining systems (or sites)

with different sampling intensity (C_1 and C_2) or systems with different dynamics, e.g., vertical mixing regimes (C_3). The scenario *D* extends the scheme examined in the scenario *A* by increasing the prior standard deviations of the system specific parameters. This experiment relaxes our confidence in the prior knowledge used to formulate the global priors and broadens the parameter space examined during the calibration of the two submodels. Based on these scenarios, the hierarchical modeling framework can be summarized as follows (Fig. 3.1a):

$$y_{ijk} \sim N(f(\theta_k, x_{ik}, y_{0k}), \sigma_{ijk}^2) \quad \textbf{(3-2)}$$

$$\theta_k \sim N(\theta, \tau_k^2); \; y_{0k} \sim N(y_{1k}, \kappa_k^2) \quad \textbf{(3-3)}$$

$$log(\theta) \sim N(\mu, \tau^2) \quad \textbf{(3-4)}$$

$$\sigma_{ijk}^2 = \delta_{jk}^2 + \varepsilon_{ijk}^2 \quad \textbf{(3-5)}$$

$$\delta_{jk}^2 \sim Inv\text{-}Gamma(0.01, 0.01) \quad \textbf{(3-6)}$$

$$\tau_k^2 = (\alpha_1 \times \theta)^2; \; \kappa_k^2 = (\alpha_2 \times y_{ik})^2; \; \varepsilon_{ijk}^2 = (\alpha_3 \times y_{ijk})^2 \quad \textbf{(3-7)}$$

$$i = 1,....n \qquad j = 1,....,m \qquad k = 1,...,o$$

where y_{ijk} is the *i*th observed value of the *j*th state variable in the system (or site of the same system) *k*; $f(\theta_k, x_{ik}, y_{0k})$ is the numerical solution of the eutrophication model; x_{ik} is a vector of time dependent control variables (e.g., boundary conditions, forcing functions) describing the environmental conditions in the system (or site of the same system) *k*, the vector θ_k is a time independent set of the calibration model parameters (i.e., the 14 parameters in Table 3.2) derived from *k* system-specific normal distributions with means drawn from the global prior θ and standard deviations τ_k equal to α_1 (=15, 35) % of the corresponding mean values; μ, τ^2 represent the first and second order moments of the

hyperparameter distributions; y_{0k} corresponds to the concentrations of the state variables at the initial time point t_0 derived from normal prior distributions with mean values the January monthly averages y_{1k} and standard deviation that was α_2 (=15) % of the mean value for each state variable j; δ_{jk} is a state variable and system-specific error term representing the discrepancy between the model structure and the natural system dynamics; ε_{ijk} is the measurement error associated with each observation y_{ijk} assumed to be α_3 (=15, 25) % of the corresponding values; *m, n,* and *o* correspond to the number of state variables (m= 4), the number of observations in time used to calibrate the model (n = 4, 6, and 12 average monthly values), and the number of systems (or sites of the same system) incorporated into the hierarchical framework (o=2), respectively.

We also examined if a refined parameterization stemming from a well-studied system can improve model performance in less intensively studied systems (scenario *E*). Namely, the system represented from the first submodel underwent a preliminary training (calibration) prior to the configuration of the hierarchical framework. The updated parameter distributions served as the global priors which then were used to delineate the two system-specific parameter spaces (Fig. 3.1b). The first submodel was subject to a second calibration exercise with a qualitatively similar dataset, whereas the second submodel was firstly tested against an eutrophic dataset (E_1) and subsequently against a system for which only four seasonal averages were available (E_2). Under the fifth scenario, the hierarchical framework can be summarized as follows:

$$y_{ijk} \sim N(f(\theta_k, x_{ik}, y_{0k}), \sigma_{ijk}^2) \quad \textbf{(3-8)}$$

$$\theta_k \sim N(\theta, \tau_k^2); \; y_{0k} \sim N(y_{1k}, \kappa_k^2) \quad \textbf{(3-9)}$$

$$log(\theta) \sim N_l(\hat{\theta}, \Sigma) \quad \textbf{(3-10)}$$

$$\sigma_{ijk}^2 = \delta_{jk}^2 + \varepsilon_{ijk}^2 \quad \textbf{(3-11)}$$

$$\delta_{j1}^2 \sim Inv\text{-}Gamma(\alpha, \beta) \quad \textbf{(3-12)}$$

$$\delta_{j2}^2 \sim Inv\text{-}Gamma(0.01, 0.01) \quad \textbf{(3-13)}$$

$$\tau_k^2 = (\alpha_1 \times \theta)^2;\ \kappa_k^2 = (\alpha_2 \times y_{ik})^2;\ \varepsilon_{ijk}^2 = (\alpha_3 \times y_{ijk})^2 \quad \textbf{(3-14)}$$

$$i = 1,....,n \qquad j = 1,....,4 \qquad k = 1,2 \qquad l = 14$$

where θ represents the global prior drawn from a l-dimensional multivariate normal distribution with mean $\hat{\theta}$ and covariance matrix Σ derived from the original model calibration in the well-studied system; and α, β correspond to the shape and scale parameters of the updated j inverse gamma distributions after the first model training.

3.2.2 Mathematical model

We used a zero-dimensional (single compartment) model that considers the flows of mass among four state variables: phosphate (PO_4^{3-}), phytoplankton (*PHYT*), zooplankton (*ZOOP*), and detritus (*DET*). The mathematical description of the eutrophication model and the definition of the model parameters can be found in Arhonditsis et al. (2007; 2008b) (see Appendix A: Figure A1 and Tables A1). The phosphate equation considers the phytoplankton uptake, the proportion of the zooplankton excretion and mortality/predation that is returned back to the system as dissolved phosphorus. Epilimnetic phosphate levels are also fuelled by the bacteria-mediated mineralization of detritus, exogenous loading, and are subject to seasonally varying diffusive mixing with the hypolimnion. The equation for phytoplankton biomass considers phytoplankton production and losses due to basal metabolism, settling and herbivorous zooplankton grazing. The growth of phytoplankton is regulated from the

physical (light and temperature) conditions and the phosphorus availability. Phytoplankton and detritus are two alternative food sources of zooplankton with equal palatability. Both herbivory and detrivory were formulated using the Holling Type III function, and a sigmoid closure term was selected to represent a ‘‘switchable’’ type of predator behaviour controlled by a prey threshold concentration (Edwards and Yool, 2000). The particulate phosphorus (detritus) is fuelled by phytoplankton respiration, a fraction of the zooplankton growth that represents the faecal pellets, and exogenous loading. Detritus is transformed to phosphate by seasonally-forced mineralization processes and sinks out of the epilimnion at a constant rate.

The well-studied system (submodel 1) in the hierarchical model configuration was represented from the average Lake Washington conditions; a mesotrophic system with limnological processes strongly dominated by a recurrent spring diatom bloom with epilimnetic chlorophyll concentration peaks on average at 10 μg/L, which is approximately three times higher than the summer concentrations when the system is phosphorus limited (Arhonditsis et al., 2003). The hypothetical systems in the second submodel represent oligotrophic conditions, mesotrophic conditions in less-studied systems, and eutrophic conditions with monomictic or dimictic mixing patterns, which exchange information via the hierarchical structure with the first submodel. In our analysis, the average input total phosphorus (TP) concentrations for the oligo-, meso-, and eutrophic environments correspond to 50 (32.5 μg TP L^{-1}), 100 (65 μg TP L^{-1}), and 200% (130 μg TP L^{-1}) of the reference conditions in Lake Washington, respectively. Based on these loading scenarios, the model was run using the posterior medians presented in Arhonditsis et al. (2008b). The simulated monthly averages provided the mean values of normal distributions with standard deviations assigned to be 15% of the

monthly values for each state variable along with the hypolimnetic phosphate (Zhang and Arhonditsis, 2008). These distributions were then sampled to generate the oligo-, meso- and eutrophic datasets used for the Bayesian model calibration.

3.2.3 Numerical approximations for posterior distributions

The calibration vector consists of the same 14 parameters used in previous applications of the model (Arhonditsis et al., 2007; 2008b). The prior distributions of the hyperparameters or global priors (Eq. 3-3) were formulated on the basis of existing knowledge (e.g., field observations, laboratory studies, literature information and expert judgment) of the relative plausibility of their values. In this study, we identified the global minimum and maximum values for each parameter, and then we assigned lognormal distributions parameterized such that 95% of the parameter values were lying within the literature ranges (Steinberg et al., 1997). The global prior distributions of the model parameters are presented in Table 3.2. The numerical approximations of the posterior distributions were obtained using the general normal-proposal Metropolis algorithm along with an ordered overrelaxation (Spiegelhalter et al., 2003). This MCMC scheme generates multiple samples per iteration and reduces the within-chain correlations by selecting a value that is negatively correlated with the current one of each stochastic node (Neal, 1998). The posterior simulations were based on one chain with starting point a vector obtained from an earlier optimization of the model with the Fletcher–Reeves conjugate-gradient method (Chapra and Canale, 1998). We used 50,000 iterations and convergence was assessed with the modified Gelman–Rubin convergence statistic (Brooks and Gelman, 1998). Our framework was implemented in the WinBUGS Differential Interface (WBDiff); an interface that allows numerical solution of systems of ordinary differential equations (ODEs) within the WinBUGS software. The ODEs were

solved using the fourth-order Runge-Kutta method with a time resolution of 3.5 days (a sample of WinBUGS code presented in Appendix B).

3.2.4 Model updating

We used the MCMC estimates of the mean and standard deviation parameter values along with the covariance structure to update the model (Legendre and Legendre, 1998). Under the assumption of a multinormal distribution for the log-transformed parameter values, the conditional distributions are given by:

$$\hat{\theta}_{i|j} = \hat{\theta}_i + [\theta_j - \hat{\theta}_j]\Sigma_j^{-1}\Sigma_{i,j} \quad \textbf{(3-15)}$$

$$\Sigma_{i|j} = \Sigma_i - \Sigma_{j,i}\Sigma_j^{-1}\Sigma_{i,j} \qquad j \in \{i+1,...n\} \quad \textbf{(3-16)}$$

where $\hat{\theta}_{i|j}$ and $\Sigma_{i|j}$ correspond to the mean value and the dispersion matrix of the parameter i conditional on the parameter vector j; the values of the elements Σ_i $\Sigma_{i,j}$ and Σ_j correspond to the variance and covariance of the two subset of parameters; and $\hat{\theta}_i, \hat{\theta}_j, \theta_j$ correspond to the posterior mean and random values of the parameters i and j, respectively. The shape and scale parameters of the inverse-gamma distributions used to represent our updated beliefs for the values of the seasonally invariant discrepancy terms (Eq. 3-12) were estimated with the method of moments (Bernardo and Smith, 1994; page 434). We also examined the sensitivity of our results to these informative priors using alternative ones that reflected lower confidence in the estimated discrepancy term values (Qian and Reckhow, 2007).

3.3 Results

The MCMC sequences of the models converged rapidly (≈5000 iterations) and the statistics reported herein were based on the last 45,000 draws by keeping every 4th iteration (thin=4). The evaluation of the degree of updating of model input parameters was based on the shifts of the most possible values and the reduction of the parameter uncertainty. The relative differences between prior and posterior estimates of the mean values and standard deviations of the 14 model parameters are presented in Fig. 3.2. The majority of the parameters were characterized by significant shifts of their posterior means relative to the global priors assigned to the first four scenarios (*A, B, C*, and *D*). Some parameters showed an increase of their central tendency values in all the scenarios examined, e.g., the phytoplankton respiration rate (r) (15-81%), the zooplankton mortality rate (d) (5-165%), and the zooplankton grazing half-saturation constant (μ) (16-182%). There were also parameters with consistently decreased posterior mean values, such as the detritus sinking rate (ψ) (54 to 84%), the detritus mineralization rate (φ) (17-79%), and the zooplankton excretion fraction (β) with 14 to 39% decrease. Notably, the mean values of some parameters significantly varied among the different scenarios, e.g., the phytoplankton sinking loss rate (s) (-68 to 172%), the half-saturation constant for predation (*pred*) (-18 to 149%), and the regeneration of zooplankton predation excretion (γ) with -26% to 15% relative change. The majority of the posterior standard deviations decreased relative to the values assigned to the hyperparameters, such as the maximum phytoplankton growth rate (a) (30-72%), the phytoplankton sinking loss rate (s) (8-78%), and the detritus sinking rate (ψ) (27-93%). However, there were also cases with significantly increased posterior standard deviations and the most characteristic examples were the zooplankton mortality rate (d) (110-620%), the half-saturation constant for predation (*pred*) (1-329%), and the zooplankton grazing half-saturation constant (μ) (20-404%).

We also compare the posterior parameter patterns when the model was calibrated against individual datasets representing oligo-, meso-, and eutrophic conditions and those obtained when crossing sites of different trophic states under the hierarchical framework, i.e., scenarios *A* and *D* (Fig. 3.3). [The MCMC estimates of the mean values and standard deviations of the model stochastic nodes (parameters and error terms) derived from the first and fourth scenarios are provided in the Appendix C.] Generally, the relaxation of the prior precisions of the system specific parameters and the broadening of the sampled parameter space (scenario *D*) resulted in higher posterior standard deviations. Importantly, the previously reported inflation of the standard deviation of parameters associated with the zooplankton feeding kinetics (μ) and mortality (*d, pred*) is only manifested with the hierarchical setting. We also note the significant increase of the posterior means of the same parameters in the mesotrophic and –especially- the eutrophic submodels. The phytoplankton respiration rate (*r*) demonstrated significant increase of the first and second order moments relative to the estimates obtained when the model was calibrated against the eutrophic dataset. The same trend was observed with the half-saturation constant for PO_4^{3-} uptake (*e*) in all the oligotrophic submodels. The latter scenarios were also characterized by a consistent decrease of the central tendency and dispersion values of the cross-thermocline exchange rate (*k*), the phytoplankton respiration (*r*) and sinking loss rates (*s*), the detritus remineralization (φ) and sinking rates (ψ).

The posterior estimates of the mean values and standard deviations of the 14 model parameters with the third scenario are shown in Table 3.3 and Fig. 3.4. The first sub-scenario (C_1) aimed to combine two datasets representing similar dynamics but different sampling intensity, i.e., twelve monthly values versus four seasonal averages for

each state variable, and our results show that the posterior means and standard deviations of the two submodels were very similar. Relatively similar results were also found with the second sub-scenario (C_2), although some variation exists with regards to the posterior moments of the cross-thermocline exchange rate (k), the half-saturation constant for PO_4^{3-} uptake (e), and the phytoplankton respiration rate (r). The same parameters along with the half-saturation constant for predation (*pred*), the zooplankton grazing half-saturation constant (μ), and the phytoplankton sinking velocity (s) were moderately (or significantly) different when examining systems with different trophic states and vertical mixing regimes, i.e., mesotrophic monomictic versus eutrophic dimictic lakes. The temporally invariant error terms ($\sigma_{j,\ j=PO4,\ PHYT,\ ZOOP,\ DET}$) delineate a constant zone around the model predictions that accounts for the discrepancy between model structure and natural system dynamics. The first and second order moments of the posterior distributions of the error terms associated with the model predictions in the "well-studied" system were fairly constant across the three scenarios (C_{11}, C_{21}, and C_{31}). Interestingly, the lower error values were found when the model was calibrated against seasonal data (C_{12}), whereas the use of data collected only from the stratified period increased the model error (scenario C_{22}); especially for the zooplankton biomass (σ_{ZOOP} with mean and standard deviation equal to 33.45 and 23.59 μg C L^{-1}, respectively). The scenario C_{32} of the eutrophic dimictic lake resulted in very high error values and particularly the error terms associated with phytoplankton (σ_{PHYT} with a mean of 246.7 μg C L^{-1} and a standard deviation of 153.3 μg C L^{-1}) and zooplankton biomass (σ_{ZOOP} with mean and standard deviation equal to 68.76 and 63.26 μg C L^{-1}, respectively).

The parameter posterior statistics along with the model error terms with global priors based on the updated conditional distributions of the 14 parameters along with

informative inverse-gamma distributions for the seasonally invariant discrepancy terms are presented in Table 3.4 and Fig. 3.5. The posterior means and standard deviations of the first submodel remained fairly stable under the two sub-scenarios E_1 and E_2 examined. It should also be noted that the shifts of the posterior means were less than 40% relative to the updated global priors, whereas the majority of the standard deviations were significantly reduced (see also Fig. 3.2). On the other hand, the calibration of the second model with an eutrophic dataset (scenario E_{12}) resulted in posteriors alike those obtained for the first submodel. Notable exceptions were the half-saturation constant for PO_4^{3-} uptake (e), the zooplankton grazing half-saturation constant (μ), and the half-saturation constant for predation (*pred*). Furthermore, in a similar manner to the scenario C_1, the use of four seasonal averages provided very similar posterior means and standard deviations between the two submodels. The scenario E_{22} also resulted in fairly low mean values of the model error terms, although the corresponding coefficients of variation (standard deviation/mean) were much higher. The same high coefficients of variation characterized the model error terms (σ_j) under the scenario E_{12}, but the posterior means were also significantly higher than the submodel of the scenario E_{11}.

The comparison between the observed and posterior predictive monthly distributions indicates that the plankton models calibrated under the Bayesian hierarchical structure provided accurate system representations for all the scenarios examined. In particular, the first submodel of the third scenario resulted in median predictions along with 95% credible intervals that closely describe the observed data, despite the slight underestimation of the spring plankton biomass peaks (Fig. 3.6). We also highlight the robustness of the model predictions of the first submodel, regardless of the dataset used to calibrate the second one. On the other hand, the median model predictions for

chlorophyll *a*, zooplankton, phosphate and total phosphorus matched the seasonal data (scenario C_{12}), except from the zooplankton mean spring biomass. In the same scenario, the wider uncertainty bands reflect the higher variability (measurement error) associated with the seasonal average values. The calibration of the second submodel against the dataset from the stratified period resulted in close reproduction of the summer plankton biomass levels as well as the contemporaneous phosphorus variability (scenario C_{22}). Furthermore, the median predictions along with the uncertainty bounds delineated a zone that closely represented the dynamics of the eutrophic dimictic system during the open surface period (scenario C_{32}).

In the fifth scenario, the predictive median values along with the uncertainty bounds of the updated model provided similar results to the submodel 1 of the third scenario and all the observed monthly values were included within the 95% credible intervals (Fig. 3.7). However, the zooplankton median predictions still underestimated the late spring biomass, which was also the case with the second submodel of the scenario E_2, i.e., eutrophic dataset with twelve monthly observations. The latter scenario resulted in a notably accurate reproduction of the chlorophyll *a*, total phosphorus, and phosphate seasonal cycle. Finally, the use of updated global priors did not improve model fit against the dataset that consists of four seasonal averages. The wide prediction bounds included all the observed values, but the median spring zooplankton predictions failed to capture the concurrent observed biomass levels.

3.4 Discussions and Conclusions

The philosophical and pragmatic differences between Bayesian and frequentist methods of inference have been extensively debated in the ecological literature (Dennis, 1996; Ellison, 1996; 2004). The distinctions arise from the different definitions of probability (long-run relative frequencies of events vis-á-vis an individual's degree of belief in the likelihood of an event), the use of prior knowledge along with the sample data, and the treatment of model parameters as random variables or as fixed quantities (Ellison, 2004). Recently, however, Clark (2003, 2005) offered a different perspective arguing that the assumptions of frequentist and simple Bayesian models are more similar than are usually perceived in ecological studies and that only the hierarchical Bayes is a distinctly different framework to accommodate the complexity in environmental systems. Hierarchical Bayes relaxes the fundamental assumption that there is an underlying "true" parameter value that is gradually approximated with increasing sample size. Using simple empirical models with a large number of hierarchies and spatiotemporally variant parameters, the latter feature has been shown to provide an effective means for addressing difficult space-time problems (Borsuk et al., 2001; Wikle, 2003a; Malve and Qian, 2006). Our objective herein was to demonstrate how the hierarchical Bayes can be used to simultaneously calibrate mathematical models in multiple sites with different ecological dynamics or amount of information available.

The degree of updating of the model input parameters from prior to posterior is usually evaluated using three different criteria: (i) shift in the most likely value, (ii) reduction in the parameter uncertainty, and (iii) change in the shape of the distribution (Endres and Schindelin, 2003). In this study, although we have not quantified the change in the shape from prior to posterior parameter distributions, the first two criteria did reveal interesting results with regards to the degree of updating under the hierarchical

model configuration. First, we highlight the often significant shifts of the posterior means and the increased standard deviations of the zooplankton mortality rate (*d*), the half-saturation constant for predation (*pred*), and the zooplankton grazing half-saturation constant (μ). These posterior patterns probably indicate that the zooplankton feeding kinetics and the mortality/higher predation rates (the so-called closure term) are primarily used to accommodate the site-specific variability and therefore are more resistant to the Bayesian shrinkage effect. Shrinkage is a well-known phenomenon in both Bayesian and frequentist statistics in which individual estimates are shrunk toward the overall mean when they are derived jointly rather than independently (Efron and Morris, 1975; Gelman and Pardoe, 2006). This finding reiterates the well-documented profound impact of these parameters upon the dynamics of plankton ecosystem models and underscores the importance of developing articulate site specific prior probability distributions when data from different study sites are combined under the hierarchical structure (Edwards and Yool, 2000; Franks, 2002; Arhonditsis and Brett, 2004). The rest calibration vector can be classified into two groups: (i) parameters that depending on the scenario examined can play an active role during the model training process, e.g., the half-saturation constant for PO_4^{3-} uptake (*e*), phytoplankton respiration (*r*) and sinking (*s*) rates, the detritus sinking (ψ) and mineralization (φ) rates, (ii) parameters with relatively unaltered posterior moments comparing with the values assigned to the global priors, e.g., the zooplankton growth efficiency (*a*) and excretion fraction (β), and the regeneration of zooplankton predation excretion (γ). Overall, these results are similar to those reported in earlier applications of the same four state variable model structure (Arhonditsis et al., 2007; 2008b). The consistent increase/decrease of the central tendency values of some parameters, such as the phytoplankton respiration rate (*r*), the detritus sinking rate (ψ), and the detritus mineralization rate (φ), probably indicates that the initial estimates

obtained from the literature review misrepresented the underlying ecological processes; at least under the setting (e.g., datasets, model structure) used in this analysis. We also note the relatively greater shifts in the mean parameter values when relaxing our confidence in the prior knowledge used to formulate the global priors (scenario *D*). The sensitivity of the first-order posterior moments to the assigned site-specific parameter precisions suggests that the broadening of the parameter space examined allows the identification of regions of higher model performance but also increases the standard deviations of the parameter marginal distributions (see the differences of the parameter standard deviations between the scenarios *A* and *D* in Figs. 3.2 and 3.3).

The Bayesian hierarchical proposition may be useful for a variety of aquatic science and ecological modeling applications in which partial, but not complete, commonality can be assumed among the modelled units. A characteristic case is the Laurentian Great Lakes region where the most degraded areas are nearshore zones above the summer thermocline adjacent to the mouths of large rivers and enclosed bays/harbours with restricted mixing with offshore water. These areas are intermediate zones in that they receive highly polluted inland waters from watersheds with significant agricultural, urban and/or industrial activities while mixing with offshore waters having different biological and chemical characteristics (Nicholls, 1999; Rockwell et al., 2005; Winter et al., 2007). We believe that this type of spatial heterogeneity cannot be fully accommodated by the typical practice of developing spatially explicit mechanistic models with common parameter values over the entire systems. Rather, the practical compromise between entirely site-specific and globally-common parameter estimates offered by the hierarchical approach may be a conceptually more sound strategy (Fig. 3.8); that is, how realistic is to assume that the same phytoplankton growth rate occurs throughout the

waterbody? Importantly, our illustration showed that such model configuration does not negate the basic premise for using process-based models, i.e., reproduction of the observed system dynamics while gaining mechanistic insights, and it does provide parameter posteriors that have meaningful ecological interpretation. For example, the posterior means for the half-saturation constant for PO_4^{3-} uptake (*e*) after updating the model against individual datasets representing oligo-, meso-, and eutrophic conditions were equal to 5.75, 13.17, and 22.05 μg P L^{-1}, respectively (Table C1). These values are ecologically plausible and depict the continuum between phytoplankton communities dominated by species with strong (e.g., diatom-like) and weak (e.g., cyanobacteria-like) P competition abilities. With the hierarchical scheme, the relative magnitude of the same parameter remained unaltered across the three states, although their absolute values were somewhat different (Tables C2 & C4). Furthermore, the wider observational range stemming from the combination of sites that represent different trophic conditions (scenarios *A* and *D*) consistently reduced the error terms associated with the phosphate (σ_{PO4}) and detritus (σ_{DET}) equations, whereas variant results were found for the phytoplankton (σ_{PHYT}) and zooplankton (σ_{ZOOP}) error terms depending on the scenarios examined. Realistic parameter values and reduced error terms were also derived from the second experiment that simulates the case in which inshore and offshore areas with different observed variability of a mesotrophic lake are combined under the hierarchical structure.

We also examined the ability of the Bayesian hierarchical framework to provide a mechanism for pooling information from systems with different sampling intensity and strengthen the predictive ability in individual sites. Indeed, our analysis showed that primarily the scenario that uses seasonal averages for the state variables (C_1) and

secondarily the one using data solely from the stratified period (C_2) resulted in very similar posterior parameter moments between the two locations, providing confidence in the ecological foundation of the model at the less studied system. Furthermore, aside from the previously mentioned low precisions of the parameters associated with the zooplankton feeding kinetics and mortality rates, the differences between the posterior first and second order moments of the hyperparameters and the system specific parameters were also quite small (Fig. 3.9); that is, the site specific parameters converged toward the global means but these shifts were not accompanied by a significant shrinkage of the corresponding parameter standard deviations (Gelman and Pardoe, 2006). The comparison between the observed and posterior predictive monthly distributions along with the values of the error terms can also be used to dictate the optimal type of information required to improve the predictive power of the model. For example, the calibration of the model with data collected once per season results in very wide uncertainty bands and thus less useful for water quality management. Furthermore, although the median predictions closely matches the majority of the observed data and the values of the error terms were notably lower, the model fails to capture the timing of the spring phytoplankton bloom and does not reproduce the contemporaneous peak of the zooplankton biomass. Interestingly, the latter problems were not alleviated when the model of the less intensively studied system was combined with a refined model parameterization based on a well-studied site. On the other hand, the use of data collected with higher frequency but exclusively from the stratified period overcomes the misrepresentation of the spring plankton dynamics and also reduces the predictive uncertainty. Similar experiments can be designed regarding the spatiotemporal sampling intensity or the collection of data on parameters versus data on output variables and the subsequent assessment of the value of information can further optimize the existing

monitoring programs and assist model-based decision making and management (Dorazio and Johnson, 2003; Van Oijen et al., 2005). Finally, we note the overwhelmingly high error values resulting from a hierarchical structure that combines a mesotrophic monomictic with an eutrophic dimictic system. These results are not surprising as it would seem counterintuitive to improve ecological forecasts by exchanging information between systems that have so significant functional and structural differences. This experiment merely aimed to provide an additional sensitivity analysis with regards to the role of the different parameters in accommodating the variability of the two datasets.

In conclusion, we introduced a Bayesian hierarchical framework that enables the development of robust probabilistic analysis of error and uncertainty in model predictions by explicitly taking into account the measurement error, parameter uncertainty, and model structure imperfection. Our intent was to illustrate how this approach can be used to transfer knowledge in space, and therefore to simultaneously calibrate process-based models in multiple sites.

Tables

Table 3.1 The scenarios examined under the Bayesian hierarchical configuration of the mathematical model.

Scenario No.	*Sub-model*	*Measurement Error*	*Parameter precision*	*Interannual variability*	*Trophic state*	*Observed Data Availability*
A_1	1	15%	15%	15%	Mesotrophic	12 monthly values
	2	15%	15%	15%	Oligotrophic	12 monthly values
A_2	1	15%	15%	15%	Mesotrophic	12 monthly values
	2	15%	15%	15%	Eutrophic	12 monthly values
B_1	1	15%	15%	15%	Mesotrophic	12 monthly values
	2	15%	15%	30%	Mesotrophic	12 monthly values
C_1	1	15%	15%	15%	Mesotrophic	12 monthly values
	2	25%	15%	15%	Mesotrophic	4 seasonal values
C_2	1	15%	15%	15%	Mesotrophic	12 monthly values
	2	15%	15%	15%	Mesotrophic	6 monthly values during the stratified period
C_3	1	15%	15%	15%	Mesotrophic	12 monthly values
	2	15%	15%	15%	Eutrophic Dimictic	6 monthly values during the ice-free period
D_1	1	15%	35%	15%	Mesotrophic	12 monthly values
	2	15%	35%	15%	Oligotrophic	12 monthly values
D_2	1	15%	35%	15%	Mesotrophic	12 monthly values
	2	15%	35%	15%	Eutrophic	12 monthly values
E_1	1	15%	Updated Prior	15%	Mesotrophic	12 monthly values
	2	15%	15%	15%	Eutrophic	12 monthly values
E_2	1	15%	Updated Prior	15%	Mesotrophic	12 monthly values
	2	25%	15%	15%	Mesotrophic	4 seasonal values

Table 3.2 The prior probability distributions of the hyperparameters.

Parameter	*Units*	*Mean*	*S.D.*
Maximum phytoplankton growth rate (a)	day^{-1}	1.446	0.308
Zooplankton mortality rate (d)	day^{-1}	0.173	0.021
Half-saturation constant for predation (*pred*)	$mg\ C\ m^{-3}$	54.61	13.94
Half-saturation constant for PO_4^{3-} uptake (e)	$mg\ P\ m^{-3}$	10.93	4.818
Cross-thermocline exchange rate (k)	day^{-1}	0.037	0.013
Phytoplankton respiration rate (r)	day^{-1}	0.117	0.070
Phytoplankton sinking loss rate (s)	day^{-1}	0.040	0.032
Zooplankton growth efficiency (a)		0.366	0.126
Zooplankton excretion fraction (β)		0.293	0.111
Regeneration of zooplankton predation excretion (γ)		0.293	0.111
Maximum zooplankton grazing rate (λ)	day^{-1}	0.609	0.107
Zooplankton grazing half-saturation coefficient (μ)	$mg\ P\ m^{-3}$	6.575	1.867
Detritus remineralization rate (φ)	day^{-1}	0.092	0.032
Detritus sinking rate (ψ)	day^{-1}	0.142	0.084

Table 3.3 *Scenario C.* Markov Chain Monte Carlo posterior estimates of the mean values and standard deviations of the model stochastic nodes.

Nodes	C_1				C_2				C_3			
	1		*2*		*1*		*2*		*1*		*2*	
	Mean	*S. D.*	*Mean*	*S. D.*	*Mean*	*S. D.*	*Mean*	*S. D.*	*Mean*	*S. D.*	*Mean*	*S. D.*
a	1.314	0.140	1.330	0.158	1.307	0.116	1.306	0.128	1.361	0.157	1.331	0.140
d	0.197	0.055	0.182	0.045	0.216	0.059	0.203	0.053	0.234	0.072	0.209	0.050
pred	54.37	22.64	59.25	26.09	56.24	21.58	46.43	24.41	55.26	21.21	60.84	35.64
e	13.05	2.895	10.92	3.122	15.84	2.907	22.11	11.17	15.09	3.815	24.64	7.687
k	0.022	0.007	0.025	0.016	0.019	0.005	0.043	0.022	0.030	0.010	0.024	0.016
r	0.197	0.027	0.197	0.050	0.178	0.025	0.161	0.057	0.181	0.034	0.211	0.075
s	0.030	0.013	0.033	0.018	0.018	0.009	0.017	0.009	0.027	0.013	0.110	0.029
α	0.376	0.143	0.360	0.136	0.481	0.154	0.471	0.162	0.497	0.180	0.502	0.187
β	0.229	0.081	0.237	0.088	0.245	0.091	0.252	0.095	0.230	0.092	0.240	0.092
γ	0.266	0.104	0.275	0.105	0.253	0.096	0.248	0.097	0.286	0.123	0.284	0.126
λ	0.581	0.115	0.576	0.114	0.599	0.107	0.593	0.112	0.659	0.121	0.660	0.124
μ	9.896	3.529	8.453	2.968	11.01	3.752	11.15	3.929	10.47	3.496	8.886	3.044
φ	0.050	0.011	0.053	0.023	0.040	0.013	0.040	0.026	0.052	0.018	0.067	0.030
ψ	0.030	0.006	0.028	0.008	0.033	0.008	0.038	0.016	0.038	0.010	0.038	0.023
σ_{PO4}	0.796	0.335	1.383	1.230	0.712	0.303	1.024	0.638	0.709	0.316	5.666	6.063
σ_{PHYT}	8.516	12.13	7.062	15.21	6.906	9.113	9.520	18.30	8.727	11.70	246.7	153.3
σ_{ZOOP}	28.79	12.69	7.989	13.97	24.63	12.19	33.45	23.59	22.80	12.78	68.76	63.26
σ_{DET}	2.261	1.072	1.486	1.926	2.568	1.234	2.904	2.384	2.637	1.471	15.71	7.939

Table 3.4 *Scenario E.* Markov Chain Monte Carlo posterior estimates of the mean values and standard deviations of the model stochastic nodes.

Nodes	E_1				E_2			
	1		*2*		*1*		*2*	
	Mean	*S. D.*	*Mean*	*S. D.*	*Mean*	*S. D.*	*Mean*	*S. D.*
a	1.209	0.069	1.195	0.071	1.271	0.048	1.271	0.068
d	0.234	0.024	0.303	0.045	0.204	0.023	0.222	0.055
pred	54.23	7.908	113.0	29.71	53.49	8.616	58.62	22.62
e	13.87	1.856	30.08	4.635	15.62	1.811	13.02	2.377
k	0.026	0.004	0.023	0.005	0.022	0.003	0.018	0.008
r	0.143	0.014	0.150	0.021	0.154	0.019	0.174	0.053
s	0.025	0.005	0.020	0.006	0.022	0.005	0.027	0.016
α	0.655	0.131	0.665	0.129	0.496	0.104	0.494	0.114
β	0.192	0.061	0.191	0.078	0.207	0.055	0.208	0.069
γ	0.174	0.043	0.152	0.045	0.273	0.098	0.283	0.111
λ	0.730	0.097	0.743	0.091	0.685	0.100	0.686	0.105
μ	9.984	1.429	15.34	5.493	9.026	1.628	11.910	3.935
φ	0.050	0.011	0.046	0.019	0.051	0.013	0.043	0.018
ψ	0.040	0.006	0.041	0.016	0.044	0.007	0.026	0.007
σ_{PO4}	0.893	0.290	1.658	0.778	0.800	0.258	1.000	0.959
σ_{PHYT}	2.962	4.822	10.24	16.32	3.113	5.194	7.964	17.29
σ_{ZOOP}	14.50	4.151	21.37	10.56	16.75	5.412	8.158	14.34
σ_{DET}	4.312	1.037	9.673	3.210	4.136	0.959	1.461	1.947

Figures

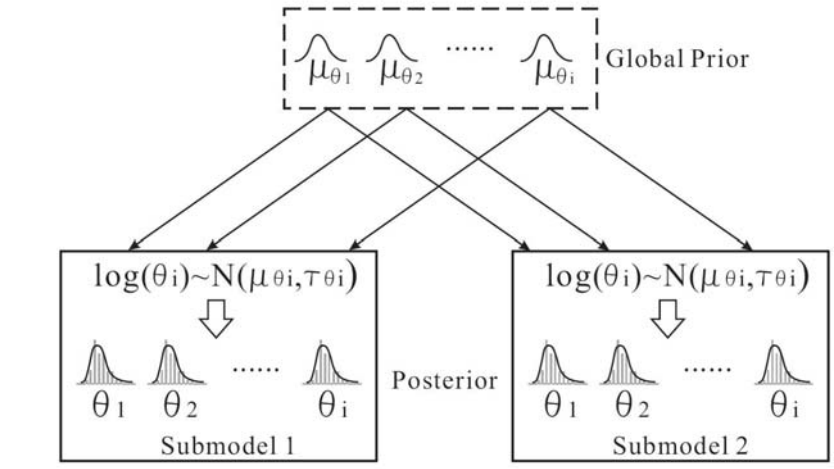

(a)

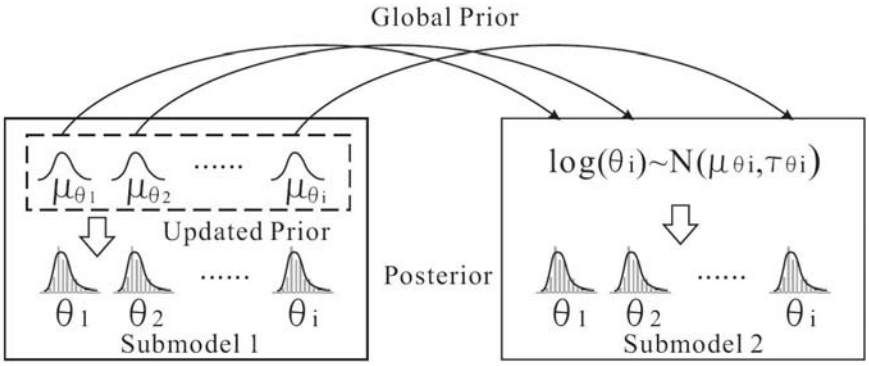

(b)

Figure 3.1 The structure of the two hierarchical frameworks examined: **(a)** scenarios *A, B, C,* and *D*; **(b)** scenario *E*.

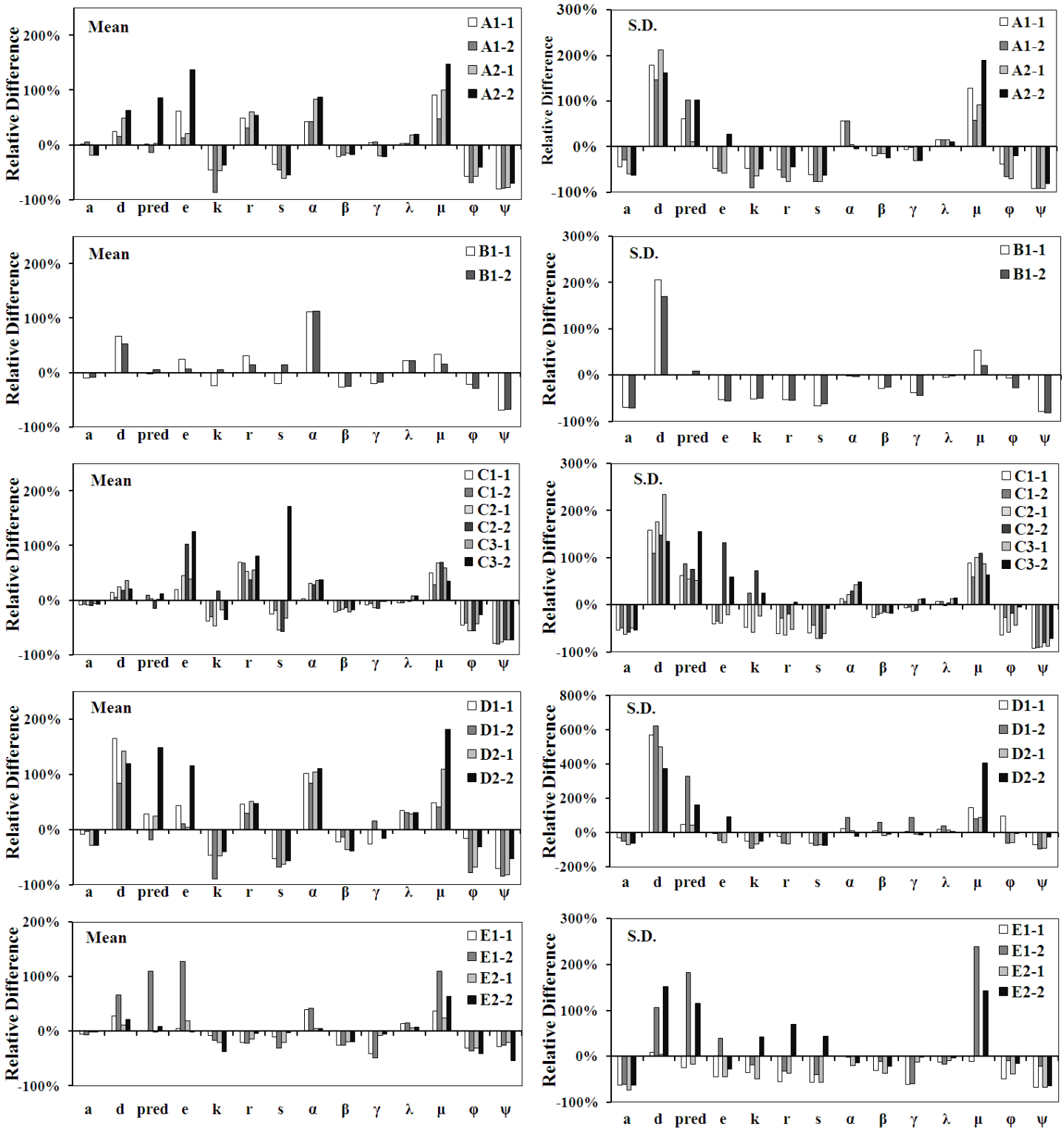

Figure 3.2 The relative difference between posterior estimates of the mean values and standard deviations and the corresponding prior distributions of the model parameters.

$$Relative\ difference = \frac{Posterior - Prior}{Prior} \times 100\%.$$

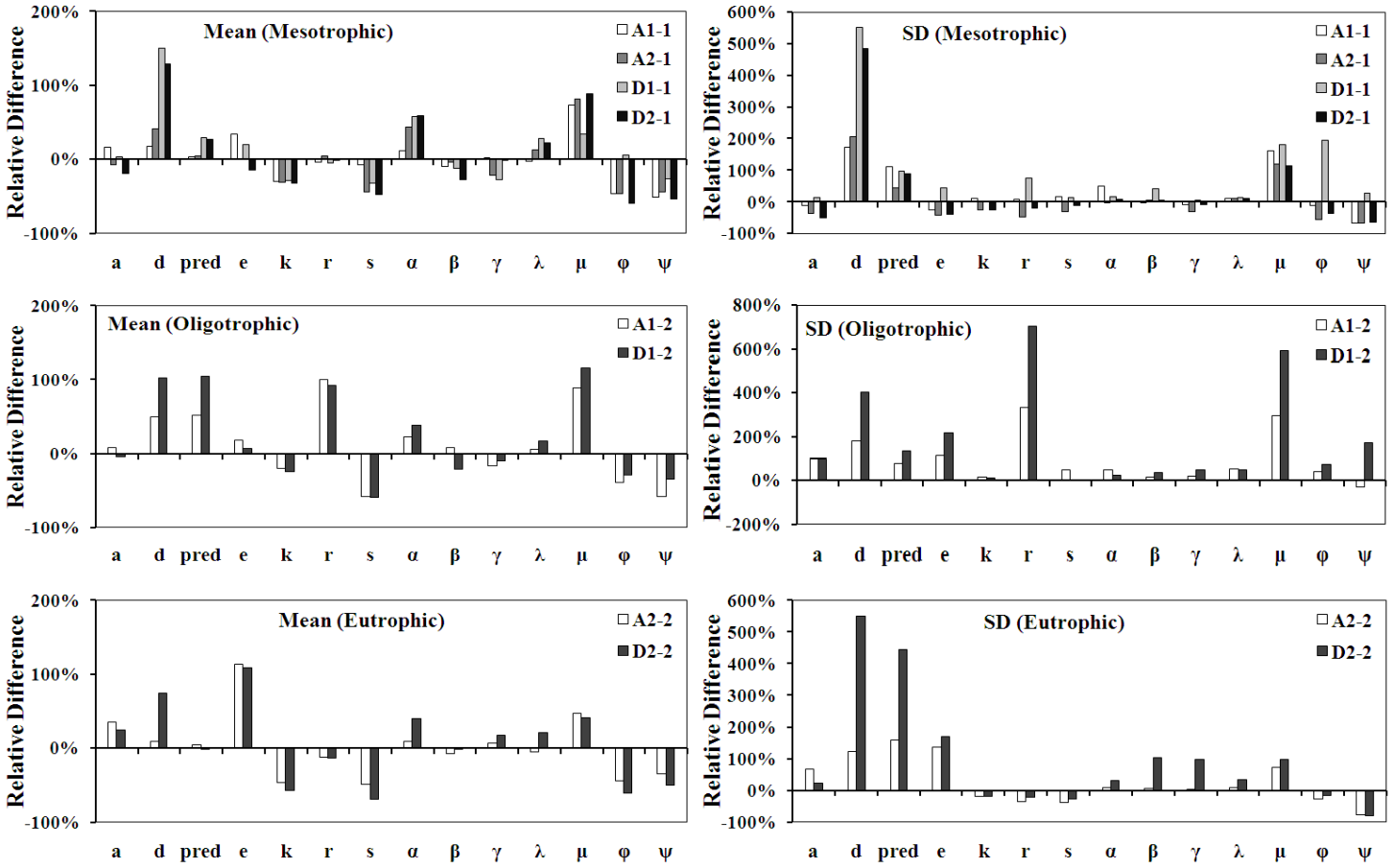

Figure 3.3 The relative difference between the posterior parameter estimates obtained after model calibration against individual datasets representing oligo-, meso- and eutrophic conditions and the hierarchical settings examined in the scenarios *A* and *D*.

$$Relative\ difference_i = \frac{Hierarchical_i - Nonhierarchical_i}{Nonhierarchical_i} \times 100\%$$

i =oligotrophic, mesotrophic, eutrophic

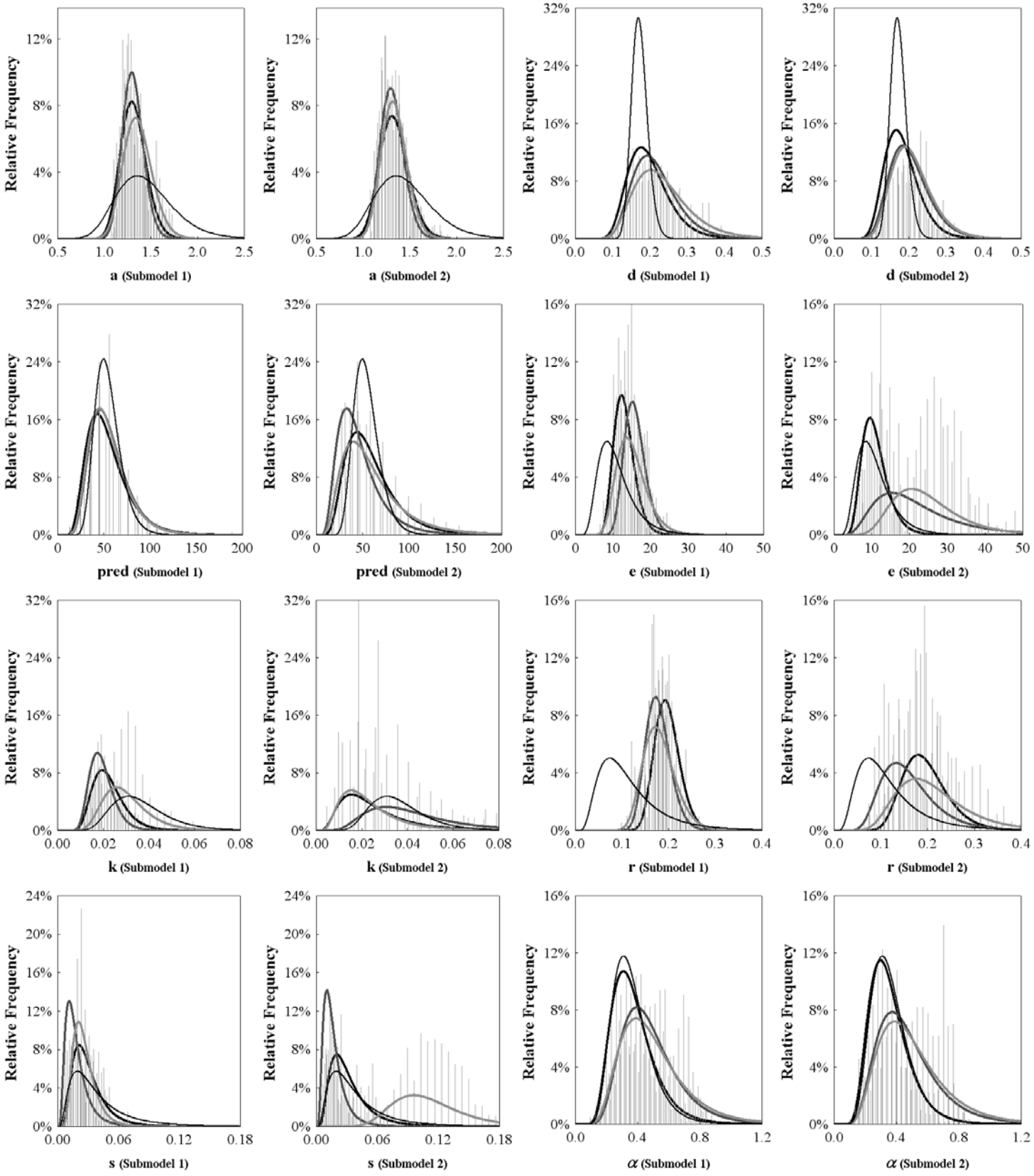
Relative Frequency
a (Submodel 1)
a (Submodel 2)
d (Submodel 1)
d (Submodel 2)
pred (Submodel 1)
pred (Submodel 2)
e (Submodel 1)
e (Submodel 2)
k (Submodel 1)
k (Submodel 2)
r (Submodel 1)
r (Submodel 2)
s (Submodel 1)
s (Submodel 2)
α (Submodel 1)
α (Submodel 2)

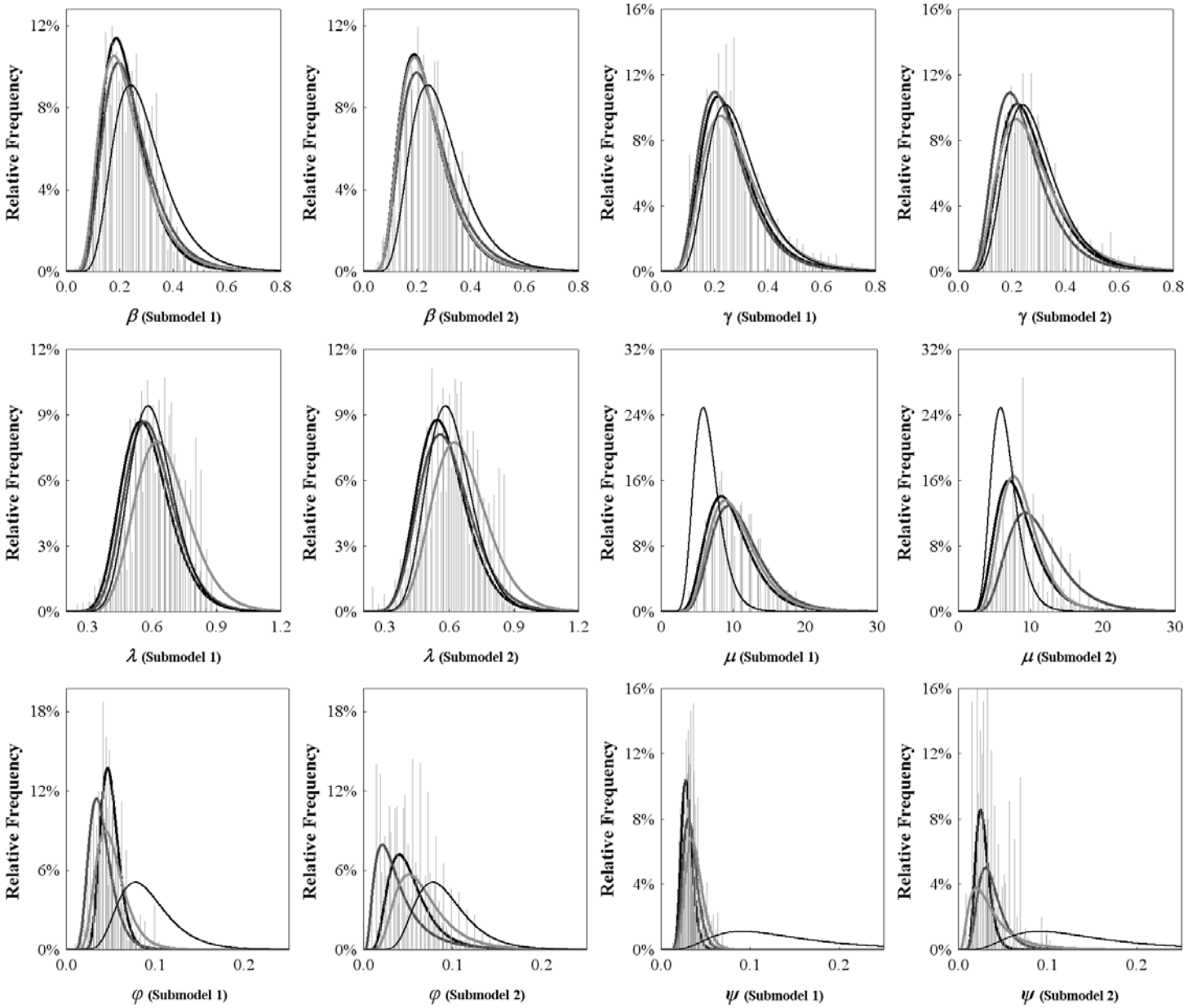

Figure 3.4 *Scenario C.* Prior (thin black lines) and posterior (C_1: thick black lines, C_2: thick grey lines, and C_3: thick light grey lines) parameter distributions.

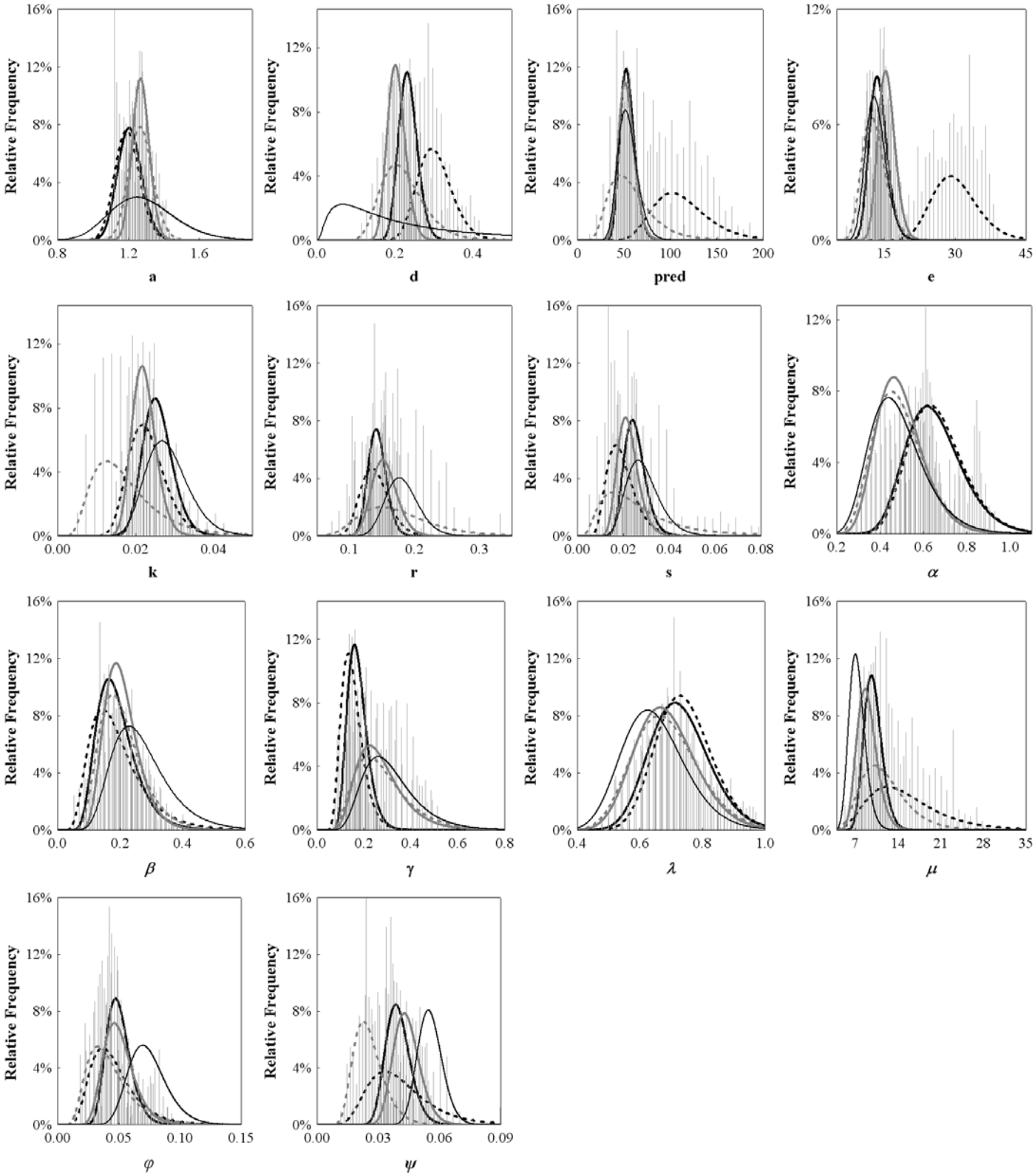

Figure 3.5 *Scenario E.* Prior (thin black lines) and posterior (E_1 submodel 1: thick black lines, E_1 submodel 2: thick black dashed lines, E_2 submodel 1: thick gray lines, and E_2 submodel 2: thick dashed grey lines) parameter distributions.

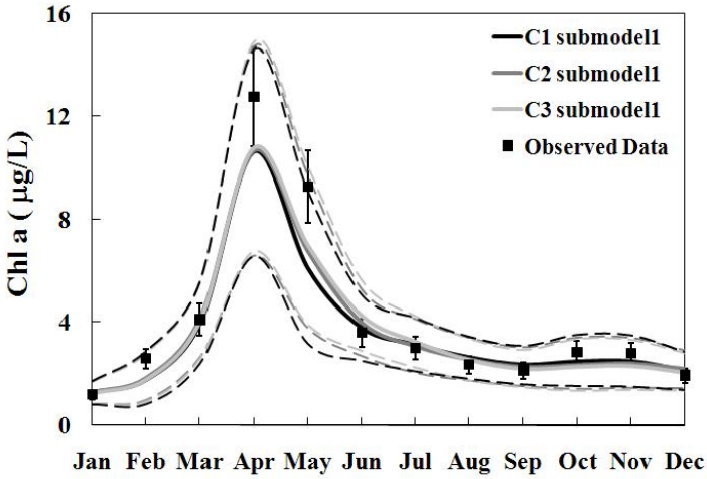
Chl a (μg/L)
16
12
8
4
0
C1 submodel1
C2 submodel1
C3 submodel1
Observed Data
Jan Feb Mar Apr May Jun Jul Aug Sep Oct Nov Dec

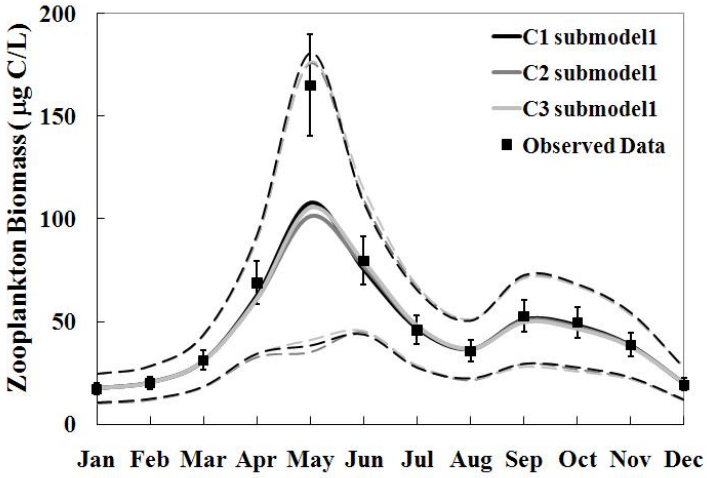
Zooplankton Biomass (μg C/L)
200
150
100
50
0
C1 submodel1
C2 submodel1
C3 submodel1
Observed Data
Jan Feb Mar Apr May Jun Jul Aug Sep Oct Nov Dec

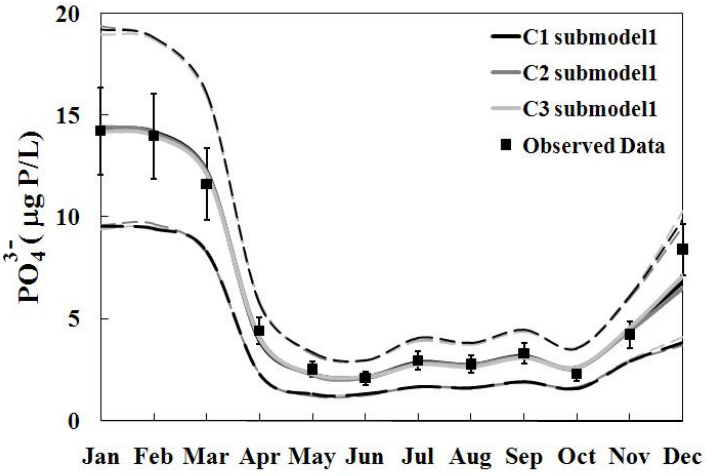
PO_4^{3-} (μg P/L)
20
15
10
5
0
C1 submodel1
C2 submodel1
C3 submodel1
Observed Data
Jan Feb Mar Apr May Jun Jul Aug Sep Oct Nov Dec

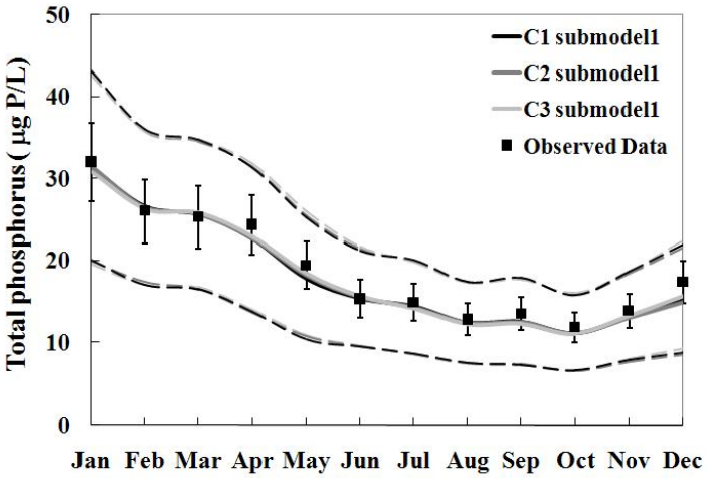
Total phosphorus (μg P/L)
50
40
30
20
10
0
C1 submodel1
C2 submodel1
C3 submodel1
Observed Data
Jan Feb Mar Apr May Jun Jul Aug Sep Oct Nov Dec

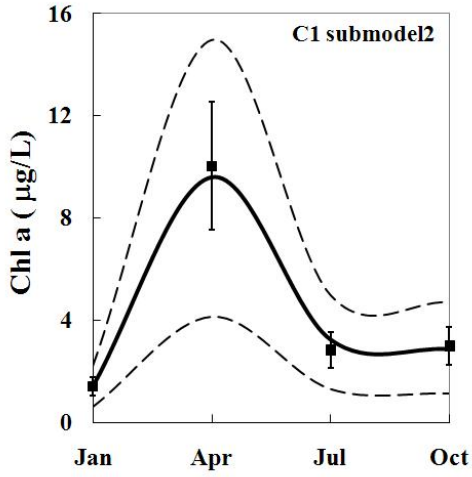
Chl a (μg/L)
16
12
8
4
0
C1 submodel2
Jan
Apr
Jul
Oct

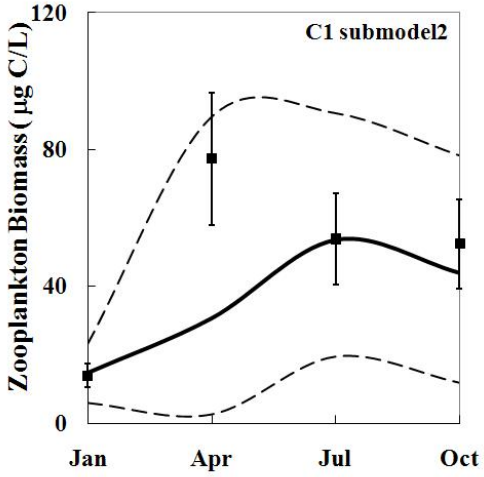
Zooplankton Biomass (μg C/L)
120
80
40
0
C1 submodel2
Jan
Apr
Jul
Oct

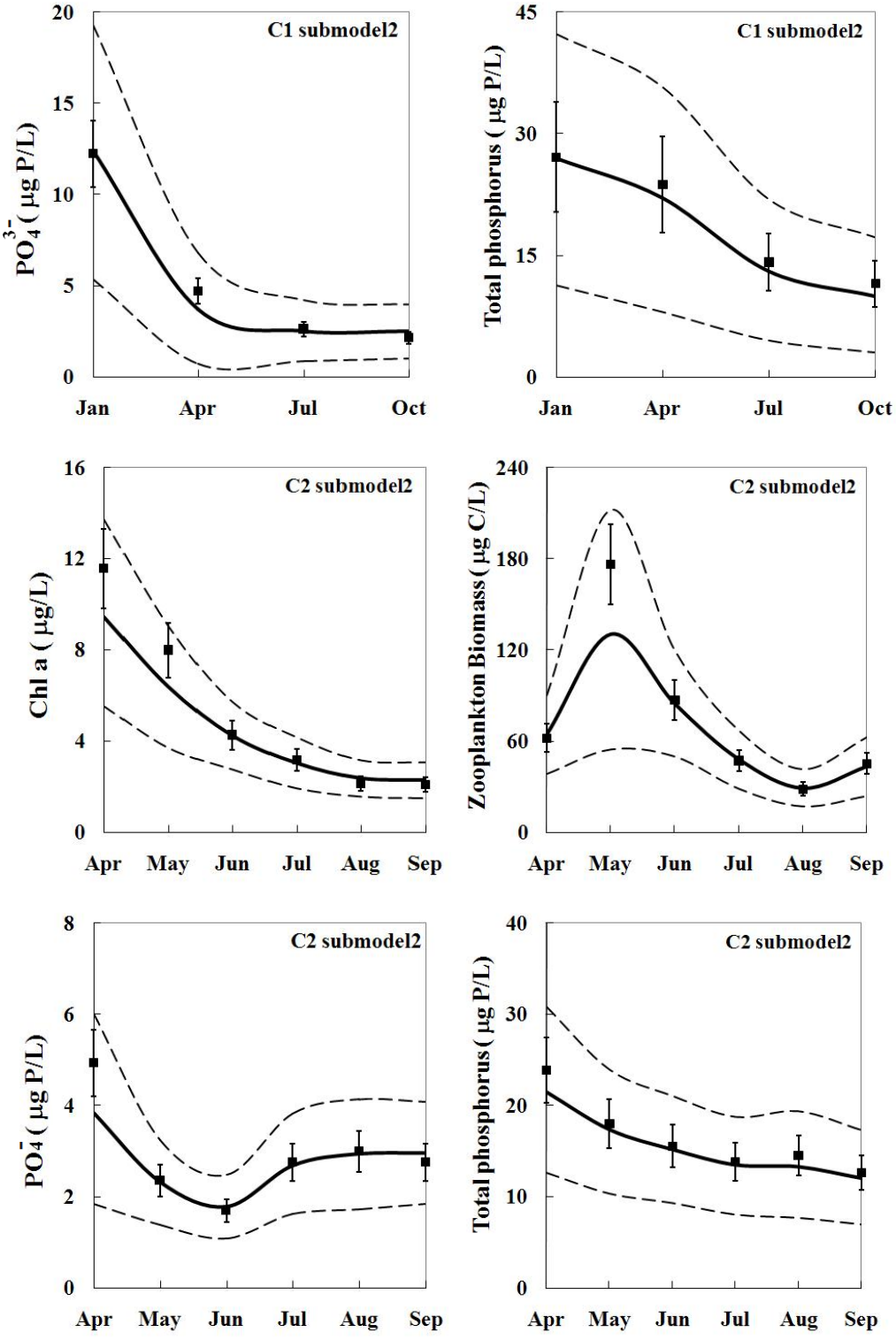
C1 submodel2
PO_4^{3-} (µg P/L)
20
15
10
5
0
Jan
Apr
Jul
Oct
C1 submodel2
Total phosphorus (µg P/L)
45
30
15
0
Jan
Apr
Jul
Oct
C2 submodel2
Chl a (µg/L)
16
12
8
4
0
Apr
May
Jun
Jul
Aug
Sep
C2 submodel2
Zooplankton Biomass (µg C/L)
240
180
120
60
0
Apr
May
Jun
Jul
Aug
Sep
C2 submodel2
PO_4^{-} (µg P/L)
8
6
4
2
0
Apr
May
Jun
Jul
Aug
Sep
C2 submodel2
Total phosphorus (µg P/L)
40
30
20
10
0
Apr
May
Jun
Jul
Aug
Sep

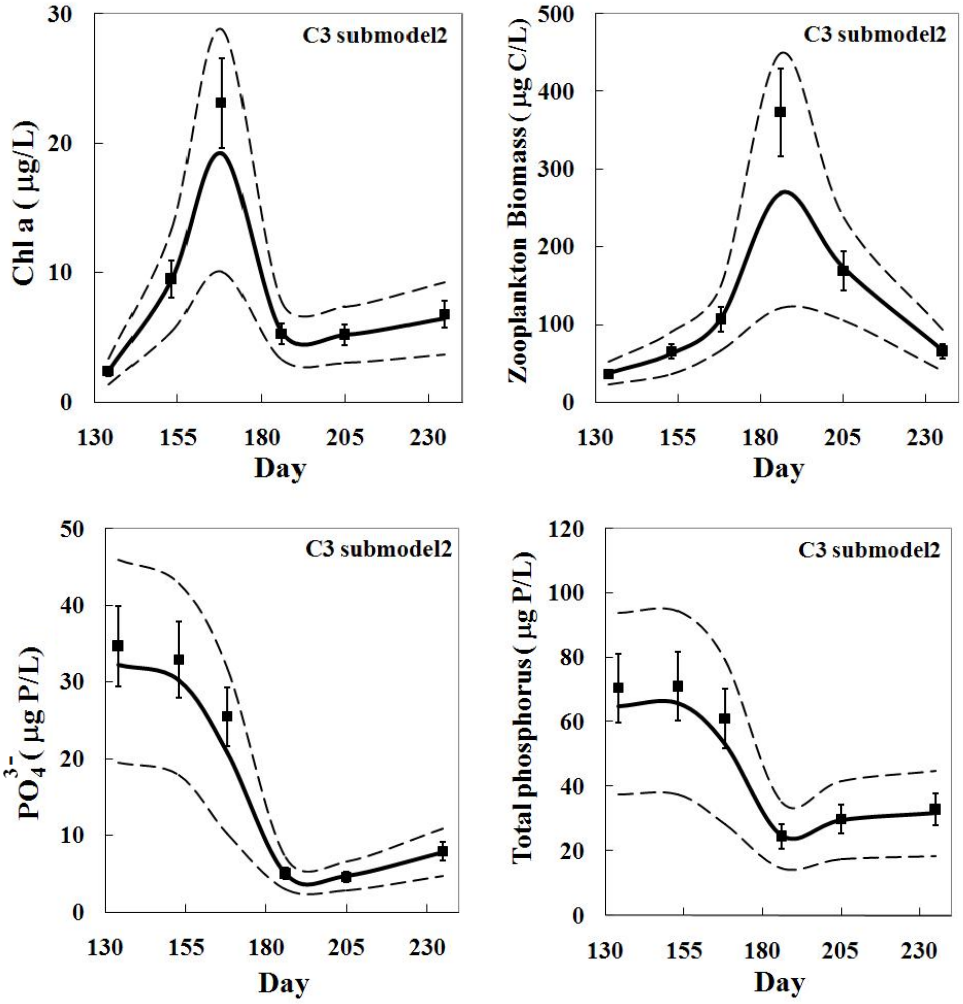

Figure 3.6 *Scenario C.* Comparison between the observed and posterior predictive distributions. Solid line corresponds to the median value of model predictions and dashed lines correspond to the 2.5 and 97.5% credible intervals. The square dots represent the observed data, while the error bars reflect the measurement error.

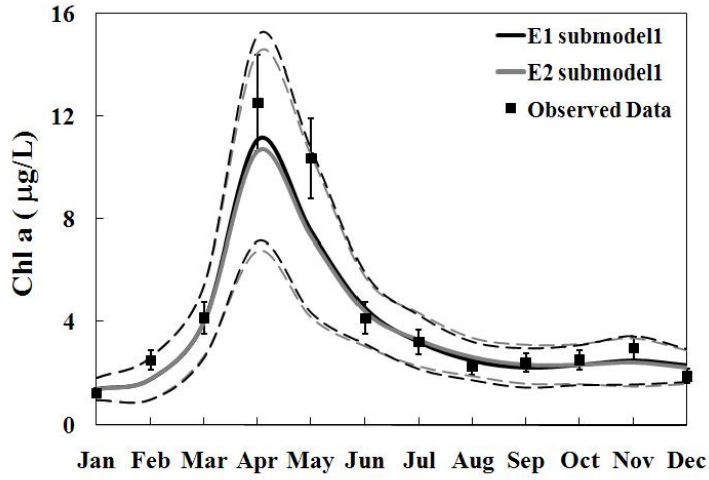
Chl a (μg/L)
16
12
8
4
0
E1 submodel1
E2 submodel1
Observed Data
Jan Feb Mar Apr May Jun Jul Aug Sep Oct Nov Dec

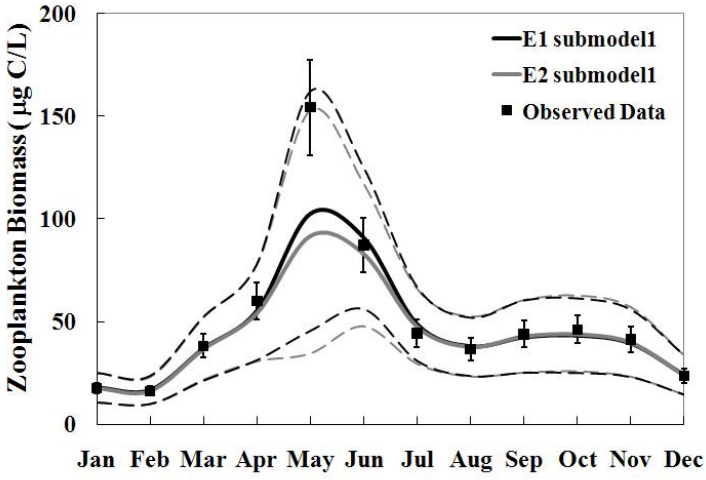
Zooplankton Biomass (μg C/L)
200
150
100
50
0
E1 submodel1
E2 submodel1
Observed Data
Jan Feb Mar Apr May Jun Jul Aug Sep Oct Nov Dec

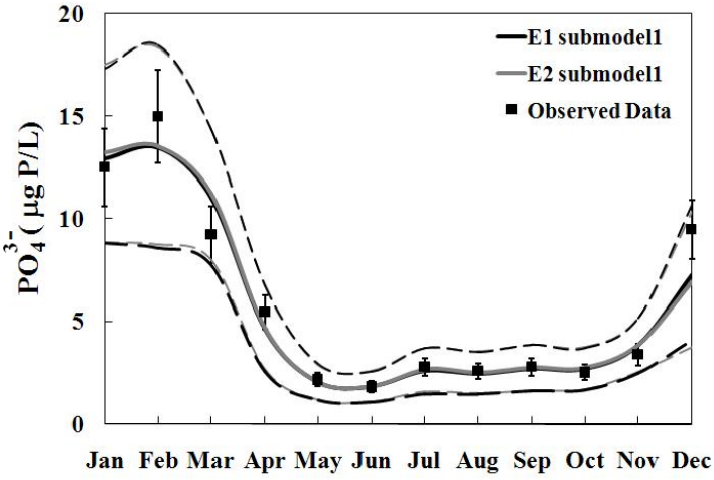
PO43- (μg P/L)
20
15
10
5
0
E1 submodel1
E2 submodel1
Observed Data
Jan Feb Mar Apr May Jun Jul Aug Sep Oct Nov Dec

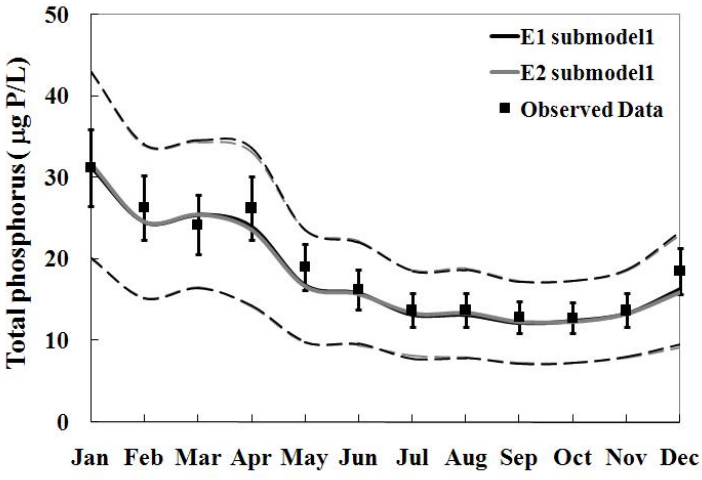
Total phosphorus (μg P/L)
50
40
30
20
10
0
E1 submodel1
E2 submodel1
Observed Data
Jan Feb Mar Apr May Jun Jul Aug Sep Oct Nov Dec

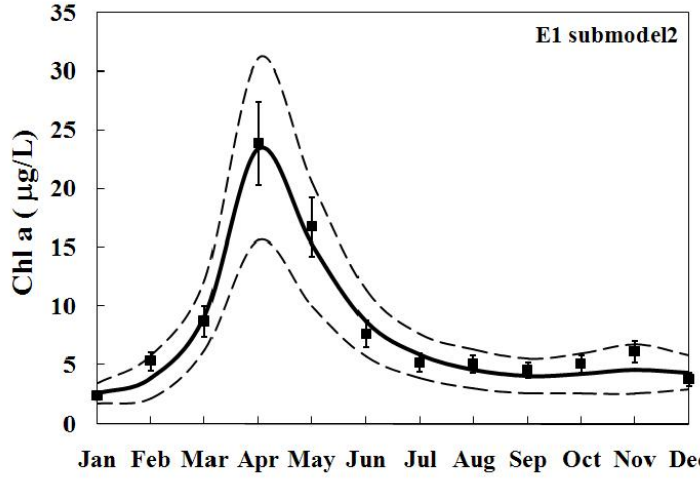
Chl a (μg/L)
35
30
25
20
15
10
5
0
E1 submodel2
Jan Feb Mar Apr May Jun Jul Aug Sep Oct Nov Dec

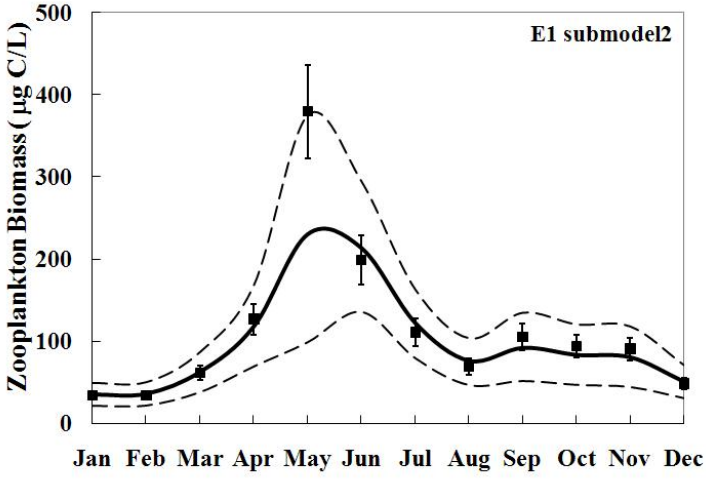
Zooplankton Biomass (μg C/L)
500
400
300
200
100
0
E1 submodel2
Jan Feb Mar Apr May Jun Jul Aug Sep Oct Nov Dec

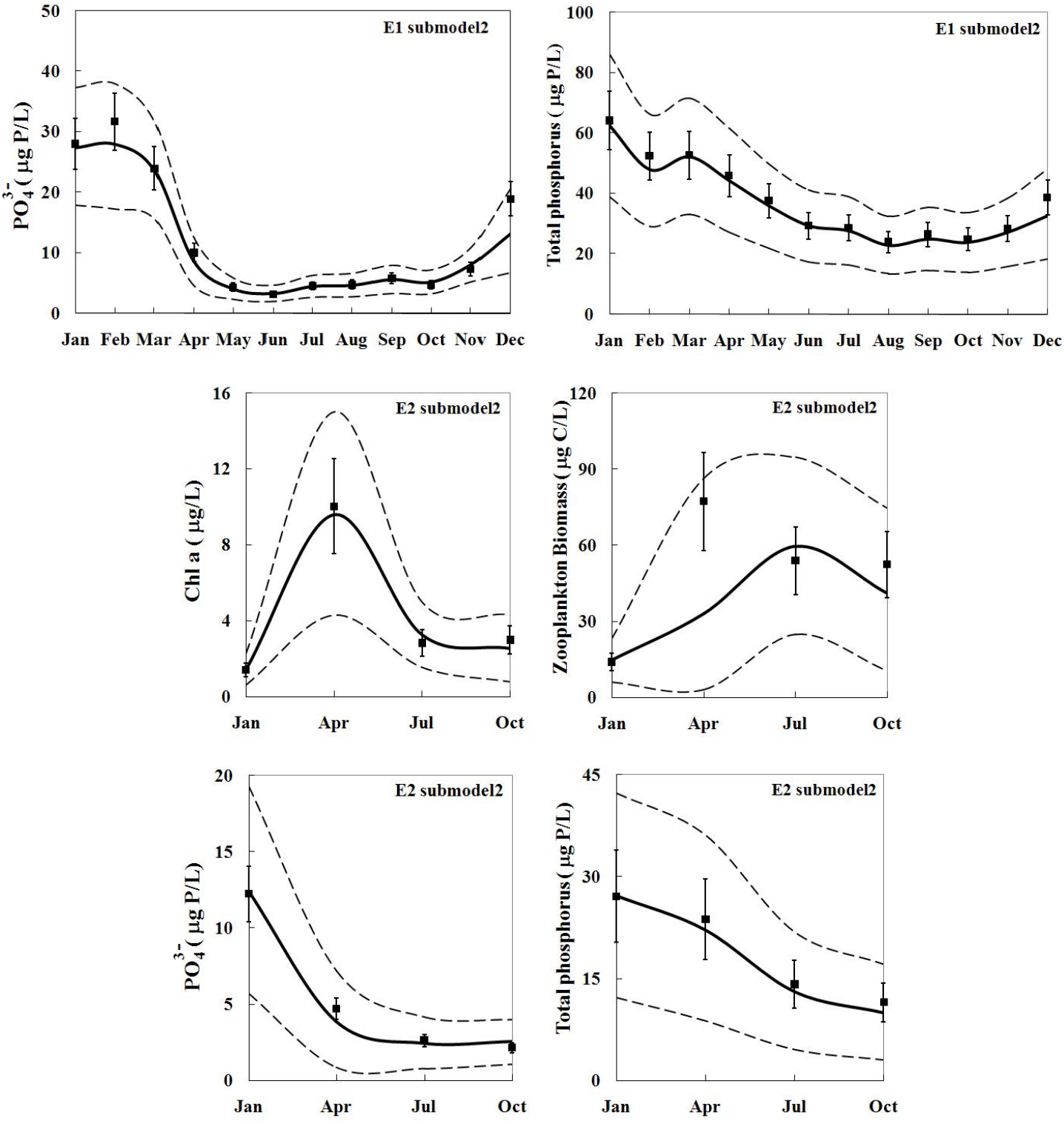

Figure 3.7 *Scenario E.* Comparison between the observed and posterior predictive distributions. Solid line corresponds to the median value of model predictions and dashed lines correspond to the 2.5 and 97.5% credible intervals. The square dots represent the observed data, while the error bars reflect the measurement error.

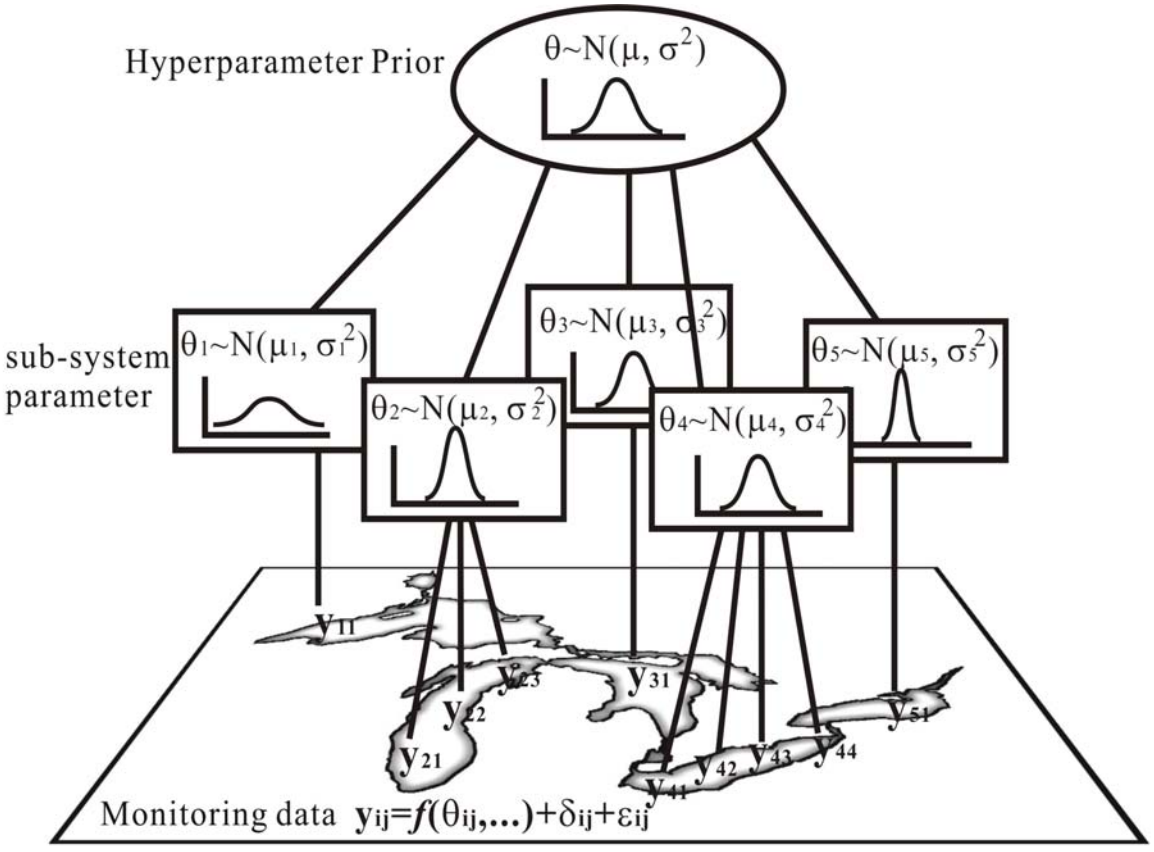

Figure 3.8 A conceptual application of the Bayesian hierarchical framework to allow the transfer of information in space.

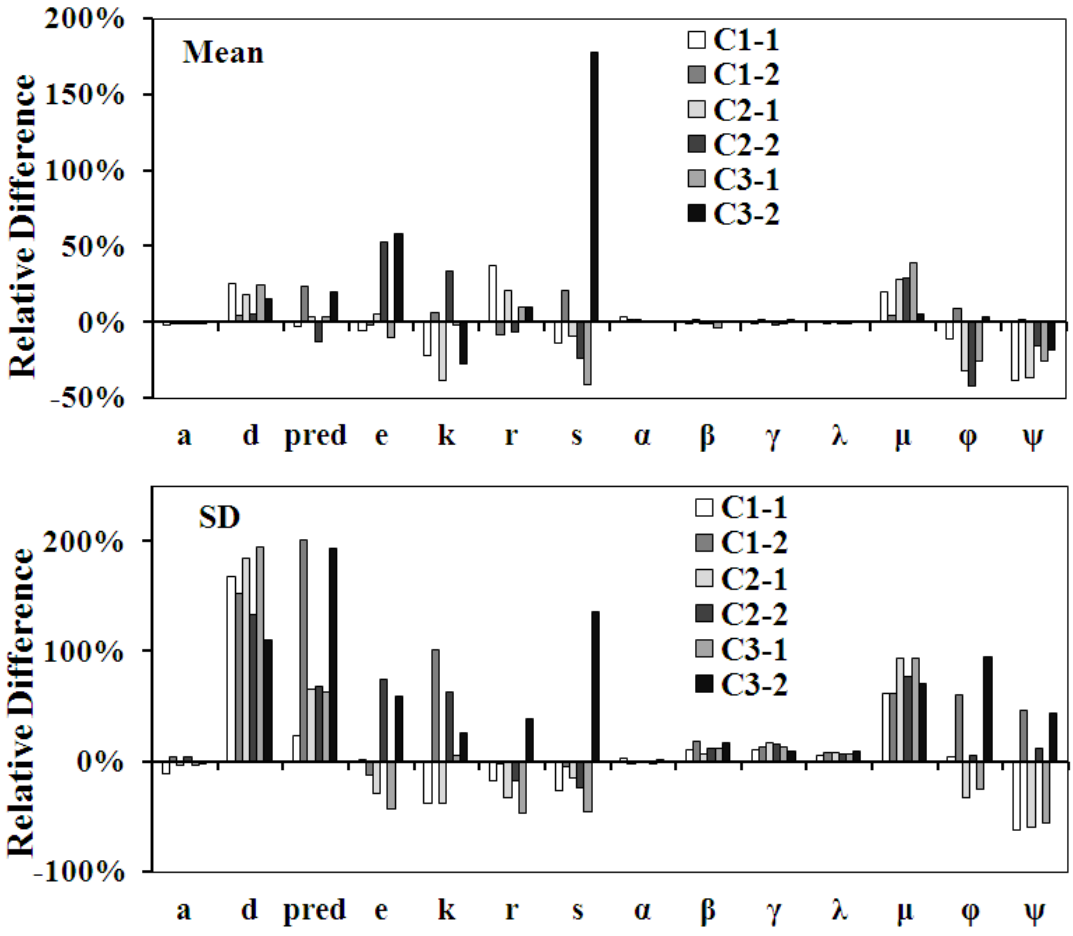

Figure 3.9 *Scenario C.* The relative difference between posterior estimates of the mean values and standard deviations of the hyperparameters and the system specific parameters.

$$Relative\ difference = \frac{Parameter_k - Global\ parameter}{Global\ parameter} \times 100\%$$

k = submodel 1, 2

Chapter 4: Future Research Perspectives

In this work, we focused on two methodological frameworks that integrate environmental process-based (mathematic) models with Bayesian analysis. The results showed that Bayesian approach provides a convenient means for characterizing uncertainty in model predictions. The Bayesian calibration is well suited for stakeholders and decision makers to make reflective judgments and rational determinations for sustainable environmental management problems.

Here, we highlight some of the unresolved technical aspects and future perspectives in the general Bayesian analysis and Bayesian hierarchical scheme.

i) *Prior assumptions on parameter distributions and model structure:* The prior distributions assigned to the model parameters would affect the updating results. Especially in hierarchical models, the global prior distributions of hyperparameters have received considerable attention in the Bayesian literature (Box and Tiao, 1973; Spiegelhalter et al., 2003; Gelman et al., 1995), and special emphasis has been placed on the use of noninformative priors for hierarchical variance parameters (Gelman, 2005). In the context of the present analysis, we also caution to carefully select the priors for the error terms representing the discrepancy between the model structure and the natural system dynamics, as our experience was that some of the results presented herein were sensitive to the pertinent selection. We also note the instrumental role of the parameters associated with the zooplankton feeding kinetics and the mortality/higher predation rates in accommodating the site specific variability. In this regard, an appealing next step would be the development of a prescriptive approach for optimizing the structure of hierarchical modeling constructs by choosing site specific closure terms (linear, quadratic,

hyperbolic, sigmoid) or functional forms for zooplankton grazing (linear, saturating, saturating with feeding threshold, acclimating to ambient food) on the basis of the posterior parameter and model endpoint patterns.

ii) *Hierarchical Bayes and spatially explicit mathematical models:* The description of spatial and spatiotemporal environmental processes has been the focus of several Bayesian modeling studies, and the existing propositions involve general hierarchical spatial model frameworks (Cressie, 2000; Wikle, 2003a), Markov random field models (Besag et al., 1995), hierarchical spatio-temporal models (Wikle et al., 1998), spatiotemporal dynamic models (Wikle et al., 2001), and spatiotemporal models that are simplified by dimension reduction (Berliner et al., 2000) or by conditioning on processes considered to be latent or hidden (Hughes and Guttorp, 1994). In the present study, we advocated the relaxation of the assumption of globally-common parameter values used in coupled physical-biogeochemical models and the adoption of hierarchical statistical formulations reflecting the more realistic notion that each site is unique but shares some commonality of behaviour with other sites of the same system. The proposed hierarchical structure will be easily employed with model segmentations of 5-10 completely-mixed boxes without significant increase of the computation demands, while future research should also evaluate formulations that explicitly consider the spatiotemporal dependence patterns of the parameter values and model error terms.

iii) *Mathematical models fitted on cross-system data:* In aquatic ecosystem modeling, cross-system data have been used in a global sense to develop empirical relationships between catchment features and nutrient loading (Howarth et al., 1996), lake morphometric/hydraulic characteristics and total phosphorus concentrations (Brett and Benjamin, 2008), light/nutrient availability and phytoplankton levels (Smith, 1986; Malve and Qian, 2006), algal and

zooplankton biomass (McCauley and Kalff, 1981). In this direction, the proposed framework is a logical advancement that allows developing models with stronger mechanistic foundation while remaining within the bounds of data-based parameter estimation (Borsuk et al., 2001). The main advantage of such hierarchical model configuration will be the effective modeling of systems with limited information by borrowing strength from well-studied systems. Indeed, our analysis showed that this approach provides ecologically meaningful parameter estimates at locations with limited data as well as site-specific predictions with more realistic uncertainty ranges than the conventional pooled approaches. Future research should identify the most appropriate criteria (trophic status, morphological characteristics) for delineating the number of levels and type of groups included in the hierarchical structures, thereby optimizing the transfer of information across systems, e.g., see the geomorphological typology presented in Malve and Qian (2006).

iv) *Water quality management:* The former application has illustrated some of the practical benefits from the Bayesian calibration framework, such as the assessment of the exceedance frequency and confidence of compliance of different water quality standards, support of probabilistic statements on cause-effect relationships pertaining to water quality management, alignment with the policy practice of adaptive management implementation, and optimization of monitoring programs using value of information concepts from decision theory (Arhonditsis et al., 2007; 2008a, b). The hierarchical framework can also be used to generalize the recently presented Bayesian approach for combining model results and monitoring data to assess water quality (Qian and Reckhow, 2007). Namely, the initial model forecasts (where the predictive distribution for one site indicates a "high" probability of non-attaining water quality criteria or, alternatively, an "unacceptably high" variance) can dictate which of the systems with limited data should be monitored. We can then pool information from both the monitoring data and the

initial model forecasts (e.g., variance-weighted combination of the two sources of information) which provides the basis for future management actions. It is anticipated that these probabilistic statements (derived from process-based models) along with the iterative (sequential updating) nature of the proposed Bayesian framework will provide a useful tool for policy analysis.

References

Arhonditsis, G.B., and Brett, M.T. 2004. Evaluation of the current state of mechanistic aquatic biogeochemical modeling. *Mar. Ecol. Prog. Ser*. 271:13-26.

Arhonditsis, G.B., and Brett, M.T. 2005a. Eutrophication model for Lake Washington (USA) Part I - model description and sensitivity analysis. *Ecol. Model.* 187(2-3):140-178.

Arhonditsis, G.B., and Brett, M.T. 2005b. Eutrophication model for Lake Washington (USA) Part II - model calibration and system dynamics analysis. *Ecol. Model*. 187(2-3):179-200.

Arhonditsis, G., Tsirtsis, G., and Karydis, M. 2002. The effects of episodic rainfall events to the dynamics of coastal marine ecosystems: applications to a semi-enclosed gulf in the Mediterranean. *Sea. J. Mar. Syst*. 35(3-4):183-205. Arhonditsis, G.B., Brett, M.T., and Frodge, J., 2003. Environmental control and limnological impacts of a large recurrent spring bloom in Lake Washington, USA. *Environ. Manage.* 31(5): 603–618.

Arhonditsis, G.B., Adams-VanHarn, B.A., Nielsen, L., Stow, C.A., and Reckhow, K.H. 2006. Evaluation of the current state of mechanistic aquatic biogeochemical modeling: citation analysis and future perspectives. *Environ. Sci. Technol*. 40(21):6547-6554.

Arhonditsis, G.B., Qian, S.S., Stow, C.A., Lamon, E.C., and Reckhow, K.H. 2007. Eutrophication risk assessment using Bayesian calibration of process-based models: Application to a mesotrophic lake. *Ecol. Model*. 208(2-4):215-229.

Arhonditsis, G.B., Papantou, D., Zhang, W., Perhar, G., Massos, E., and Shi, M. 2008a. Bayesian calibration of mechanistic aquatic biogeochemical models and benefits for environmental management. *J. Mar. Syst*.73(1-2):8-30.

Arhonditsis, G.B., Perhar, G., Zhang, W., Massos, E., Shi, M., and Das, A. 2008b. Addressing equifinality and uncertainty in eutrophication models. *Water Resour. Res*. 44:W01420.

Anderson, T.R., 2005. Plankton functional type modeling: running before we can walk? *J. Plankton Res.* 27(11):1073-1081.

Anderson, T.R., 2006. Confronting complexity: reply to Le Quere and Flynn. *J. Plankton Res.* 28(9): 877-878.

Beck, M.B., 1987. Water-quality modeling - a review of the analysis of uncertainty. *Water Resour. Res.* 23(11):1393-1442.

Berliner, L.M. 1996. Hierarchical Bayesian time series models. In: *Maximum Entropy and Bayesian Methods* (eds Hanson, K. and Silver, R.). Norwell: Kluwer pp. 15-22.

Berliner, L.M., Wikle, C.K., and Cressie, N. 2000. Long-lead prediction of Pacific SSTs via Bayesian Dynamic Modeling. *J. Climate*. 13(22): 3953-3968.

Bernardo, J.M., and Smith, A.F.M. 1994. *Bayesian Theory*. New York: John Wiley & Sons.

Besag, J., Green, P., Higdon, D. and Mengersen, K. 1995. Bayesian computation and stochastic systems. *Stat. Sci*. 10(1): 3–66.

Beven, K.J. 1993. Prophecy, reality and uncertainty in distributed hydrological modeling. *Adv. Water Resour*. 16(1):41-51.

Beven, K.J. 2001. *Rainfall-Runoff Modeling: The Primer*. New York: John Wiley.

Beven, K.J. 2006. A manifesto for the equifinality thesis. *J. Hydrol*. 320(1-2):18-36.

Bierman, V.J., and Dolan, D.M. 1986. Modeling of phytoplankton in Saginaw Bay. 1. Calibration Phase. J. Environ. Eng.-ASCE. 112(2): 400-414.

Bierman, V.J., Kaur, J., DePinto, J.V., Feist, T.J., and Dilks, D.W. 2005. Modeling the role of zebra mussels in the proliferation of blue-green algae in Saginaw Bay, Lake Huron. *J. Great Lakes Res.* 31(1): 32-55.

Borsuk, M.E., Stow, C.A., and Reckhow, K.H. 2002. Predicting the frequency of water quality standard violations: a probabilistic approach for TMDL development. *Environ. Sci. Technol*. 36(10):2109-2115.

Borsuk, M.E., Stow, C.A., and Reckhow, K.H. 2004. A Bayesian network of eutrophication models for synthesis, prediction, and uncertainty analysis. *Ecol. Model*. 173(2-3):219-239.

Bowerman, W.W., Carey. J., Carpenter, D., Colborn, T., DeRosa, C., Fournier, M., Fox, G.A., Gibson, B.L., Gilbertson, M., Henshel, D., McMaster, S., and Upshur, R. 1999. Is it time for a Great Lakes Ecosystem Management Agreement separate from the Great Lakes Water Quality Agreement? *J. Great Lakes Res.* 25(2): 237-238.

Box, G.E.P., and Tiao,G.C.1973. *Bayesian Inference in Statistical Analysis*. Reading: Addison-Wesley.

Brett, M.T., and Benjamin, M.M. 2008. A review and reassessment of lake phosphorus retention and the nutrient loading concept. *Freshwater Biol*. 53(1): 194-211.

Brett, M.T., Arhonditsis, G.B., Mueller, S.E., Hartley, D.M., Frodge, J.D., and Funke, D.E. 2005. Non-point-source impacts on stream nutrient concentrations along a forest to urban gradient. *Environ. Manage*. 35(3) 330-342.

Brun, R., Reichert, P., and Kunsch, H.R. 2001. Practical identifiability analysis of large environmental simulation models. *Water Resour. Res.* 37(4): 1015-1030.

Brooks, S.P., and Gelman, A. 1998. Alternative methods for monitoring convergence of iterative simulations. *J. Comput. Graph*. Stat. 7(4): 434-455.

Cerco, C.F., and Cole, T.M. 1994. *CE-QUAL-ICM: a three-dimensional eutrophication model, version 1.0. User's Guide*. US Army Corps of Engineers Waterways Experiments Station. Vicksburgh, MS.

Chapra, S.C., and Canale, R.P. 1998. *Numerical Methods for Engineers* (3rd Ed.). New York: McGraw-Hill.

Chen, C.F., Ma, H.W., and Reckhow, K.H. 2007. Assessment of water quality management with a systematic qualitative uncertainty analysis. *Sci. Total Environ.* 374(1): 13-25.

Clark, J.S. 2003. Uncertainty in population growth rates calculated from demography: the hierarchical approach. *Ecology*. 84(6): 1370-1381.

Clark, J.S. 2005. Why environmental scientists are becoming Bayesians. *Ecol. Lett.* 8(1): 2-14.

Clark, J.S., Dietze, M., Chakraborty, S., Agarwal, P.K., Ibanez, I., LaDeau, S., and Wolosin, M. 2007. Resolving the biodiversity paradox. *Ecol. Lett.* 10(8): 647-659.

Cressie, N. 2000. Spatial statistics and environmental sciences. *Proceedings of the Section on Statistics and the Environment*. Alexandria: American Statistical Association. pp. 1-10.

Denman, K.L. 2003. Modeling planktonic ecosystems: parameterizing complexity. *Prog. Oceanogr.* 57 (3-4):429-452.

Dennis, B. 1996. Discussion: should ecologists become Bayesians? *Ecol. Appl*. 6(4): 1095-1103.

Dorazio, R.M., and Johnson, F.A. 2003. Bayesian inference and decision theory - A framework for decision making in natural resource management. *Ecol. Appl*. 13(2):556-563.

DiToro, D.M., Thomas, N.A., Herdendorf, C.E., Winfield, R.P., and Connolly, J.P. 1987. A post audit of a Lake Erie eutrophication model. *J. Great Lakes Res.* 13(4):801-825.

Edwards, A.M., and Yool, A. 2000. The role of higher predation in plankton population models. *J. Plankton Res*. 22(6):1085-1112.

Efron, B., and Morris, C.N. 1975. Data analysis using Stein's estimator and its generalizations. *J. Am. Stat. Assoc*. 70(350): 311–319.

Ellison, A.M. 1996. An introduction to Bayesian inference for ecological research and environmental decision-making. *Ecol. Appl*. 6(4): 1036-1046.

Ellison, A.M. 2004. Bayesian inference in ecology. *Ecol. Lett*. 7(6): 509-520.

Endres, D.M., and Schindelin, J.E. 2003. A new metric for probability distributions. *IEEE T. Inform. Theory*. 49(7): 1858-1860.

Engeland, K., and Gottschalk, L. 2002. Bayesian estimation of parameters in a regional hydrological model. *Hydrol. Earth Syst. Sci.* 6: 883-898.

Franks, P.J.S. 2002. NPZ models of plankton dynamics: their construction, coupling to physics, and application. *J. Oceanogr.* 58: 379–387.

Gelman, A. 2005. Analysis of variance -Why it is more important than ever. *Ann. Stat*. 33(1): 1-31.

Gelman, A., and Pardoe, L. 2006. Bayesian measures of explained variance and pooling in multilevel (hierarchical) models. *Technometrics*. 48(2): 241-251.

Gelman, A., Carlin, J.B., Stern, H.S., and Rubin, D.B. 1995. *Bayesian Data Analysis*. New York: Chapman and Hall.

Gilks, W.R., Richardson, S., and Spiegelhalter, D.J. (Eds.) 1998. *Markov Chain Monte Carlo in Practice*. London:Chapman & Hall/CRC.

Hampton, S.E. 2005. Increased niche differentiation between two Conochilus species over 33 years of climate change and food web alteration. *Limnol. Oceanogr.* 50(2): 421-426.

Hartig, J.H., Zarull, M.A., and Law, N.L. 1998. An ecosystem approach to Great Lakes management: Practical steps. *J. Great Lakes Res.* 24(3): 739-750.

Higdon, D., Kennedy, M., Cavendish, J.C., Cafeo, J.A., and Ryne, R.D. 2004. Combining field data and computer simulations for calibration and prediction. *SIAM J. Sci. Comput*. 26(2):448-466.

Hong, B.G., Strawderman, R.L., Swaney, D.P., and Weinstein, D.A. 2005. Bayesian estimation of input parameters of a nitrogen cycle model applied to a forested reference watershed, Hubbard Brook Watershed Six. *Water Resour. Res.* 41(3): W03007.

Howarth, R.W., Billen, G., Swaney, D., Townsend, A., Jaworski, N., Lajtha, K., Downing, J.A., Elmgren, R., Caraco, N., Jordan, T., Berendse, F., Freney, J., Kudeyarov, V., Murdoch, P., and Zhu, Z. 1996. Regional nitrogen budgets and riverine N&P fluxes for the drainage to the North Atlantic Ocean: Natural and human influences. *Biogeochemistry*. 35(1): 75-139.

Hughes, J.P., and Guttorp, P. 1994. Incorporating spatial dependence and atmospheric data in a model of precipitation. *J. Appl. Meteorol*. 33(12): 1503–1515.

Jassby, A.D., and Platt, T. 1976. Mathematical formulation of relationship between photosunthesis and light for phytoplankton. *Limnol. Oceanogr*. 21(4):540-547.

Jorgensen, S.E., Nielsen, S.E., and Jorgensen, L.A. 1991. *Handbook of Ecological Parameters and Ecotoxicology*. New York:Elsevier Publications.

Krantzberg, G. 2004. Science must inform Great Lakes policy. *J. Great Lakes Res.* 30(4):573-574.

Lam, D.C.L., Schertzer, W.M., and Fraser, A.S. 1987a. Oxygen depletion in Lake Erie – modeling the physical, chemical, and biological interactions, 1972 and 1979. *J. Great Lakes Res.* 13(4):770-781.

Lam, D.C.L., Schertzer, W.M., and Fraser, A.S. 1987b. A post-audit analysis of the NWRI 9-box water-quality model for Lake Erie. *J. Great Lakes Res.* 13(4): 782-800.

Lampert, W., and Sommer, U. 1997. *Limnoecology: the ecology of lakes and streams*. New York:Oxford University Press.

Leon, L.K., Imberger, J., Smith, R.E.H., Hecky, R.E., Lam, D.C.L., and Schertzer, W.M. 2005. Modeling as a tool for nutrient management in Lake Erie: a hydrodynamics study. *J. Great Lakes Res.* 31(sup2): 309-318.

Ludwig, D. 1996. Uncertainty and the assessment of extinction probabilities. *Ecol. Appl*. 6(4):1067-1076.

Malve, O., and Qian, S.S. 2006. Estimating nutrients and chlorophyll a relationships in Finnish lakes. *Environ. Sci. Technol*. 40(24): 7848-7853.

Malve, O., Laine, M., and Haario, H. 2005. Estimation of winter respiration rates and prediction of oxygen regime in a lake using Bayesian inference. *Ecol. Model.* 182(2): 183-197.

Malve, O., Laine, M., Haario, H., Kirkkala, T., and Sarvala, J. 2007. Bayesian modelling of algal mass occurrences - using adaptive MCMC methods with a lake water quality model. *Environ. Modell. Softw.* 22(7): 966-977.

McBride, G.B., and Ellis, J.C. 2001. Confidence of compliance: A Bayesian approach for percentile standards. *Water Res*. 35(5):1117-1124.

McCauley, E., and Kalff, J. 1981. Empirical relationships between phytoplankton and zooplankton biomass in lakes. *Can. J. Fish. Aquat. Sci*. 38(1): 458–463.

Michielsens, C., and McAllister, M. 2004. A Bayesian hierarchical analysis of stock-recruit data: quantifying structural and parameter uncertainties. *Can. J. Fish. Aquat. Sci*. 61(6): 1032-1047.

Mills, E.L., Casselman, J.M., Dermott, R.J., Fitzsimons, D., Gal, G., Holeck, K.T., Hoyle, J.A., Johannsson, O.E., Lantry, B.F., Makarewicz, J.C., Millard, E.S., Munawar, I.F., Munawar, M., O'Gorman, R., Owens, R.W., Rudstam, L.G., Schaner, T., and Stewart T.J. 2003. Lake Ontario: food web dynamics in a changing ecosystem (1970–2000). *Can. J. Fish. Aquat. Sci.* 60(4):471-490.

Minns, C.K., and Kelso, J.R.M. 2000. NO! It is time for a Great Lakes Ecosystem Management Agreement that SUBSUMES the Great Lakes Water Quality Agreement. *J. Great Lakes Res.* 26(1):1-2.

Neal, R. 1998. Suppressing random walks in Markov chain Monte Carlo using ordered over-relaxation. In: Jordan, M.I. (Ed.) *Learning in Graphical Models*. pp. 205-230. Dordrecht:Kluwer Academic Publishers.

Nicholls, K.H. 1999. Effects of temperature and other factors on summer phosphorus in the inner Bay of Quinte, Lake Ontario: implications for climate warming. *J. Great Lakes Res*. 25(2): 250-262.

Office of Water. 2007. *Guidelines for Preparation of the Comprehensive State Water Quality Assessments*. U.S. Washington, DC: Environmental Protection Agency.

Omlin, M., and Reichert, P. 1999. A comparison of techniques for the estimation of model prediction uncertainty. *Ecol. Model.* 115(1): 45-59.

Page, T., Beven, K.J., and Whyatt, J.D. 2004. Predictive capability in estimating changes in water quality: Long-term responses to atmospheric deposition. *Water Air Soil Pollut.* 151(1-4): 215-244.

Qian, S.S., and Reckhow, K.H. 2007. Combining model results and monitoring data for water quality assessment. *Environ. Sci. Technol*. 41(14):5008-5013.

Qian, S.S., Stow, C.A., and Borsuk, M.E. 2003. On Monte Carlo methods for Bayesian inference. *Ecol. Model.* 159(2-3): 269-277.

Reichert, P., and Omlin, M. 1997. On the usefulness of overparameterized ecological models. *Ecol. Model*. 95(2-3): 289-299.

Reichert, P., Schervish, M., and Small, M.J. 2002. An efficient sampling technique for Bayesian inference with computationally demanding models. *Technometrics.* 44(4): 318-327.

Rivot, E., and Prévost, E. 2002. Hierarchical Bayesian analysis of capture-mark-recapture data. *Can. J. Fish. Aquat. Sci*. 59(11): 1768–1784.

Rivot, E., Prévost, E., Cuzol, A., Bagliniere, J.L., and Parent, E. 2008. Hierarchical Bayesian modelling with habitat and time covariates for estimating riverine fish population size by successive removal method. *Can. J. Fish. Aquat. Sci*. 65(1): 117-133.

Rockwell, D.C., Warren, G.J., Bertram, P.E., Salisbury, D.K., and Burns, N.M. 2005. The US EPA Lake Erie indicators monitoring program 1983-2002: Trends in phosphorus, silica, and chlorophyll a in the central basin. *J. Great Lakes Res*. 31(Suppl. 2): 23-34.

Royle, J.A., Berliner, L.M., Wikle, C.K., and Milliff, R. 1999. A hierarchical spatial model for constructing wind fields from scatterometer data in the Labrador Sea. *Case Studies in Bayesian Statistics* (Eds. C. Gatsonis et al). pp. 367–382. Springer-Verlag.

Schindler, D.W. 1997. Widespread effects of climatic warming on freshwater ecosystems in North America. *Hydrol. Process.* 11(8): 1043-1067.

Schindler, D.W. 2001. The cumulative effects of climate warming and other human stresses on Canadian freshwaters in the new millennium. *Can. J. Fish. Aquat. Sci.* 58(1): 18-29.

Schindler, D.W. 2006. Recent advances in the understanding and management of eutrophication. *Limnol. Oceanogr*. 51(1): 356-363.

Schladow, S.G., and Hamilton, D.P. 1997. Prediction of water quality in lakes and reservoirs. 2. Model calibration, sensitivity analysis and application. *Ecol. Model*. 96(3):111-123.

Smith, V.H. 1986. Light and nutrient effects on the relative biomass of blue-green algae in lake phytoplankton. *Can. J. Fish. Aquat. Sci*. 43(1): 148-153.

Spiegelhalter, D., Thomas, A., Best, N., and Lunn, D. 2003. *WinBUGS User Manual, Version 1.4*. Available at http://www.mrc-bsu.cam.ac.uk/bugs.

Steinberg, L.J., Reckhow, K.H., and Wolpert, R.L. 1997. Characterization of parameters in mechanistic models: a case study of a PCB fate and transport model. *Ecol. Model*. 97(1-2):35-46.

Stow, C.A., Reckhow, K.H., Qian, S.S., Lamon, E.C., Arhonditsis, G.B., Borsuk, M.E., and Seo, D. 2007. Approaches to evaluate water quality model parameter uncertainty for adaptive tmdl implementation. *J. Am. Water Resour. As*. 43(6):1499-1507.

Straile, D. 2002. North Atlantic Oscillation synchronizes food-web interactions in central European lakes. *P. Roy. Soc. Lond. B. Bio.* 269(1489): 391-395.

Thomas, C.D., Bodsworth, E.J., Wilson, R.J., Simmons, A.D., Davies, Z.G., Musche, M., and Conradt, L. 2001. Ecological and evolutionary processes at expanding range margins. *Nature.* 411(6837): 577-581.

Tian, R.C., Vezina, A.F., Starr, M., and Saucier, F. 2001. Seasonal dynamics of coastal ecosystems and export production at high latitudes: a modeling study. *Limnol. Oceanogr*. 46(8):1845-1859.

Van Oijen, M., Rougier, J., and Smith, R. 2005. Bayesian calibration of process-based forest models: bridging the gap between models and data. *Tree Physiol*. 25(7):915–927.

Walters, C.J. 1986. *Adaptive Management of Renewable Resources*. New York:McMillan.

Weyhenmeyer, G.A. 2004. Synchrony in relationships between the North Atlantic Oscillation and water chemistry among Sweden's largest lakes. *Limnol. Oceanogr.* 49(4): 1191-1201.

Wild, P., Hordan, R., LePlay, A., and Vincent, R. 1996. Confidence intervals for probabilities of exceeding threshold limits with censored log-normal data. *Environmetrics*. 7(3):247-259.

Wikle, C.K. 2003a. Hierarchical models in environmental science. *Int. Stat. Rev.* 71(2): 181-199.

Wikle, C.K. 2003b. Hierarchical Bayesian models for predicting the spread of ecological processes. *Ecology.* 84(6): 1382-1394.

Wikle, C.K., Berliner, L.M. and Cressie, N. 1998. Hierarchical Bayesian space-time models. *J. Envir. Ecol. Stat*. 5(2): 117-154.

Wikle, C.K., Milliff, R.F., Nychka. D., and Berliner, L.M. 2001. Spatiotemporal hierarchical Bayesian modeling: Tropical ocean surface winds. *J. Am. Stat. Assoc.* 96(454): 382-397.

Wikle, C.K., Berliner, L.M., and Milliff, R.F. 2003. Hierarchical Bayesian approach to boundary value problems with stochastic boundary conditions. *Mon. Weather. Rev.* 131(6): 1051-1062.

Winter, J.G., Eimers, M.C., Dillon, P.J., Scott, L.D., Scheider, W.A., and Willox, C.C. 2007. Phosphorus inputs to lake simcoe from 1990 to 2003: Declines in tributary loads and observations on lake water quality. *J. Great Lakes Res.* 33(2): 381-396.

Wroblewski, J.S. 1977. Model of phytoplankton plume formation during variable Oregon upwelling. *J. Mar*. 35(2):357-394.

Wyatt, R.J. 2002. Estimating riverine fish population size from single- and multiple-pass removal sampling using a hierarchical model. *Can. J. Fish. Aquat. Sci*. 59(4): 695-706.

Zhang, W., and Arhonditsis, G.B. 2008. Predicting the frequency of water quality standard violations using Bayesian calibration of eutrophication models. *J. Great Lakes Res.* In press.

Appendix

Appendix A NPZD model structure

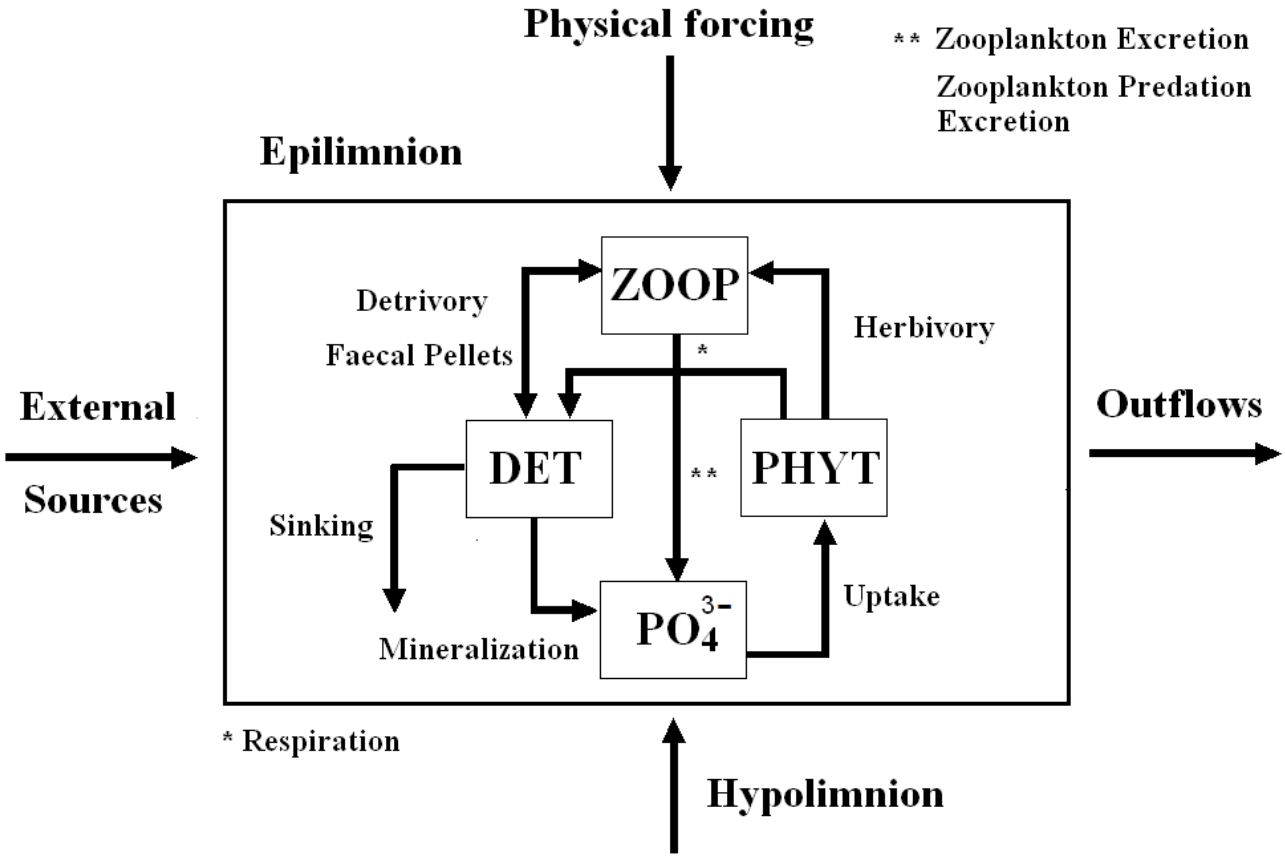

Figure A1 The phosphate-detritus-phytoplankton-zooplankton model structure. Arrows indicate flows of matter through the system. System equations and parameter definitions are provided in Tables A1 and Table 3.2.

Table A1 The specific functional forms of the NPZD eutrophication model.

$$\frac{dPO_4}{dt} = -\frac{PO_4}{e+PO_4}\mathrm{a}\sigma_{(t)}PHYT\ P/C_{phyto} + \frac{\beta\lambda\left((PHYT\cdot P/C_{phyto})^2+\omega DET^2\right)}{\mu^2+(PHYT\cdot P/C_{phyto})^2+\omega DET^2}\sigma_{(tz)}ZOOP\ P/C_{zoop}$$

$$+\gamma d\sigma_{(tz)}\frac{ZOOP^3}{pred^2+ZOOP^2}P/C_{zoo} + \phi\sigma_{(t)}DET + k(1-\sigma_{(t)})(PO_{4(hypo)}-PO_4) + PO_{4exog}$$

$$-outflows\cdot PO_4$$

$$\sigma_{(t)} = \frac{(1-\varepsilon\cos(\frac{2\pi t}{365}))}{1+\varepsilon}\quad \sigma_{(tz)} = \frac{(1-\varepsilon\cos(\frac{2\pi t}{365}-0.5))}{1+\varepsilon}$$

$$outflows = 0.0028+0.0014\sin(2\pi(t/365+0.12))$$

$$\frac{dPHYT}{dt} = \frac{PO_4}{e+PO_4}\mathrm{a}\sigma_{(t)}PHYT - r\sigma_{(t)}PHYT - \frac{\lambda(PHYT\cdot P/C_{phyto})^2}{\mu^2+(PHYT\cdot P/C_{phyto})^2+\omega DET^2}\sigma_{(tz)}ZOOP$$

$$-sPHYT - outflows\cdot PHYT$$

$$\frac{dZOOP}{dt} = \frac{\alpha\lambda\left((PHYT\cdot P/C_{phyto})^2+\omega DET^2\right)}{\mu^2+(PHYT\cdot P/C_{phyto})^2+\omega DET^2}\sigma_{(tz)}ZOOP - d\sigma_{(tz)}\frac{ZOOP^3}{pred^2+ZOOP^2} - outflows\cdot ZOOP$$

$$\frac{dDET}{dt} = r\sigma_{(t)}PHYT\ P/C_{phyto} + \frac{\left[(1-\alpha-\beta)(PHYT\cdot P/C_{phyto})^2-(\alpha+\beta)\omega DET^2\right]\lambda}{\mu^2+(PHYT\cdot P/C_{phyto})^2+\omega DET^2}\sigma_{(tz)}ZOOP\ P/C_{zoop}$$

$$-\varphi\sigma_{(t)}DET - \psi DET + DET_{exog} - outflows\cdot DET$$

Appendix B WinBUGS code for the Bayesian Hierarchical model

The following WinBUGS code is for the Bayesian Hierarchical model *Scenario A_1* in Chapter 3:

```
model {

#   Mechanistic Model (Note:  S=1 Mesotrophic, S=2  Oligotrophic)
for (i in 1:S) {
solution[i, 1:n.grid, 1:dim] <- ode.block(init[i,1:dim], grid[1:n.grid], D(C[i,1:dim], t), origin,
tol)
D(C[i,PO4[i]], t) <- -pcp*a[i]*Fp[i]*sigmat[i]*C[i,PHYT[i]]
                          +(beta[i]*lamda[i]*(pow(PhytP[i],2)+omega*pow(C[i,DET[i]],2))
                          *sigmatz[i]*C[i,ZOOP[i]]*pcz)
                         /(pow(me[i],2)+pow(PhytP[i],2)+omega*pow(C[i,DET[i]],2))
                         +(gamma[i]*d[i]*sigmatz[i]*pow(C[i,ZOOP[i]],3)*pcz)
                        /(pow(pred[i],2)+pow(C[i,ZOOP[i]],2)) +phi[i]*sigmat[i]*C[i,DET[i]]
                        +k[i]*(1-sigmat[i])*(PO4hypo[i]-C[i,PO4[i]])+PO4exog[i]-
outflows*C[i,PO4[i]]
D(C[i,PHYT[i]], t) <- a[i]*Fp[i]*sigmat[i]*C[i,PHYT[i]] -r[i]*sigmat[i]*C[i,PHYT[i]]
                          -(lamda[i]*(pow(PhytP[i],2))*sigmatz[i]*C[i,ZOOP[i]])
                          /(pow(me[i],2)+pow(PhytP[i], 2)+omega*pow(C[i,DET[i]],2))
                          -s[i]*C[i,PHYT[i]]-outflows*C[i,PHYT[i]]
D(C[i,ZOOP[i]], t) <- (alpha[i]*lamda[i]*(pow(PhytP[i],2)+omega*pow(C[i,DET[i]],2))
                           *sigmatz[i]*C[i,ZOOP[i]])
                           /(pow(me[i],2)+pow(PhytP[i],2)+omega*pow(C[i,DET[i]],2))
                           -
(d[i]*sigmatz[i]*pow(C[i,ZOOP[i]],3))/(pow(pred[i],2)+pow(C[i,ZOOP[i]],2))
                           -outflows*C[i,ZOOP[i]]
D(C[i,DET[i]], t) <- r[i]*sigmat[i]*C[i,PHYT[i]]*pcp
                         +(((1-alpha[i]-beta[i])*pow(PhytP[i],2)-(alpha[i]+beta[i])
                         *omega*pow(C[i,DET[i]],2))*lamda[i]*sigmatz[i]*C[i,ZOOP[i]]*pcz)
                          /(pow(me[i],2)+pow(PhytP[i], 2)+omega*pow(C[i,DET[i]],2))
                         -phi[i]*sigmat[i]*C[i,DET[i]]-psi[i]*C[i,DET[i]]+DETexog[i]-
outflows*C[i,DET[i]]
PhytP[i]<-C[i,PHYT[i]]*pcp
Fp[i]<- C[i,PO4[i]]/(C[i,PO4[i]]+e[i])
#   Parameter hierarchical structure
log(a[i]) <- lna[i]
lna[i]  ~ dnorm(atrans,preca[i])
preca[i]<-1/pow(0.15*atrans,2)
log(d[i]) <- lnd[i]
lnd[i] ~ dnorm(dtrans,precd[i])
precd[i]<-1/pow(0.15*dtrans,2)
log(pred[i]) <- lnpred[i]
lnpred[i] ~ dnorm(predtrans, precpred[i])
precpred[i]<-1/pow(0.15*predtrans,2)
```

```
log(e[i]) <- lne[i]
lne[i] ~ dnorm(etrans, prece[i])
prece[i]<-1/pow(0.15*etrans,2)
log(k[i]) <- lnk[i]
lnk[i] ~ dnorm(ktrans, preck[i])
preck[i]<-1/pow(0.15*ktrans,2)
log(r[i]) <- lnr[i]
lnr[i] ~ dnorm(rtrans, precr[i])
precr[i]<-1/pow(0.15*rtrans,2)
log(s[i]) <- lns[i]
lns[i] ~ dnorm(strans,precs[i])
precs[i]<-1/pow(0.15*strans,2)
log(alpha[i]) <- lnalpha[i]
lnalpha[i] ~ dnorm(alphatrans, precalpha[i])
precalpha[i]<-1/pow(0.15*alphatrans,2)
log(beta[i]) <- lnbeta[i]
lnbeta[i] ~ dnorm(betatrans, precbeta[i])
precbeta[i]<-1/pow(0.15*betatrans,2)
log(gamma[i]) <- lngamma[i]
lngamma[i] ~ dnorm(gammatrans, precgamma[i])
precgamma[i]<-1/pow(0.15*gammatrans,2)
log(lamda[i]) <- lnlamda[i]
lnlamda[i] ~ dnorm(lamdatrans, preclamda[i])
preclamda[i]<-1/pow(0.15*lamdatrans,2)
log(me[i]) <- lnme[i]
lnme[i] ~ dnorm(metrans, precme[i])
precme[i]<-1/pow(0.15*metrans,2)
log(phi[i]) <- lnphi[i]
lnphi[i] ~ dnorm(phitrans,precphi[i])
precphi[i]<-1/pow(0.15*phitrans,2)
log(psi[i]) <- lnpsi[i]
lnpsi[i] ~ dnorm(psitrans, precpsi[i])
precpsi[i]<-1/pow(0.15*psitrans,2)
        }
sigmat[1] <- (1-epsilon1*cos((2*3.14159*t)/104))/(1+epsilon1)
sigmat[2] <- (1-epsilon2*cos((2*3.14159*t)/104))/(1+epsilon2)
sigmatz[1] <- (1-epsilon1*cos((2*3.14159*t)/104-0.5))/(1+epsilon1)
sigmatz[2] <- (1-epsilon2*cos((2*3.14159*t)/104-0.5))/(1+epsilon2)
#  Boundary conditions:
PO4hypo[1]<- 0.000000001558893*pow(t,6)-0.000000434309987*pow(t,5)
                    +0.000041682779882 5628*pow(t,4)-0.001543158*pow(t,3)
                    +0.015065585*pow(t,2)+0.08878439*t+12.3813609435
PO4hypo[2]<- 0.00000000272837*pow(t,6)-0.000000774928*pow(t,5)
                     +0.0000747704*pow(t,4)-0.00257711*pow(t,3)
                     +0.00242661*pow(t,2)+1.00447*t+22.3926
PO4exog[1]<- -0.000000000012403*pow(t,6) + 0.000000003955862*pow(t,5)
                     -0.000000479071768 *pow(t,4)+0.000027615963954 1091*pow(t,3)
```

-0.000775946*pow(t,2)+0.009286105*t+0.022415321272
PO4exog[2]<- -0.000000000005632783*pow(t,6)+0.000000001818671*pow(t,5)
-0.000000223327130*pow(t,4)+0.000013063819200*pow(t,3)
-0.000372098*pow(t,2)+0.004519269*t+0.01172135
DETexog[1]<- -0.000000000020726*pow(t,6)+0.000000005716774*pow(t,5)
-0.000000538746690*pow(t,4)+0.000018621702669*pow(t,3)
-0.000017044227089*pow(t,2)-0.011206669*t+0.288576694063
DETexog[2]<- -0.000000000009965121*pow(t,6)+0.000000002746906*pow(t,5)
-0.000000258027240*pow(t,4)+0.000008789937823*pow(t,3)
+0.000002590822239*pow(t,2)-0.005689981*t+0.1446479
outflows<-0.0028+0.0014*sin(2*3.14159*(t/104+0.12))
# **Model global parameters prior:**
atrans ~ dnorm(0.347, 22.525)
dtrans ~ dnorm(-1.763, 65.828)
predtrans ~ dnorm(3.969, 15.836)
etrans ~ dnorm(2.303, 5.631)
ktrans ~ dnorm(-3.363, 8.967)
rtrans ~ dnorm(-2.303, 3.222)
strans ~ dnorm(-3.454, 2.041)
alphatrans ~ dnorm(-1.060, 8.967)
betatrans ~ dnorm(-1.295, 7.466)
gammatrans ~ dnorm(-1.295, 7.466)
lamdatrans ~ dnorm(-0.511, 32.691)
metrans ~ dnorm(1.844, 12.890)
phitrans ~ dnorm(-2.446, 8.967)
psitrans ~ dnorm(-2.100, 3.371)
# **Initial conditions:**
for (i in 1:S) {
init[i,PO4[i]] <- PO4o[i]; init[i,PHYT[i]] <- PHYTo[i];
init[i,ZOOP[i]] <- ZOOPo[i]; init[i,DET[i]] <- DETo[i]
PO4ostd[i]<-1/pow(0.15*PO4o[i],2)
PO4o[i]~dnorm(PO4omu[i],PO4ostd[i])I(0,)
PHYTostd[i]<-1/pow(0.15*PHYTo[i],2)
PHYTo[i]~dnorm(PHYTomu[i],PHYTostd[i])I(0,)
ZOOPostd[i]<-1/pow(0.15*ZOOPo[i],2)
ZOOPo[i]~dnorm(ZOOPomu[i],ZOOPostd[i])I(0,)
DETostd[i]<-1/pow(0.15*DETo[i],2)
DETo[i]~dnorm(DETomu[i],DETostd[i])I(0,)
}
PO4omu[1] <- 14.24726837
PO4omu[2] <- 6.180139616
PHYTomu[1] <- 59.77109509
PHYTomu[2] <- 33.88162719
ZOOPomu[1] <- 17.2799879
ZOOPomu[2] <- 8.492516905
DETomu[1] <- 16.90430875
DETomu[2] <- 7.314716529

```
#  Model Likelihood:
for (i in 1:S) {
          for (j in 1:n.grid) {
                for (q in 1:dim) {
        obtau[i,j,q]<-1/pow(0.15*data[i,j,q],2)
        obsigma[i,j,q]<-sqrt(1/obtau[i,j,q])
        Interdata[i,j,q] ~ dnorm(solution[i,j,q], mtau[i,q])
         data[i,j,q] ~ dnorm(Interdata[i,j,q], obtau[i,j,q])
         Preddata[i,j,q] ~ dnorm(Interdata[i,j,q], obtau[i,j,q])
        }}}
for (i in 1:S) {
        for (q in 1:dim) {
        mtau[i,q]~dgamma(0.01,0.01)
        msigma[i,q]<-sqrt(1/mtau[i,q])
        }}}
#    Inference Data:
list(
S = 2,
PO4 = c(1,1), PHYT = c(2,2), ZOOP = c(3,3), DET = c(4,4),
n.grid = 12,
dim = 4,
origin = 0,
tol = 0.00000001,
grid = c(4.6, 13.1, 21.7, 30.3, 39.1, 47.7, 56.6, 65.1, 74.0, 82.9, 91.7, 100.3),
data = structure(.Data = c(14.24726837,59.77109509,17.2799879,16.90430875,
13.99423926,129.7519023,20.12119105,10.10776343,
11.63240118,205.4647507,31.09868422,10.59293302,
4.42669556,639.0460477,69.02204047,10.36347722,
2.52358068,464.5307313,165.1322121,9.960077036,
2.095617637,180.3841684,79.74873375,10.55995282,
2.966957698,150.4655553,45.90881535,9.723150468,
2.785277238,117.8737581,35.7416764,8.282708645,
3.322557068,106.8030325,52.65677917,8.624109062,
2.300312757,142.6370131,49.56776042,7.447291406,
4.23556492,139.3428599,38.74035428,7.576533256,
8.417786282,96.94063701,19.35311914,7.544966479,
6.180139616,33.88162719,8.492516905,7.314716529,
7.227069737,63.1075345,9.767450612,4.493065289,
5.228115639,92.75624665,19.11291589,5.801092145,
2.763422765,278.0850346,29.98995456,5.532943047,
1.20819773,234.942107,94.72277278,4.501100966,
0.875468887,87.8290718,48.99289999,5.786532918,
1.395636012,69.37206523,26.33857668,4.969518264,
1.428236856,55.36434294,18.33184026,4.557439217,
1.562754024,51.04038084,20.87849253,4.75999908,
0.970056068,75.77579426,29.52406742,3.522486371,
2.025392248,61.21856031,22.35026172,4.041977169,
```

4.810957004,56.39059175,12.72811693,4.055796807),.Dim=c(2,12,4)),
epsilon1 = 0.9,
epsilon2 = 0.85,
pcp=0.015,
pcz=0.029,
omega=1
)
Initial Values:
list(atrans=0.405465, alphatrans=-0.79851, betatrans= -1.60944, dtrans=-1.89712,
etrans=2.564949, ktrans=-2.99573, rtrans=-1.89712, strans=-3.21888, gammatrans=-
0.69315, lamdatrans=-0.51083, metrans=1.558145, phitrans=-2.99573, psitrans= -
2.52573, predtrans=4.174387,
lna=c(0.693147,0.693147), lnalpha=c(-0.79851,-0.79851), lnbeta=c(-1.60944,-1.60944),
lnd=c(-1.83258,-1.83258), lne=c(2.484907, 2.484907), lnk=c(-2.99573, -2.99573),
lnr=c(-1.89712,-1.89712), lns=c(-3.21888,-3.21888), lngamma=c(-0.51083,-0.51083),
lnlamda=c(-0.51083,-0.51083), lnme=c(1.386294,1.386294), lnphi=c(-2.99573,-
2.99573), lnpsi=c(-2.30259, -2.30259), lnpred=c(3.806662, 3.806662),
PO4o = c(14.24726837,6.180139616),
PHYTo = c(59.77109509,33.88162719),
ZOOPo = c(17.2799879,8.492516905),
DETo= c(16.90430875,7.314716529),
mtau= structure(.Data = c(0.1,0.1,0.1,0.1,0.1,0.1,0.1,0.1),
                                    .Dim=c(2,4)),
Preddata = structure(.Data =c(14.24726837,59.77109509,17.2799879,16.90430875,
13.99423926,129.7519023,20.12119105,10.10776343,
11.63240118,205.4647507,31.09868422,10.59293302,
4.42669556,639.0460477,69.02204047,10.36347722,
2.52358068,464.5307313,165.1322121,9.960077036,
2.095617637,180.3841684,79.74873375,10.55995282,
2.966957698,150.4655553,45.90881535,9.723150468,
2.785277238,117.8737581,35.7416764,8.282708645,
3.322557068,106.8030325,52.65677917,8.624109062,
2.300312757,142.6370131,49.56776042,7.447291406,
4.23556492,139.3428599,38.74035428,7.576533256,
8.417786282,96.94063701,19.35311914,7.544966479,
6.180139616,33.88162719,8.492516905,7.314716529,
7.227069737,63.1075345,9.767450612,4.493065289,
5.228115639,92.75624665,19.11291589,5.801092145,
2.763422765,278.0850346,29.98995456,5.532943047,
1.20819773,234.942107,94.72277278,4.501100966,
0.875468887,87.8290718,48.99289999,5.786532918,
1.395636012,69.37206523,26.33857668,4.969518264,
1.428236856,55.36434294,18.33184026,4.557439217,
1.562754024,51.04038084,20.87849253,4.75999908,
0.970056068,75.77579426,29.52406742,3.522486371,
2.025392248,61.21856031,22.35026172,4.041977169,
4.810957004,56.39059175,12.72811693,4.055796807),

```
                                                    .Dim=c(2,12,4)),
Interdata = structure(.Data = c(14.24726837,59.77109509,17.2799879,16.90430875,
13.99423926,129.7519023,20.12119105,10.10776343,
11.63240118,205.4647507,31.09868422,10.59293302,
4.42669556,639.0460477,69.02204047,10.36347722,
2.52358068,464.5307313,165.1322121,9.960077036,
2.095617637,180.3841684,79.74873375,10.55995282,
2.966957698,150.4655553,45.90881535,9.723150468,
2.785277238,117.8737581,35.7416764,8.282708645,
3.322557068,106.8030325,52.65677917,8.624109062,
2.300312757,142.6370131,49.56776042,7.447291406,
4.23556492,139.3428599,38.74035428,7.576533256,
8.417786282,96.94063701,19.35311914,7.544966479,
6.180139616,33.88162719,8.492516905,7.314716529,
7.227069737,63.1075345,9.767450612,4.493065289,
5.228115639,92.75624665,19.11291589,5.801092145,
2.763422765,278.0850346,29.98995456,5.532943047,
1.20819773,234.942107,94.72277278,4.501100966,
0.875468887,87.8290718,48.99289999,5.786532918,
1.395636012,69.37206523,26.33857668,4.969518264,
1.428236856,55.36434294,18.33184026,4.557439217,
1.562754024,51.04038084,20.87849253,4.75999908,
0.970056068,75.77579426,29.52406742,3.522486371,
2.025392248,61.21856031,22.35026172,4.041977169,
4.810957004,56.39059175,12.72811693,4.055796807),
                                                    .Dim=c(2,12,4)))
```

Appendix C Posterior estimates for Bayesian Hierarchical Models

Table C1: Markov Chain Monte Carlo posterior estimates of the mean values and standard deviations of the model stochastic nodes against three datasets representing oligo-, meso-, and eutrophic conditions.

Nodes	*Oligotrophic*		*Mesotrophic*		*Eutrophic*	
	Mean	*S. D.*	*Mean*	*S. D.*	*Mean*	*S. D.*
a	1.129	0.130	1.273	0.189	1.073	0.058
d	0.182	0.024	0.183	0.022	0.188	0.020
pred	45.04	10.98	53.68	10.50	66.75	15.61
e	5.749	0.947	13.17	3.336	22.05	2.928
k	0.008	0.001	0.028	0.006	0.029	0.006
r	0.174	0.035	0.180	0.031	0.090	0.009
s	0.043	0.012	0.028	0.011	0.044	0.008
α	0.481	0.182	0.469	0.132	0.560	0.079
β	0.256	0.088	0.256	0.088	0.224	0.073
γ	0.287	0.106	0.297	0.113	0.275	0.064
λ	0.659	0.113	0.641	0.110	0.686	0.077
μ	6.597	1.724	7.280	1.624	8.577	1.362
φ	0.051	0.015	0.073	0.021	0.088	0.018
ψ	0.045	0.028	0.055	0.020	0.101	0.023
σ_{PO4}	5.272	0.487	14.43	1.661	27.51	2.464
σ_{PHYT}	38.59	4.383	69.35	8.032	131.5	14.86
σ_{ZOOP}	9.750	1.449	20.02	3.824	36.42	4.822
σ_{DET}	7.657	0.968	19.05	3.677	36.68	5.324

Table C2: *Scenario A.* Markov Chain Monte Carlo posterior estimates of the mean values and standard deviations of the model stochastic nodes.

Nodes	A_1				A_2			
	1		*2*		*1*		*2*	
	Mean	*S. D.*	*Mean*	*S. D.*	*Mean*	*S. D.*	*Mean*	*S. D.*
a	1.472	0.168	1.525	0.216	1.172	0.123	1.159	0.114
d	0.215	0.060	0.199	0.053	0.257	0.067	0.282	0.056
pred	55.08	22.36	46.93	28.35	56.13	15.29	101.6	28.14
e	17.65	2.535	12.30	2.230	13.17	1.997	25.92	6.161
k	0.020	0.007	0.005	0.001	0.019	0.004	0.023	0.006
r	0.174	0.034	0.152	0.022	0.187	0.016	0.179	0.039
s	0.026	0.012	0.022	0.007	0.016	0.008	0.018	0.012
α	0.523	0.198	0.522	0.197	0.673	0.130	0.685	0.119
β	0.229	0.089	0.236	0.094	0.247	0.094	0.241	0.083
γ	0.303	0.104	0.307	0.109	0.233	0.077	0.229	0.076
λ	0.626	0.124	0.627	0.123	0.722	0.123	0.724	0.119
μ	12.60	4.276	9.703	2.952	13.17	3.565	16.22	5.416
φ	0.038	0.019	0.028	0.011	0.039	0.009	0.054	0.025
ψ	0.027	0.007	0.030	0.006	0.031	0.007	0.042	0.015
σ_{PO4}	14.50	1.241	5.689	0.514	14.44	1.283	28.21	2.283
σ_{PHYT}	65.90	7.411	35.11	3.685	66.34	6.500	119.4	13.00
σ_{ZOOP}	19.58	2.933	9.557	1.473	19.48	2.785	34.82	4.860
σ_{DET}	16.39	2.238	7.329	0.936	17.17	2.136	35.66	4.810

Table C3: *Scenario B.* Markov Chain Monte Carlo posterior estimates of the mean values and standard deviations of the model stochastic nodes.

Nodes	B_1			
	1		*2*	
	Mean	*S. D.*	*Mean*	*S. D.*
a	1.303	0.092	1.317	0.087
d	0.288	0.066	0.263	0.058
pred	53.42	14.07	57.12	15.21
e	13.66	2.278	11.61	2.129
k	0.028	0.006	0.039	0.006
r	0.153	0.033	0.134	0.032
s	0.032	0.011	0.046	0.012
α	0.772	0.126	0.779	0.121
β	0.215	0.078	0.218	0.082
γ	0.232	0.069	0.240	0.062
λ	0.738	0.103	0.739	0.105
μ	8.753	2.863	7.611	2.244
φ	0.072	0.030	0.064	0.023
ψ	0.044	0.017	0.046	0.015
σ_{PO4}	14.51	1.344	14.63	1.591
σ_{PHYT}	67.48	6.779	60.50	6.799
σ_{ZOOP}	18.49	2.601	17.24	2.373
σ_{DET}	18.16	2.352	17.21	2.416

Table C4: *Scenario D.* Markov Chain Monte Carlo posterior estimates of the mean values and standard deviations of the model stochastic nodes.

Nodes	D_1				D_2			
	1		*2*		*1*		*2*	
	Mean	*S. D.*	*Mean*	*S. D.*	*Mean*	*S. D.*	*Mean*	*S. D.*
a	1.316	0.217	1.399	0.159	1.028	0.096	1.027	0.116
d	0.458	0.143	0.317	0.154	0.417	0.128	0.379	0.101
pred	69.63	20.83	44.64	59.81	68.12	19.87	136.2	36.62
e	15.70	4.812	12.03	2.552	11.31	2.052	23.61	9.309
k	0.020	0.006	0.004	0.001	0.019	0.004	0.022	0.006
r	0.170	0.055	0.151	0.027	0.176	0.025	0.172	0.074
s	0.019	0.012	0.013	0.008	0.015	0.010	0.018	0.008
α	0.740	0.155	0.673	0.235	0.746	0.142	0.772	0.099
β	0.225	0.125	0.252	0.178	0.186	0.094	0.177	0.099
γ	0.216	0.118	0.336	0.209	0.294	0.102	0.247	0.095
λ	0.823	0.127	0.796	0.149	0.783	0.124	0.799	0.114
μ	9.783	4.563	9.280	3.407	13.730	3.508	18.55	9.417
φ	0.076	0.062	0.020	0.012	0.029	0.014	0.063	0.031
ψ	0.041	0.025	0.022	0.006	0.026	0.007	0.066	0.061
σ_{PO4}	14.13	1.367	5.837	0.548	14.98	1.344	28.74	2.622
σ_{PHYT}	64.30	6.766	34.65	3.697	67.83	6.561	124.8	14.39
σ_{ZOOP}	18.34	2.709	9.243	1.468	19.16	2.798	32.86	4.499
σ_{DET}	16.94	2.241	6.971	0.795	16.44	2.068	35.14	4.986